EXPLORING THE PINHOLE: BIOCHEMICAL AND GENETIC STUDIES ON THE PROTOTYPE PINHOLIN, S^{21}

A Dissertation

by

TING PANG

Submitted to the Office of Graduate Studies of
Texas A&M University
in partial fulfillment of the requirements for the degree of

DOCTOR OF PHILOSOPHY

May 2010

Major Subject: Biochemistry

EXPLORING THE PINHOLE: BIOCHEMICAL AND GENETIC STUDIES ON THE PROTOTYPE PINHOLIN, S^{21}

A Dissertation

by

TING PANG

Submitted to the Office of Graduate Studies of
Texas A&M University
in partial fulfillment of the requirements for the degree of

DOCTOR OF PHILOSOPHY

Approved by:

Chair of Committee,	Ryland F. Young, III
Committee Members,	Mary Bryk
	Andreas Holzenburg
	Pingwei Li
Head of Department,	Gregory D. Reinhart

May 2010

Major Subject: Biochemistry

ABSTRACT

Exploring the Pinhole:

Biochemical and Genetic Studies on the Prototype Pinholin, S^{21}. (May 2010)

Ting Pang, B.S., Wuhan University

Chair of Advisory Committee: Dr. Ryland F. Young, III

Lysis of the host by bacteriophage 21 requires two proteins: the pinholin S^{21} (forms pinholes in the cytoplasmic membrane and controls lysis timing) and the endolysin (degrades the cell wall). *S21* has a dual-start motif, encoding a holin, $S^{21}68$, and a weak antiholin, $S^{21}71$. Both proteins have two transmembrane domains (TMD) and adopt an N-in, C-in topology. The topology of $S^{21}68$ is dynamic because TMD1 is a signal-anchor-release (SAR) domain which, while initially integrated into the cytoplasmic membrane, is eventually released into the periplasm. TMD1 is dispensable because the truncated protein, $S^{21}68_{\Delta TMD1}$, retains the holin function. Adding two positive charges to N-terminus of $S^{21}68$ by an *irs* tag (RYIRS) prevents the release of TMD1. The irs$S^{21}68$ protein not only has lost its holin function, but is a potent antiholin and blocks the function of $S^{21}68$.

In this dissertation, the structure of $S^{21}68$ was suggested by incorporating electron-microscopy, biochemical, and computational approaches. The results suggest that $S^{21}68$ forms a symmetric heptamer, with the hydrophilic side of TMD2 lining the

channel of ~ 15 Å in diameter. This model also identifies two interacting surfaces, A and B, of TMD2.

A model for the pinhole formation pathway was generated from analyzing phenotypes of an extensive collection of *S*^{21} mutants. In this model, the individually folded and inserted S^{21} molecules first form the inactive dimer, with the membrane-inserted TMD1 inhibiting the lethal function of TMD2 both inter- and intra-molecularly. A second inactive dimer may form, with one TMD1 released. When both TMD1s are released, the activated dimer is formed, with the homotypic interfaces A:A interaction of the TMD2s. However, this interaction might not be stable, which will shift to heterotypic A:B interactions, allowing TMD2 to oligomerize. Finally, the pinhole forms, possibly driven by the hydration of lumenal hydrophilic residues.

In addition, the localization of pinholes was visualized by fusing the green fluorescent protein (GFP) to the C-terminus of pinholins. The results showed that pinholins form numerous small aggregates, designated as rafts, spread all over the cell body. The antiholin irsS^{21}68 not only inhibits the triggering of S^{21}68ΦGFP, but inhibits the rafts formation as well.

DEDICATION

This dissertation is dedicated to my dearest parents. I couldn't have done it without all your love and support.

ACKNOWLEDGEMENTS

I deeply appreciate my PI, Dr. Ry Young, for giving me the opportunity to study in his lab, and for his guidance on my research. The round-table meeting, the SWIM (Student Weekly Individual Meeting), and the random brainstorming with Ry was fun and very helpful. I would like to thank my committee members Dr. Mary Bryk, Dr. Andreas Holzenburg, and Dr. Pingwei Li, for their advice and support. I would also like to thank Dr. Karen Fleming for her contribution on the molecular modeling of the $S^{21}68$ pinhole structure. Special thanks goes to Ms. Daisy Wilbert for her clerical assistance and ability to solve every problem.

I would like to thank all the past and present members of the Young lab. Many thanks go to Dr. Douglas Struck for his insightful ideas and advice, and great help and support on my writing skills. I would like to thank Dr. Christos Savva for his contribution on the EM analysis of $S^{21}68$. I would also like to thank Dr. Taehyun Park, for building a great foundation on this project, and training me with a lot of experimental techniques. Many thanks goes to Anh, Brenley, Yi, Carrie, Rebecca, Joel, Liz, Jason, Thammajun, Jill, Gabby, Catrina, Samir, Kenneth, and Vlad for being my friends and giving me lots of advice, encouragement and support. The Young lab members create such a friendly, family-like environment in the lab, which I will miss a lot.

I can never appreciate my family enough, especially my mom, dad, and my grandparents. Thanks for the love, hope, patience and prayers. I would never have gone this far without all your unconditional support.

TABLE OF CONTENTS

CHAPTER Page

CHAPTER Page

CHAPTER Page

LIST OF FIGURES

FIGURE Page

FIGURE Page

LIST OF TABLES

CHAPTER I

INTRODUCTION

Discovery of bacteriophage (classification)

In 1896, on a French journal *Ann. De I' Inst. Pasteur*, E.H. Hankin, a British microbiologist working in India, published a paper called *'The bactericidal action of the waters of the Jamuna and Ganga rivers on Cholera microbes (translated title)'* (Hankin, 1896). In this paper, he showed that water from the Ganga River contained a heat-inactivatable filterable agent that killed cholera bacteria in less than 3 hours, but did not kill typhoid bacteria. This publication is believed to be the first report of the antibacterial agent which was later on named bacteriophage. A few years later, bacteriophages (phages) were discovered independently by the British pathologist Frederick Twort and the Canadian scientist Felix d'Herelle. In 1915, Twort observed 'glassy transformation (later known as lysis)' of *Staphylococcus* colonies by an unknown agent (Stent, 1963). One year later, d'Herelle then working on bacterial (*Shigella*) dysentery in Pasteur Institute in Paris observed small round, clear spots (later called 'plaques') in *Shigella* cultures from the fecal samples of sick soldiers grown on agar plates (Stent, 1963). He then used the term 'bacteriophage' from the Greek word *phagein* (to eat). He also introduced the therapeutic use of bacteriophage, which is still considered around the world as an important alternative to antibiotics as against infectious disease.

Since then, thousands of phages have been found in over 140 bacterial genera in

---

This dissertation follows the style of *Molecular Microbiology*.

archaea and eubacteria (Ackermann, 2006). New phages are still being discovered. Phages are classified by the International Committee on Taxonomy of Viruses (ICTV) according to their morphology and nucleic acid. As of 2000, ICTV recognizes one order (Caudovirales, tailed phages), 13 families, and 31 genera, containing more than 5136 phages examined by electron microscopy, which makes bacteriophage the largest viral group in nature (Ackermann, 2001, Ackermann, 2006).

Life cycle of bacteriophages

Like all other viruses, bacteriophages produce progeny intracellularly. Despite of the variety and detail, the general phage life cycle involves three steps: adsorption, infection and release (Abedon, 2006). Many phages like phage λ and T4 adsorb to bacteria through the binding of tail fibers with their specific receptors at the surface of bacteria, which include outer membrane proteins, lipopolysaccharides (LPS), teichoic acids, or even pili and flagella. The genetic components are then injected into bacterial cytoplasm. Infection can be divided into an eclipse period and a period of progeny production. The eclipse period is the interval after the phage adsorption and before the first phage production. It is either a short prevegetative, with the progeny production period immediately following, as in the phage lytic life cycle. Or it is greatly extended, as phage entering the lysogenic life cycle. In the lysogenic life cycle, phage DNA becomes a stable replicon, by integrating into the host genome, or by forming a stably replicating plasmid (Campbell, 1969). After entering into the lysogenic life cycle, phage genes are generally not expressed, except for the repressors which control the switch of

the lytic/lysogenic states. Phages which can only grow vegetatively (lytic life cycle) are termed 'virulent' or 'lytic' (Delbrück, 1942, Lwoff, 1953, Lederberg & Lederberg, 1953), like phage T4. In contrast, temperate phages, like λ, can either enter the lytic life cycle or follow a lysogenic life cycle. Bacteria lysogenized with phage DNA is hence called lysogen and the phage then is called prophage. The last step, release, can occur by various mechanisms, including lysis, extrusion, or budding (Abedon, 2006).

Strategies of releasing phage progenies from hosts

Except for the filamentous phages, almost all bacteriophages of Eubacteria release and disperse their progeny by lysing the host. Lysis of the bacteria cell can be accomplished in two ways: disruption of the cell envelope or interruption of cell wall synthesis during cell growth (Young & Wang, 2006). All double-stranded DNA (dsDNA) phages use the first strategy involving two proteins to attack each component of the envelope. The first step is a timed, lethal attack on the cytoplasmic membrane by the holin, a small membrane hole-forming protein. This activates the second step, which is degradation of the cell wall by the endolysin, a muralytic enzyme. Then, in Gram-negative bacteria, there is a third step in which the outer membrane is destroyed by another phage-encoded protein or protein complex called 'spanin'. This strategy is thus called the 'holin-endolysin-spanin' lysis system. In contrast, the latter strategy is used by the small lytic single-stranded DNA and single-stranded RNA phages, involving a single protein that blocks synthesis of intact murein. For example, the ssRNA phage Qβ encodes a protein called A_2 which inhibits MurA, the enzyme required for the first step

of cell wall synthesis (Bernhardt *et al.*, 2001b). Similarly, the E protein from the ssDNA phage ϕX174 inhibits MraY, which catalyzes a downstream step in the same pathway (Bernhardt *et al.*, 2000, Bernhardt *et al.*, 2001a). However, this Introduction will only focus on the three-step strategy used by all the dsDNA phages of Gram-negative hosts.

Holin-endolysin-spanin lysis system

Endolysins

At least four muralytic activities have been found in various phage endolysins: glycosidase and transglycosylase, which attack glycosidic bonds linking the *N*-acetylmuramic acid (MurNac) and *N*-acetylglucosamine (GlcNac) residues; amidase, which attacks the amide linkage between muramic acid and the first amino acid of the cross-linking oligopeptide; and endopeptidase, which attacks peptide bonds in that oligopeptide (Fig. 1.1) (Young, 1992).

Most known endolysins are cytoplasmic proteins, such as phage λ endolysin R and phage T4 endolysin E. λ R is a 17 kDa transglycosylase, while T4 E is a glycosidase, also known as true lysozyme. The difference between their enzymatic activities is irrelevant to the lysis event, since λ *R* defect can be complemented by T4 *e* (Young, 1992). However, neither of them can accomplish the lysis event alone, since they are trapped in the cytosol. Thus they both require another lysis protein, the holin, to make holes or lesions in the cytoplasmic membrane bilayer, in order for them to pass to the periplasm (Fig. 1.2A).

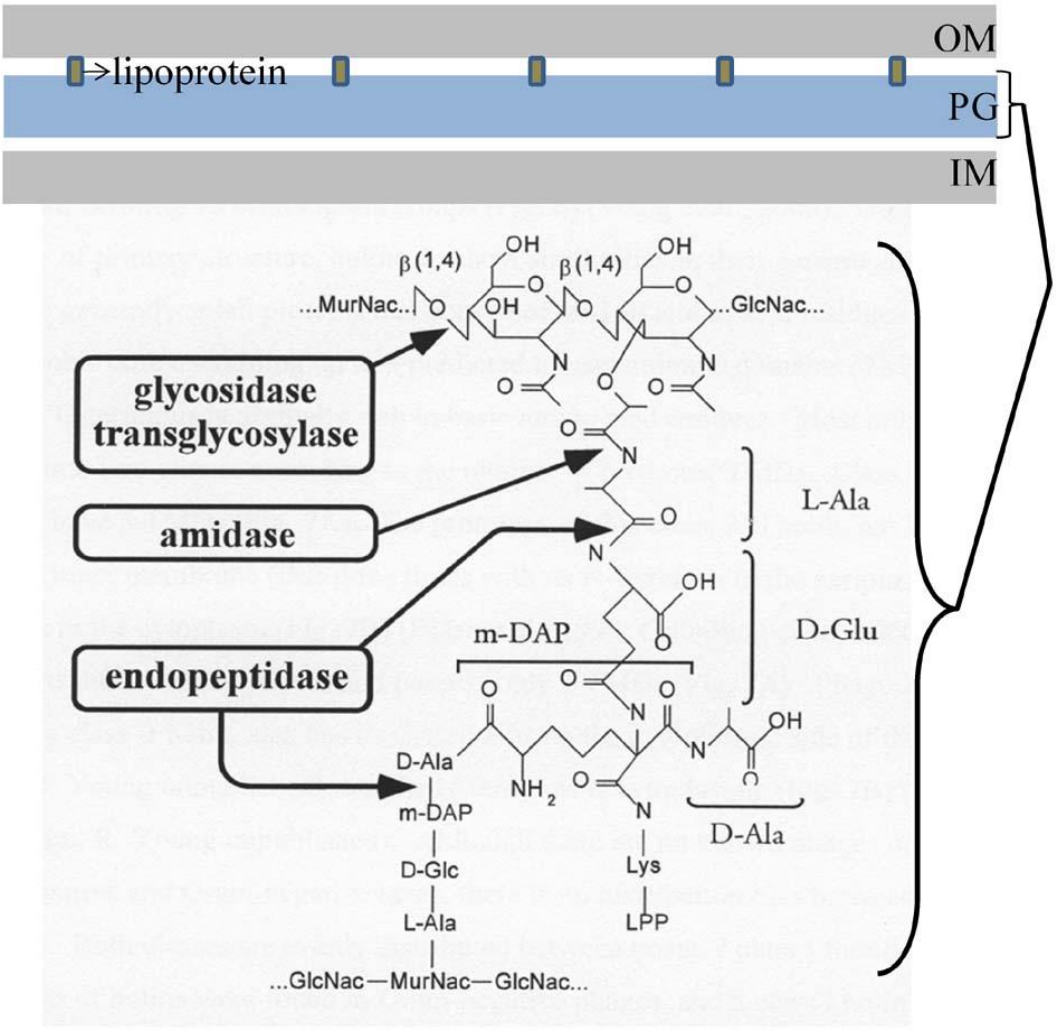

Fig. 1.1 The composition of Gram-negative bacteria peptidoglycan and the cleavage sites of endolysins. OM, outer membrane; PG, peptidoglycan; IM, inner membrane; GlcNac, N-acetylglucosamine; MurNac, N-acetylmuramic acid; m-DAP, meso-diaminopimelic acid; LPP, lipoprotein. Adopted from Ramanculov (2001) with permission.

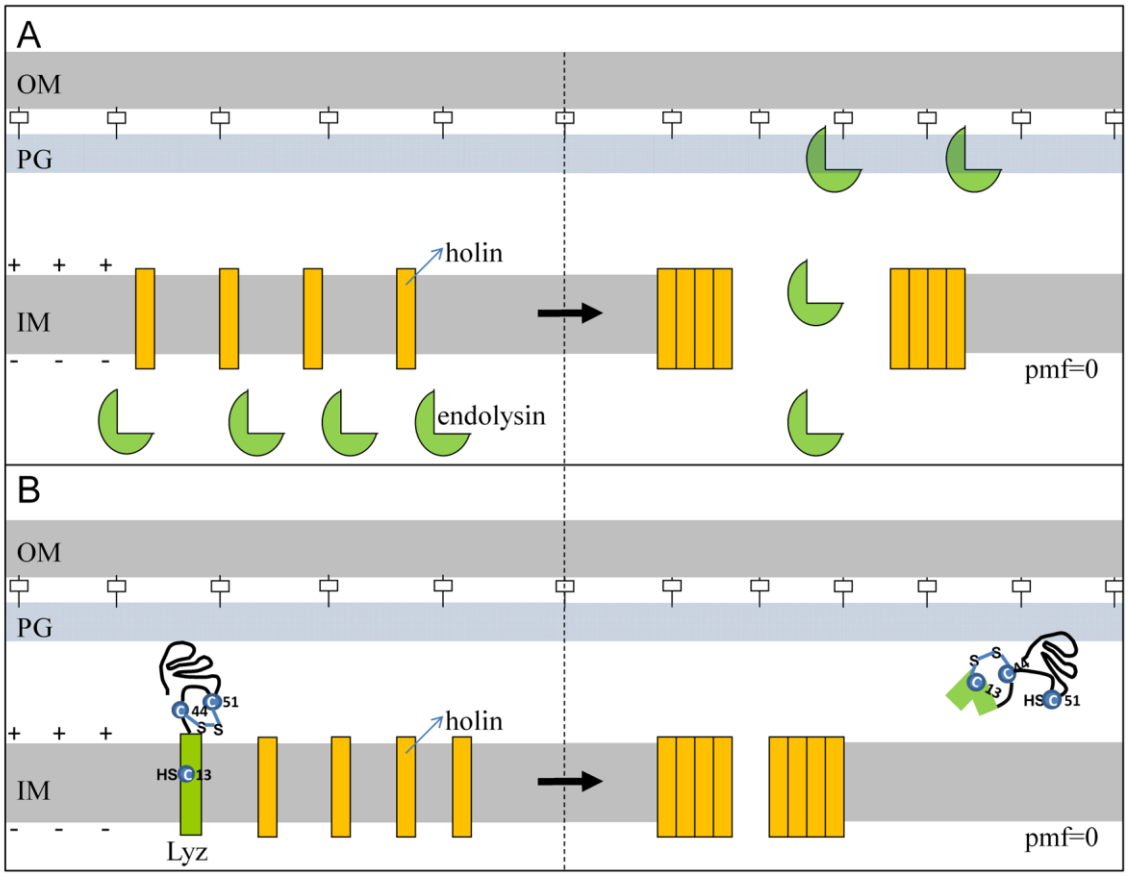

Fig. 1.2 The lysis strategies of the holin- cytoplasmic endolysin system (A) and the holin- SAR endolysin system (B). In both A and B, the localization of each protein before lysis is shown on the left; whereas the lysis mechanism is shown on the right. In A, holins (yellow rectangle) form large holes for the passage of cytoplasmic endolysins (green pie portion) to the periplasm to degrade cell wall. B represents the lysis strategy of phage P1. The endolysin Lyz has a SAR domain (green rectangle), containing a cysteine at position 13. In its periplasmic region, Cys44 and Cys51 form disulfide bond (blue lines). Disulfide isomerization occurs after the externalization of SAR domain, in which Cys13 forms disulfide bond with Cys44, leaving the catalytic Cys51 free. Thus lyz only becomes active after the release of SAR domain. Holins (orange rectangle) in this case control the lysis timing by forming holes to depolarize the membrane, which causes the immediate release of SAR-domains.

This 'large-hole forming holin with soluble endolysin' lysis system had long been viewed to be the sole paradigm of the dsDNA phage lysis system, until the discovery of a group of endolysins that could be secreted into the periplasm through their N-terminal signal sequence. A typical example is the endolysin Lys44 from *Oenococcus oeni* phage fOg44 (Sao-Jose *et al.*, 2000). It is transported to the periplasm by the *sec* translocon, and then the signal sequence is cleaved by the leader peptidase. Since these endolysins are exported directly, one might think that these endolysins would cause lysis of the host cell without the function of a holin. However, Nascimento *et al.* (2008) found out that expression of Lys44 alone did not produce the lysis of *L.lactis*, unless the lantibiotic nisin was also added. Nisin binds to the murein precursor lipid II and forms a 2.5nm cytoplasmic membrane pore. However, the adding of enduracidin, which binds to lipid II but does not form membrane pores, cannot trigger the lysis by Lys44. Thus it is likely that nisin mimics the holin in disruption of the cytoplasmic membrane electrical and chemical gradients and thus triggers the lysis event, presumably by causing activation of the Lys44 endolysin.

Among those endolysins which can be released into periplasm without the help from holin, a particularly interesting case is the endolysin Lyz from *E. coli* phage P1 (Fig. 1.2B). Lyz was the first identified SAR-endolysin, a class of enzyme which has now been found in many other phages (Xu *et al.*, 2004). 'SAR' stands for Signal-Anchor-Release. This group of endolysins has an N-terminal SAR domain, with a large C-terminal periplasmic domain. It is initially signal-anchored in the membrane in a *sec* dependent pathway, by its transmembrane domain (TMD), and then released into the

periplasm spontaneously without the cleavage of the signal sequence. The capacity of SAR domain to exit from membrane is dependent on a high content of small, weakly hydrophobic and polar residues Gly, Ala, Ser, and Thr, but the mechanism remains unclear. P1 Lyz has seven cysteines, six of which reside in the periplasmic domain, with one in the SAR domain. When SAR domain remains in the membrane, the first cysteine Cys13 is embedded in the bilayer in its sulfhydryl form, but all other six cysteines are in disulfides (Xu *et al.*, 2005). Among them, the third cysteine Cys51, which forms the catalytic triad together with Glu42 and Thr57 in the active enzyme, forms a disulfide-bond with the second cysteine Cys44 instead (Fig. 1.2B). Therefore the membrane-associated Lyz is inactive. The release of SAR from membrane activates Lyz through disulfide isomerization, which leaves the catalytic Cys51 free while Cys13 and Cys44 form disulfides. Meanwhile, the entire catalytic domain undergoes a conformational change, from three α-helices into three β-strands, and forms a catalytic cleft similar as the lysozymes (Fig. 1.3A). The externalized SAR domain still remains helical and not in contact with the body of the enzyme (Xu *et al.*, 2005).

Recently, bioinformatic surveys have shown that, at least among sequenced phage genomes, the P1 Lyz-like SAR- endolysins are not the prevalent class. Instead, a class represented by the phage 21 endolysin R^{21}, which does not have either a cysteine in the SAR domain or a catalytic cysteine (Sun *et al.*, 2009), predominates. Recently, the structure of R^{21} has been analyzed and a different regulatory mechanism has been proposed, in which the release of SAR domain from the membrane is still a critical step to activate the endolysin (Fig. 1.3B) (Sun *et al.*, 2009). In the active form of R^{21}, in

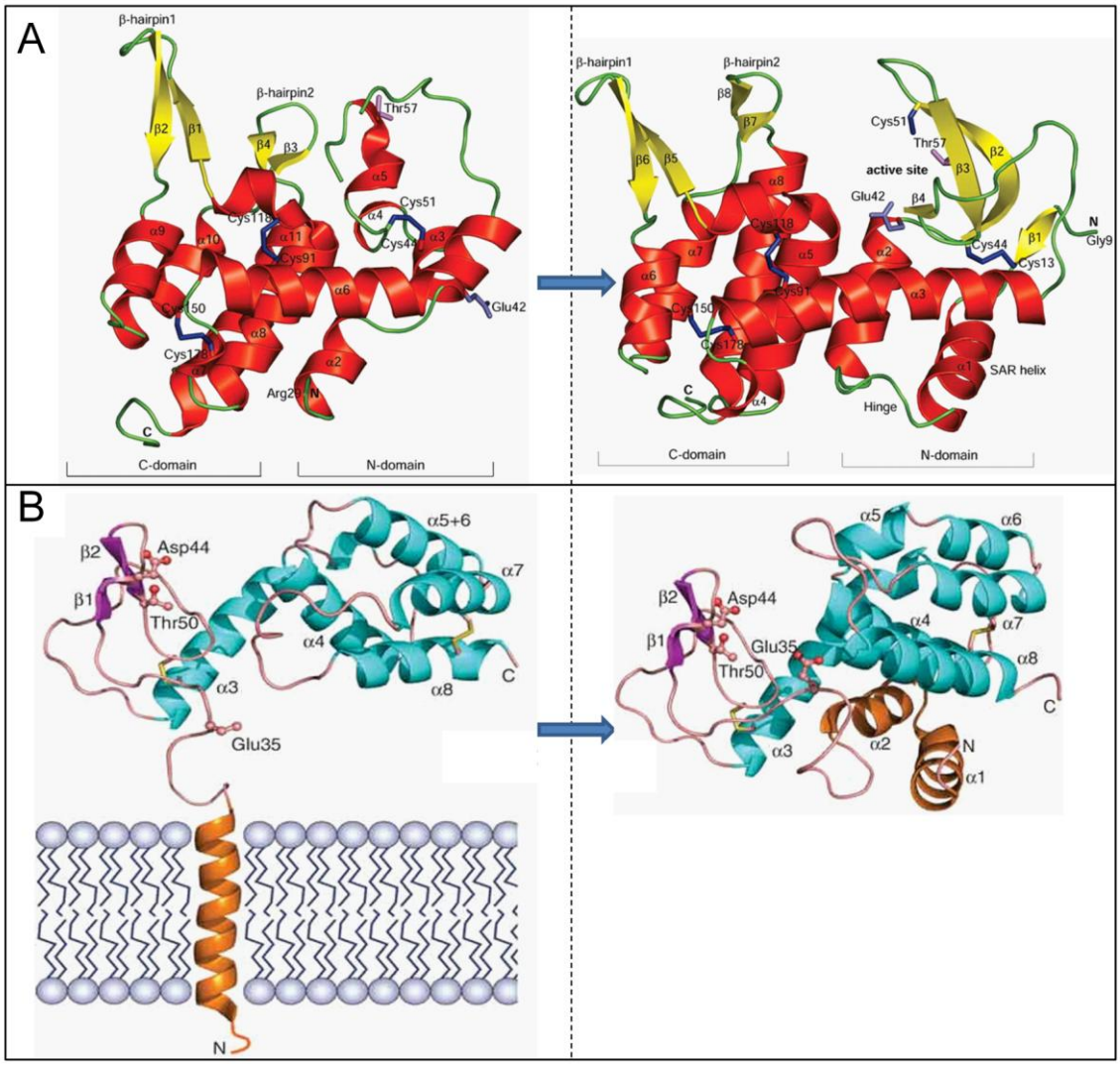

Fig. 1.3 Topological and conformational changes upon SAR-endolysin activation (A, P1 Lyz; B, R^{21}). In both A and B, the crystal structures of inactive SAR-endolysins (^{i}Lyz, $^{i}R^{21}$) are shown on the left, while the active ones (^{a}Lyz, $^{a}R^{21}$) are on the right. **A.** Colors: α helices, red; β strands, yellow; loops, green; disulfides, blue. The SAR-domain in ^{i}Lyz (residues 1 to 28) is truncated. ^{a}Lyz has additional strands β1 to β4, but lacks helices α3 to α5 of ^{i}Lyz. In addition, ^{a}Lyz has disulfide bond formed between Cys13 and Cys44, instead of Cys44 and Cys51 in ^{i}Lyz. Adopted from Xu *et al.* (2005) with permission. **B.** Colors: α helices, cyan; β strands, magenta; coils, salmon. The SAR domain is shown in orange and is depicted as a membrane-spanning helix in $^{i}R^{21}$. The catalytic triads (Glu35, Asp44, Thr50) are represented in stick-and-ball form. Disulfide linkages are represented in yellow stick. Adopted from Sun *et al.* (2009) with permission.

which the SAR domain is externalized into the periplasm, refolded into two antiparallel helices, and integrated into the main body of the enzyme, the geometry of the catalytic triad (E35, D44, and T50) is nearly identical to that in the T4 E family. However, in the inactive membrane-tethered form, the catalytic residue E35 is placed far away from the other two residues. Thus, the release of SAR domain causes its conformational change, which relocates the E35 closer to the other two catalytic residues and forms the active catalytic triad.

P1 Lyz and R^{21} are both able to lyse host cell without the presence of holin. However, lysis led by them alone is delayed and gradual (Xu *et al.*, 2004, Iida & Arber, 1977, Park *et al.*, 2007). Either the addition of a membrane energy poison, like the uncoupler dinitrophenol (DNP), or the lethal function of a holin immediately induces or dramatically accelerates lysis (Xu *et al.*, 2004, Park *et al.*, 2006). Therefore, it suggests that holin controls the lysis timing of SAR-endolysins by forming holes in the cytoplasmic membrane, which collapse the proton-motive-force (pmf) and triggers the immediate release and activation of SAR-endolysins (Fig. 1.2B). Unlike the hole formed by holins for the release of cytoplasmic endolysin, the hole formed by holins for SAR-endolysin is not required to be big enough for the passage of the endolysin. We will discuss the features of different holins associated with either cytoplasmic endolysin or SAR-endolysin in the next section.

Holins

Holins constitute a large functional group of small membrane proteins. They are

one of the most diverse functional families. More than 250 holin or putative holin genes have been found, according to a survey more than 5 years ago (Young & White, 2008). They can be grouped into 50 unrelated families using homology analysis. Although they are so diverse, most of the holins can be grouped into three topology classes (Fig. 1.4A).

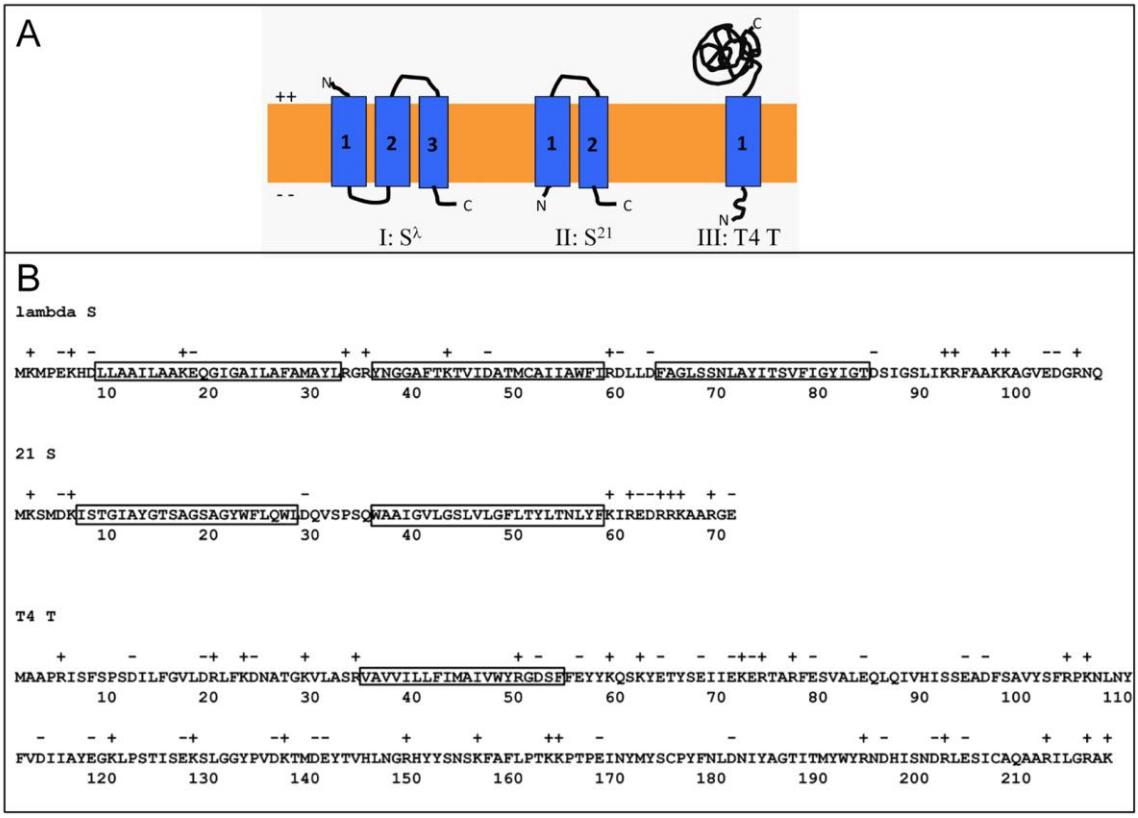

Fig. 1.4 The membrane topology (A) and the primary structure (B) of the prototype holins of each holin class. Class I, S$^{\lambda}$; class II, S^{21}; class III, T4 T. Each transmembrane domain is depicted by the blue box in A, or the clear box in B. Charge distribution is also shown on top of each residue in B.

Class I holins have three transmembrane domains, with the N-terminus out and C-terminus inside of cytoplasm; class II holins have two TMDs, with both termini inside; class III has only one TMD, with N-terminus in and C-terminus out. However, there might be more topology classes among this large and diverse group, since the membrane topology analysis is only based on primary structure, and in some cases, it is not obvious. The prototype class I, II and III holins are from bacteriophages lambda, 21 and T4, respectively (Fig. 1.4A, B). All three have been subjected to both genetic and biochemical studies.

Lambda holin S

In lambdoid phages, genes encoding the holin S, the endolysin R, and the spanin components Rz and Rz1 are clustered together in the "lysis cassette"(Young, 1992)(Fig. 1.5A). The lysis cassette is transcribed from a late gene promoter, designated $P_{R'}$ in λ. Transcription from $P_{R'}$ is constitutive, but in the absence of the anti-terminator Q, transcription is terminated at the two terminator sites ($t_{R'}$ and $t_{R'2}$) upstream of the lysis cassette, with an overall efficiency of 98%. Q-dependent transcription from $P_{R'}$ begins at around 8 minutes after infection or induction of the prophage, and continues until lysis.

Dual start motif: one gene, two proteins with opposing functions

The λ *S* gene has a 107 codon reading frame, starting with Met1-Lys2-Met3. Both the Met1 and Met3 codons are used for translational starts *in vivo*, generating two proteins, named S107 and S105 respectively, for their length in amino acid residues (Fig.

1.5A) (Bläsi *et al.*, 1990). Each of the translational starts has its own Shine-Dalgarno sequence. Although the two proteins differ only by two residues at the amino terminus, they have opposing functions. The S105 is the holin, while the longer product, S107 is not only defective in the lysis function, but also acts as an "antiholin" to inhibit the lysis function of S105. This phenomenon, that both holin and antiholin are encoded from one gene by a dual-start motif, is frequently observed in both class I and class II holin families (Wang *et al.*, 2000).

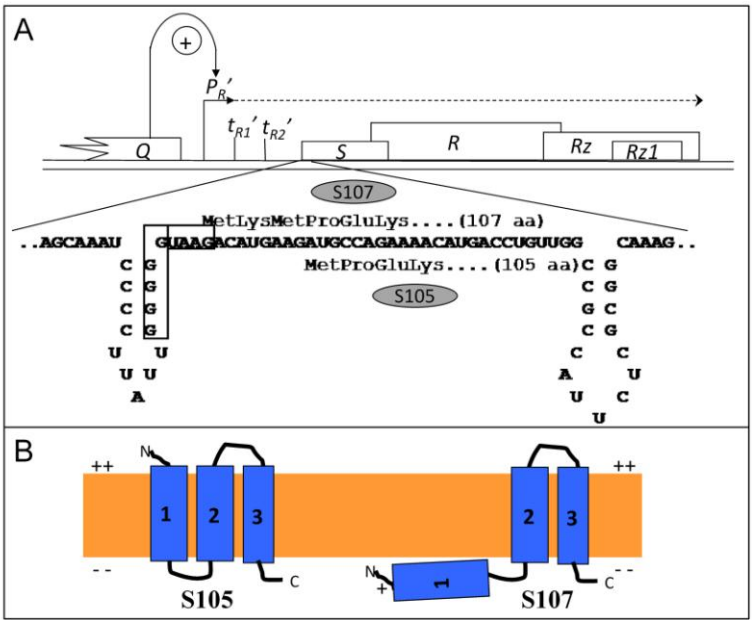

Fig. 1.5 Features of the phage lambda holin. A. The phage lambda lysis cassette. Lysis genes *S*, *R*, *Rz* and *Rz1* are transcribed from late promoter P_R', which is transactivated by the anti-terminator Q. t_R' and t_{R2}' are the terminator sites. The mRNA structure and corresponding amino acid at the beginning of *S* are shown in below. *S* has a dual-start motif, encoding the holin S105 and the antiholin S107. The Shine-Dalgarno sequences for each protein are boxed individually. Two stem-loops are formed in the mRNA structure. See text for detail. **B. The membrane topology of S105 and S107.** Colors are the same as in Fig. 1.4A.

Both *in vitro* and *in vivo* experiments revealed that the ratio of S105 molecules to S107 molecules expressed from the wildtype *λS* gene is around 2:1 (Chang *et al.*, 1995). This expression ratio is controlled by two mRNA stem-loops upstream and in the λ *S* gene (Fig. 1.5A) (Young, 1992). The upstream stem-loop is called the *sdi* (*s*tructure-*d*irected *i*nitiation) site and overlaps the Shine-Dalgarno sequence of Met1, but not of Met3. Weakening this stem-loop favors the expression of S107, decreases the ratio of S105:S107, and delays or inhibits lysis. Oppositely, weakening the second stem-loop favors the expression of S105, which increases the ratio of S105:S107 and accelerates lysis.

The only difference between S107 and S105 is the N-terminal dipeptide sequence Met1-Lys2. As a prototype of type I holins, S105 has three TMDs, with an N-out, C-in topology (Fig. 1.5B). However, the TMD1 of S107 is not inserted into the membrane until the proton- motive- force (pmf) is collapsed, probably because that the positive charge provided by Lys2 blocks the insertion of S107 TMD1 into the membrane. Presumably, this topological defect is the reason for its loss of holin function (Young & White, 2008). Indeed, either replacing Lys2 with a neutral or acidic residue, or adding an energy poison not only abolishes the antiholin function of S107, but also converts it into a holin (Bläsi *et al.*, 1989, Bläsi *et al.*, 1990, Graschopf & Bläsi, 1999, Young & White, 2008). Interestingly, an *S* allele missing the entire TMD1 acts as an antiholin, suggests that it is the absence of TMD1 from the membrane rather than its presence in the cytoplasm that blocks the holin function (White *et al.*, 2010).

Homodimers and heterodimers of S105 and S107 can be detected *in vivo* by

subjecting membranes containing S molecules to oxidative conditions (Gründling *et al.*, 2000c). This takes advantage of the presence of a unique Cys residue at position 51, in the middle of TMD2, leading to intermolecular disulfide bonds and covalent dimers that survive SDS-PAGE. Thus S107 inhibits lysis by binding to and titrating out the holin S105. Given that the ratio of S105 to S107 synthesis is ~2:1, this effectively reduces the number of S105:S105 homodimers by about 1/3 of what would be present in the absence of the antiholin. However, at the time of triggering, which is defined by the first hole formed by S105, the pmf collapses and allows the insertion of S107 TMD1, converting the heterodimers into functional holin dimers, which can be incorporated into the S holes. Thus the presence of the antiholin pool not only controls lysis timing, given that the lysis timing can be flexibly adjusted by changing the ratio of S105:S107, but also makes the lytic event a more "all or nothing" phenomenon.

Nevertheless, even in the absence of S107, the S105 holin can mediate sharply defined temporal control of lysis, indicating that the "clock" of lysis is a built-in feature of the S105 primary sequence.

Genetic and biochemical analysis of the lambda holin S105

S is a good candidate for genetic analysis for several reasons. First, it is small (107 codons). Second, its function does not appear to require other host or phage proteins, based on the observation that S holes can be formed in both *Saccharomyces cerevisiae* and mammalian cells (Garrett *et al.*, 1990, Agu *et al.*, 2007). A large collection of *S* mutant alleles was obtained by chemical-induced, and site-directed

mutagenesis methods (Raab *et al.*, 1986, White *et al.*, 2010, Zheng *et al.*, 2008). Analysis of these mutants suggested that:

1). The lysis clock is built into the primary structure of S105. Missense mutations that alter the triggering time significantly are found in all three TMDs (Raab *et al.*, 1986, White, 2008). Moreover, substituting a single amino acid (C51 and A52) with the other 19 amino acids was found to generate a wide range of timing phenotypes differences (White, 2008). The extreme cases are the two substitutions A52L and A52I, which, despite the very small differences in the substituted side chain, generate extremely early-triggering and completely non-functional holins, respectively. This suggests that the precise timing of holin function is extremely sensitive to protein-protein interactions between the alpha-helical TMDs in the bilayer.

2). The S105 hole formation is an "all or nothing" event. White (2008) fused GFP to the C-terminus of S105 and its mutants, and using real-time confocal fluorescence microscopy, observed that S105 was evenly distributed in the inner membrane until very close to its triggering time, when it forms large aggregates, at about 3 per cell. In contrast, these large aggregates, or "rafts", were not present in cells expressing the isogenic, non-functional A52V mutant.

3). The hole formation process is composed of multiple steps. S105 was shown to form DSP (Dithiobis[succinimidyl propionate])- crosslinked oligomers in the inner membrane, independent of the disulfide-bond formation of Cys51 (Johnson-Boaz *et al.*, 1994, Gründling *et al.*, 2000b). The same crosslinking experiment performed on the lysis-defective mutants revealed that, while some mutants formed oligomers

indistinguishable from the wild-type, some only formed dimers or monomers, such as A52V and A48V, respectively, although the monomer form was unstable. Taking the DSP crosslinking and S-GFP localization data together, a S105 hole formation model was proposed. Initially, S105 dimerizes in the inner membrane. At a time defined by the primary structure, the dimers form large rafts, and spontaneous channel forms due to nucleation in the middle of rafts, then suddenly large holes are formed (Fig. 1.6) (White, 2008).

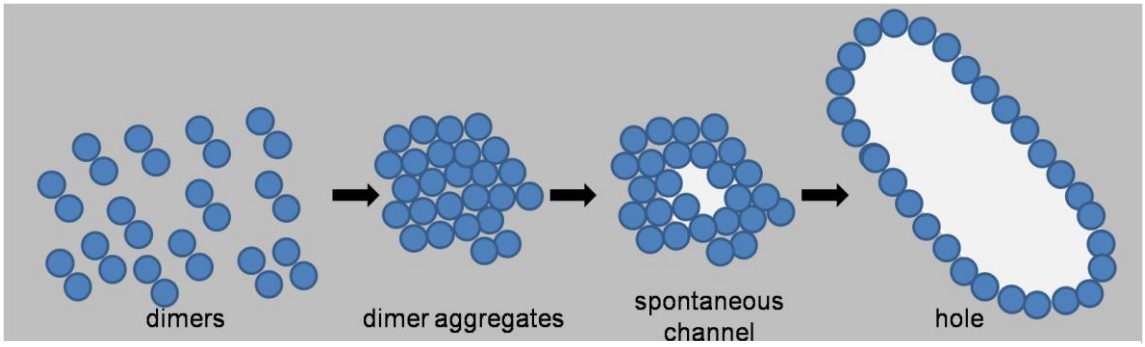

Fig. 1.6 Model for lambda S hole formation (top-down view from periplasm). Initially, S105 appears as dimers in the membrane. At a genetically defined time, the dimers form large aggregates. Spontaneous channel forms due to nucleation in the aggregates, which suddenly triggers the formation of big holes. Grey, lipid of the inner membrane; blue circle, a single S105 molecule.

4). Since mutations in all three TMDs are found to affect lysis timing, it suggests that helical packing of TMDs might be involved in the hole formation process. In support of this idea, A52L and A52I, although differed only subtly in the side chain, had dramatically opposite impact on the lysis timing, as stated above. It probably is the

change of the amino acid shape that destabilize or stabilize the helical packing, which in turn affects the hole formation.

Biochemical studies have also been conducted with S105. Purified S105 was shown to be able to permeabilize calcein-loaded liposomes (Deaton *et al.*, 2004) and form rings with large diameters (8.5 nm inner and 23 nm outer diameters) in the non-ionic detergent dodecyl maltoside (DDM) (Savva *et al.*, 2008). The height (4 nm) of the S105 ring closely matches the thickness of the lipid bilayer. As a control, the lysis-defective mutant A52V fails to form these rings. These data indicate that S105 is able to form holes *in vitro* solely by itself.

Recently, Dewey and Savva *et al.* (2010) visualized the S105 holes *in vivo* by cryo-electron microscopy and tomography. The holes formed by S105 *in vivo* were extremely large and irregular with an average diameter of around 340 nm, which is currently the largest hole known in bacteria. The unprecedented size of these holes, nearly 10-fold larger than any other protein-dependent channel structure, certainly explains how fully folded endolysin can escape after holin triggering. In fact, diameters of this size would pose no restraint even on the ~0.5 mega-Dalton R-β-galactosidase hybrids that have also been shown to function with the λ holin (Wang *et al.*, 2003).

T4 T, a large-hole holin with a single TMD

The holin T of T4 represents the type III holin family. T has no sequence similarity to the lambda holin S105, and contains only a single TMD with a large C-terminal periplasmic domain of 163 residues (Fig. 1.4B). Replacing *S* with *t* in the λ

lysis cassette results in normal, sharply-defined lysis, except that the lysis time is much earlier (at about 20 minutes, compared with 50 minutes of λ *S*). This indicates that T also forms large holes in the membrane, capable of allowing the passage of either λ R or E, the cytoplasmic T4 endolysin (Ramanculov & Young, 2001b).

t has also been subjected to genetic studies. Using a selection for retarded lysis triggering, Ramanculov and co-workers (2001c) obtained 47 single mutations scattered throughout the *t* gene. Similar to *S*, *t* has significant flexibility in terms of altering the lysis timing, even with only a single amino acid change. This suggests that the malleability of the lysis clock built into the holin genes enables phages to adapt quickly to the change of environment.

The mechanism of the lysis inhibition (LIN)

A normal T4 infection cycle, from the adsorption to lysis, lasts around 25 to 30 minutes. However, host lysis can enter into a state called Lysis Inhibition (LIN), if a secondary infection (superinfection) by a T-even phage occurs after ~3 minutes post the primary infection (Hershey, 1946a, Hershey, 1946b, Young & Wang, 2006). It is thought that this indicates that the local environment is depleted of host cells. In such a condition, it would make sense for the infection cycle to be extended, allowing continued accumulation of virions intracellularly, rather than release even more phage particles to the environment. The LIN signal is unstable; superinfections must re-occur at least every ~10 minutes. Recently, a molecular mechanism for this phenomenon has been established.

The T4 *rI* gene, encoding a *t*-specific antiholin, was found to be required for the LIN phenotype, since it inhibits T-mediated lysis in the absence of other T4 genes and even without the superinfection of T4 phages (Ramanculov & Young, 2001a). The holin T can be cross-linked into oligomers; while T and RI co-expressed in the cell can only be cross-linked into heterodimers. This suggests that RI inhibits T function by binding to it and blocking its oligomerization. RI has an N-terminal SAR domain, which serves as a secretion signal for its release from membrane into the periplasm, without proteolytic processing (Tran *et al.*, 2007) (Fig. 1.7A). The periplasmic domain of RI alone was capable of imposing LIN by binding to the periplasmic domain of T (Tran *et al.*, 2005); while the presence of SAR domain targets RI for degradation by the periplasmic protease DegP, with a half-life of ~2 minutes (Tran *et al.*, 2007). However, LIN was not significantly enhanced in a *degP*$^{-}$ host, suggesting that the periplasmic RI is functionally inactivated even when its degradation is inhibited. A model has been suggested for LIN, in which two forms of RI are involved (Tran *et al.*, 2007) (Fig. 1.7B). Without superinfection, RI is secreted to the periplasm in its active form, but is then released from the membrane and rapidly converted into an inactive form, with subsequent degradation by DegP. However, in superinfection, the DNA and likely internal proteins of the superinfected phage are diverted to the periplasm, probably serving as the LIN signal. In this case, the active form of RI might be stabilized by these signal(s), and conduct LIN.

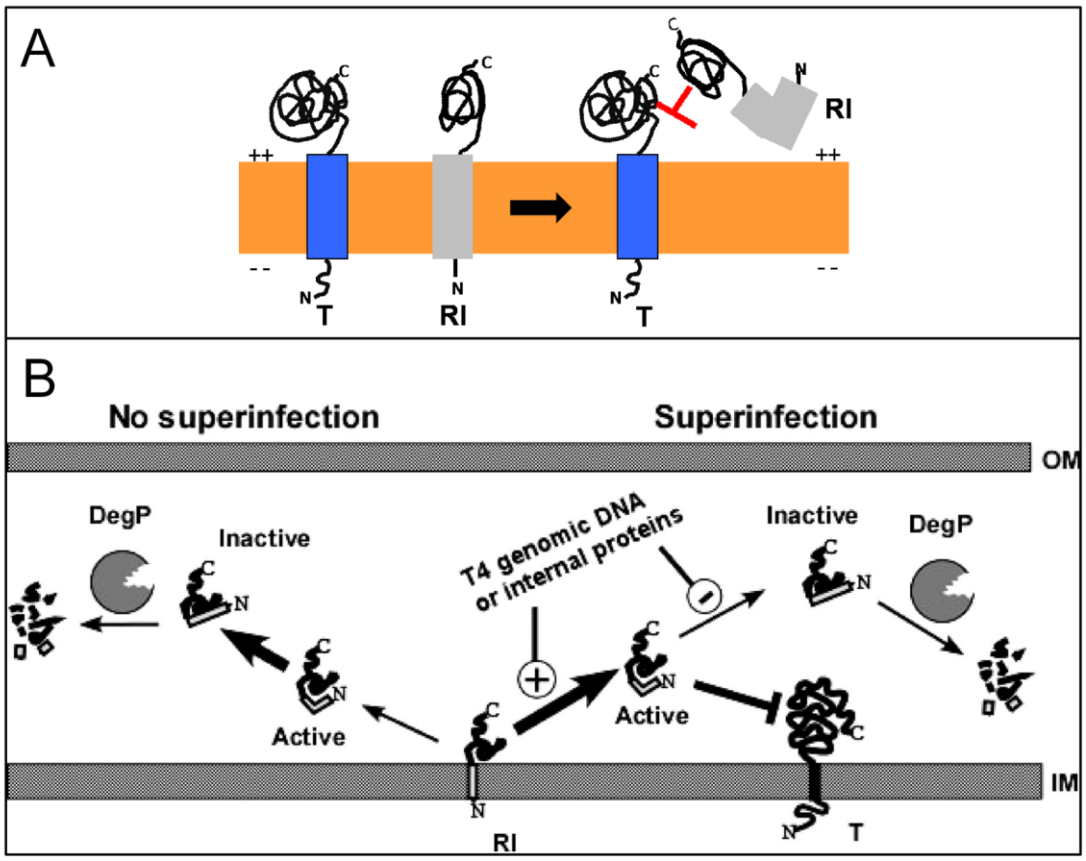

Fig. 1.7 The mechanism of LIN. A. Model for RI inhibition of T. T has a single transmembrane domain (blue box), while RI has an N-terminal SAR-domain (grey box). The externalization of RI from membrane is required for the inhibition of T-mediated lysis. The periplasmic domain of RI alone is able to inhibit T. **B. Model for LIN.** Left, without superinfection, RI is released to the periplasm and forms the active form, but is inactivated in a short period of time, and then degraded by the periplasmic protease DegP. Right, with superinfection, the active form of RI is stabilized by either the DNA or the protein injected from the superinfecting T-even phage. The active RI is able to interact with T and inhibit lysis. Adopted from Tran *et al*. (2007) with permission.

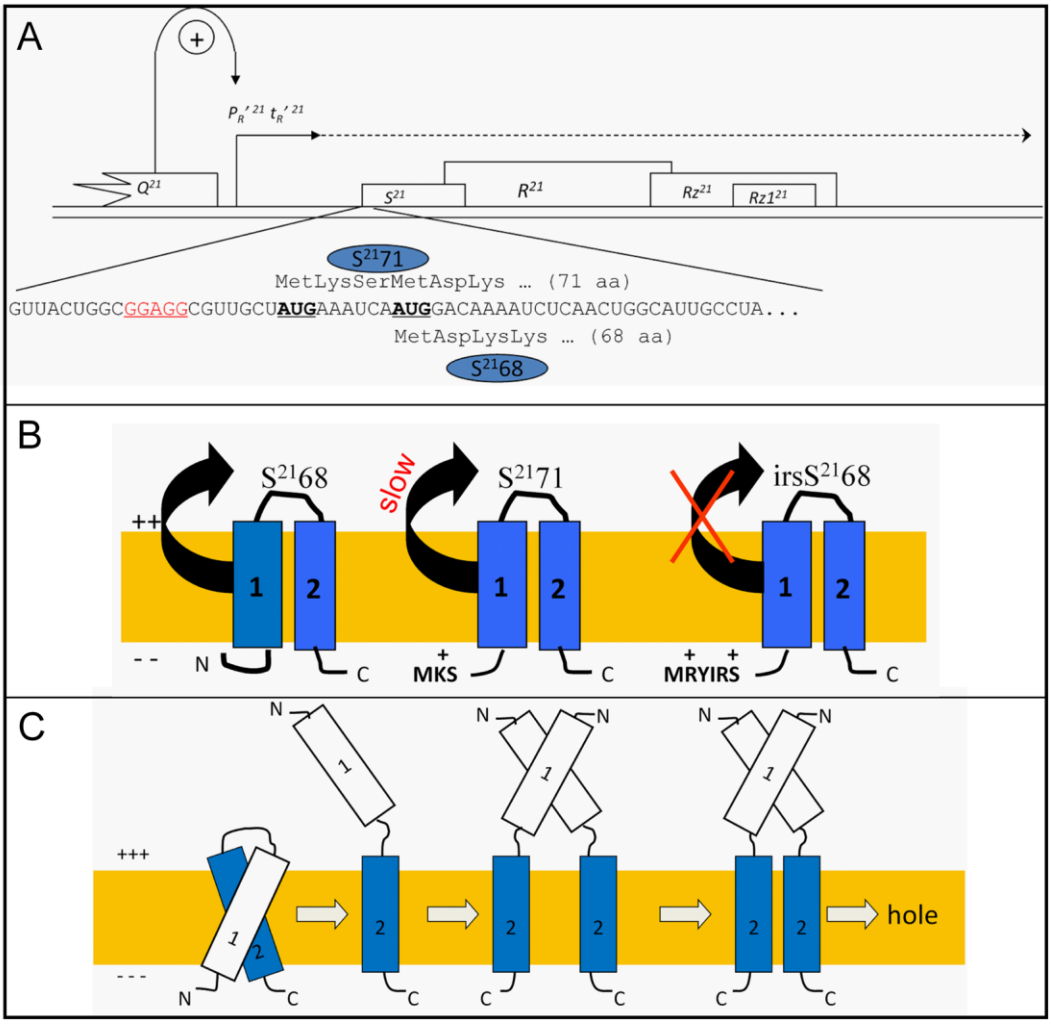

Fig. 1.8. Features of the phage 21 lysis system. A. phage 21 lysis cassette. Similar to the lysis cassette of λ, the lysis genes S^{21}, R^{21}, Rz^{21} and $Rz1^{21}$ are transcribed from late promoter $P_R'^{21}$, which is transactivated by Q^{21}. The mRNA structure and corresponding amino acid at the beginning of S^{21} are shown in below. S^{21} also has a dual-start motif, encoding both a holin, $S^{21}68$, and an antiholin, $S^{21}71$. The Shine-Dalgarno sequence for both $S^{21}68$ and $S^{21}71$ is underlined and colored in red. **B. The membrane topology of holin $S^{21}68$, the weak antiholin $S^{21}71$, and the strong antiholin $irsS^{21}68$**. Differences at the N-terminus are shown. $S^{21}71$ has one additional positive charge while $irsS^{21}68$ has two. The TMD1 is a SAR-domain. The release of TMD1 is delayed in the context of $S^{21}71$, and completely blocked in $irsS^{21}68$. It is likely that the positive charge at N-terminus blocks its release. **C. The model of hole formation by $S^{21}68$.** Initially, the two TMDs are inserted in the membrane, with TMD1 binding to TMD2. When TMD1 is released in the periplasm, periplasmic TMD1-TMD1 interactions occur. TMD2s are then free to oligomerize and form holes.

The pinholin S^{21}

In contrast to the large hole formers S105 and T, the holin S^{21} from phage 21 represents another large group of holins, the pinholin. Instead of making big holes, holes formed by phage 21 holin are not large enough to allow the passage of either the cytoplasmic λ R or T4 E or the periplasmic located marker-tagged GFP protein (Park *et al.*, 2007). Thus these holes are named 'pinholes' and the phage 21 holin is called pinholin.

Like λ *S*, *S^{21}* also has a dual-start motif, encoding both a holin $S^{21}68$ (68 amino acids), and an antiholin $S^{21}71$ (71 amino acids), with a ratio of 2:1 (Barenboim *et al.*, 1999) (Fig. 1.8A). The two products are different only by the tripeptide Met1-Lys2-Ser3 at the N-terminus of $S^{21}71$. Both $S^{21}68$ and $S^{21}71$ have two TMDs; hence S^{21} is a type II holin (Young, 2002) (Fig. 1.8B).

The topology of $S^{21}68$ is dynamic. Its TMD1 is a SAR domain, which is capable of spontaneously exiting the membrane into the periplasm (Park *et al.*, 2006). However, it is the removal of TMD1 from the membrane rather than the TMD1 itself that is required for lethal holin function (Park *et al.*, 2006). *$S^{21}68_{\Delta TMD1}$*, an *$S^{21}68$* allele lacking the TMD1, still retains its holin function. In contrast, appending the *irs* epitope (Arg-Tyr-Ile-Arg-Ser), with two positive charges, at the N-terminus of $S^{21}68$ completely abolishes the holin function (Fig. 1.8A, B). In addition, the new allele *irs$S^{21}68$*, exhibits a dominant-negative phenotype when co-expressed with *$S^{21}68$*, thus behaving as a strong antiholin. The natural antiholin $S^{21}71$, because its TMD1 is able to be released from the membrane at a delayed time, delays but does not completely block the triggering of

$S^{21}68$. Thus $S^{21}71$ is called a weak antiholin (Park *et al.*, 2006). Since irs$S^{21}68$ has two additional positive charges at its N-terminus compared to only one of $S^{21}71$, it is believed that the positive charges prevent the TMD1 from exiting the membrane and thus are responsible for the antiholin function. Moreover, Park *et al.* followed the change in the dimer/monomer ratio of $S^{21}68_{S16C}$, which forms disulfide-bond linked dimer only when the TMD1 is in the periplasm, as a function of time. It showed that the release of TMD1 from the membrane coincides with the triggering time of $S^{21}68$, which suggests that the release of TMD1 is the rate-limiting step of the $S^{21}68$ pinhole formation. Therefore, the regulation of lysis triggering time is not only dependent on the presence of $S^{21}71$, but also resides in $S^{21}68$, in which the membrane-embedded TMD1 serves as an intrinsic inhibitor domain blocking the function of TMD2 before the time of triggering.

Park *et al.* proposed a hole formation model for $S^{21}68$ (Fig. 1.8C). Initially, two TMDs of $S^{21}68$ are inserted in the membrane. Then TMD1s are gradually released into the periplasm, which leaves TMD2s free to oligomerize and form pinholes. However, in spite of the significant and interesting features of S^{21} that had been discovered, as a new class of holin, and a new lysis paradigm with the SAR- endolysin R^{21}, the details of this pinhole formation pathway were unknown.

Rz/Rz1 (spanin): the last step of lysis

The λ *Rz* gene was first identified as a site for Tn*903* insertions which caused lysis defects in the presence of millimolar concentrations of Mg^{2+} (Young *et al.*, 1979).

Later, Casjens *et al.* (1989) showed that other divalent cations also cause this phenotype. A few years later, the *Rz1* gene was discovered to be located in the +1 register within *Rz* (Hanych *et al.*, 1993) (Fig. 1.9A). Zhang *et al.* (1999) further characterized these two genes by introducing amber nonsense mutations into each gene without affecting the amino acid of the other. In the presence of 10 mM Mg^{2+}, induced lambda lysogens carrying either isogenic Rz_{am} or $Rz1_{am}$ prophages could not complete lysis; instead, they formed spherical cells, which were fragile and gradually lost refractility. This made *Rz* and *Rz1* genes unique as they share the same DNA in different reading frames and are associated with the same phenotype. However, the fact that λ lysogens are able to complete lysis without *Rz* or *Rz1* under standard laboratory condition (i.e. without high concentration of divalent cations) made these nested genes less attractive for intensive study.

Nevertheless, recently, from a comprehensive genomic search, 120 of the 137 sequenced phages of Gram-negative hosts were found to possess the *Rz/Rz1* equivalent genes (Summer *et al.*, 2007). This widespread presence in phage genomes suggested that the function of these last genes in the typical lysis cassette was significant. A year later, Berry *et al.* (2008) performed biochemical analysis on Rz and Rz1 and suggested a model for their function. Rz was identified to be an inner membrane protein having an N-terminal TMD. Rz1 is an outer membrane lipoprotein, which undergoes N- terminal signal sequence cleavage and lipid modification at Cys20 (Berry *et al.*, 2008, Kedzierska *et al.*, 1996) (Fig. 1.9B). Co-expressed Rz and Rz1 co-fractionated on isopycnic sucrose gradients, and formed a complex which could be isolated *in vitro*. Moreover, genetic

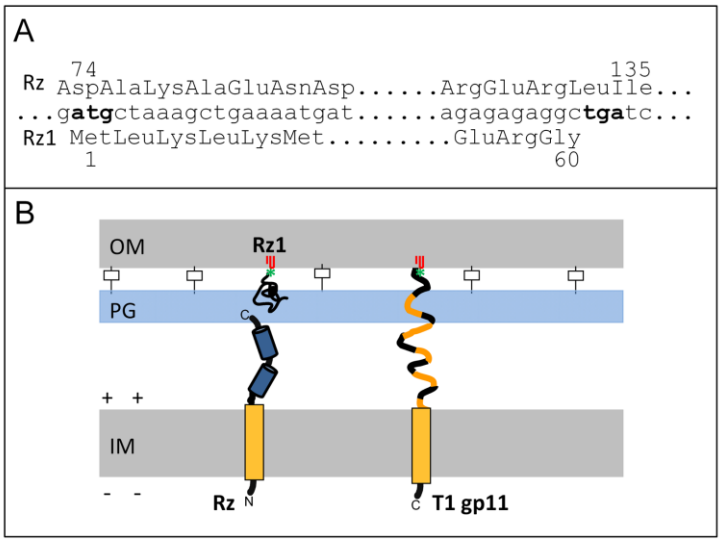

Fig. 1.9 Features of the spanin complex. A. The *Rz1* gene is encoded in the +1 reading frame within *Rz*. Part of the Rz and Rz1 reading frames are shown above and below the mRNA sequence. The start codon and stop codon of *Rz1* are shown in bold. **B. The membrane topology of Rz and Rz1, and of the spanin gp11 from phage T1.** Rz has an N-terminal TM domain (yellow rectangle) and a coiled-coil region (blue cylinder) in the periplasmic domain. Rz1 is an outer membrane lipoprotein, which has a predicted signal peptidase II cleavage site at Cys20 (Berry *et al.*, 2008). The mature Rz1 is attached to the inner leaflet of the outer membrane by the lipid decoration at Cys20. Rz and Rz1 interact with each other through their C-terminus. The T1 gp11 spanin has an N-terminal lipoprotein signal peptide as well as a C-terminal TMD, which spans the entire periplasm.

evidence also suggested that these two proteins interact. First, the phage P2 genes *lysB* and *lysC* complemented the *Rz*$^{-}$*/Rz1*$^{-}$ lysis defect only as a cognate pair, but not individually (Markov *et al.*, 2004). Secondly, yeast two-hybrid analysis indicated that gene products of the *Rz/Rz1* gene equivalent of phage T7, the *18.7* and *18.5*, interacted with each other by their C-terminal contacts (Bartel *et al.*, 1996). Finally, the discovery of the spanin gene, a single gene equivalent of *Rz*/*Rz1*, brought more emphasis to the role of Rz/Rz1 (Summer *et al.*, 2007). Spanins have an N-terminal lipoprotein signal

peptide as well as a C-terminal TMD; thus, the spanin protein must span the entire periplasm and link the inner and outer bacterial membranes (Fig. 1.9B). The fact that T1 spanin gene is able to complement the *Rz*$^{-}$*/Rz1*$^{-}$ lysis defect suggested further that Rz and Rz1 interact and link the IM and OM as a complex. Furthermore, Berry *et al.* (2008) reported that in the presence of 10 mM Mg^{2+}, cells expressing the SAR-endolysin P1 *lyz* exhibited the same lysis defect as the λ *Rz*$^{-}$ or *Rz1*$^{-}$ phenotype. This lysis defect can be eliminated by providing the *Rz/Rz1* gene pair. This result demonstrated that the Rz/Rz1 function is independent of holin function.

Berry *et al.* (2008) also suggested a three-step lysis model for dsDNA phages. Holins form holes in the inner membrane, which control the externalization of endolysins into the periplasm. After the degradation of peptidoglycan by endolysins, Rz/Rz1 or spanins facilitate the disruption of outer membranes, possibly due to the fusion of the inner and outer membranes.

α-helical membrane protein folding and stability

Membrane proteins can be divided into two general groups, the α-helices and the β-barrels. Single or multiple α-helices were found in proteins residing in cytoplasmic membrane, golgi and endoplasmic reticulum (ER), whereas β-barrels were found in bacterial, mitochondrial and chloroplast outer membranes (Meng *et al.*, 2009, Tamm *et al.*, 2004). Statistical analyses based on the hydrophobicity of proteins from genome-wide sequence data of eubacteria, archaea, and eukaryotes suggest that α-helix bundles represent about 20-30% of ORFs (Wallin & von Heijne, 1998). However, the β-barrels

are much less abundant (Bigelow *et al.*, 2004), and their folding mechanism is much different from that of α-helices. Therefore, only the folding of α-helical membrane proteins will be reviewed here.

The three-stage folding model

The α-helix membrane protein folding was previously considered as a two-stage model, in which each individual α-helix is folded and inserted into the membrane independently, followed by the interactions between helices to allow higher order folding (Popot & Engelman, 1990) (Fig. 1.10A). Biochemical analysis of bacteriorhodopsin (BR) provided solid evidence for this model. BR is a light-driven proton pump found in halobacteria. It forms a membrane protein complex composed of three identical protein chains, each rotated 120° relative to others. Each protein chain has seven transmembrane helices connected by extramembranous loops and a retinal molecule embedded deep inside (Fig. 1.10B) (Haupts *et al.*, 1999). Kahn *et al.* (1992) and Marti (1998) were able to regenerate the native structure and function of BR from a combination of polypeptides corresponding to portions of its seven TMDs. Thus, each α-helical TMD is folded and inserted into the lipid bilayer individually, and assembled together afterwards. Loops present between helices only help to stabilize the final structure (Marti, 1998).

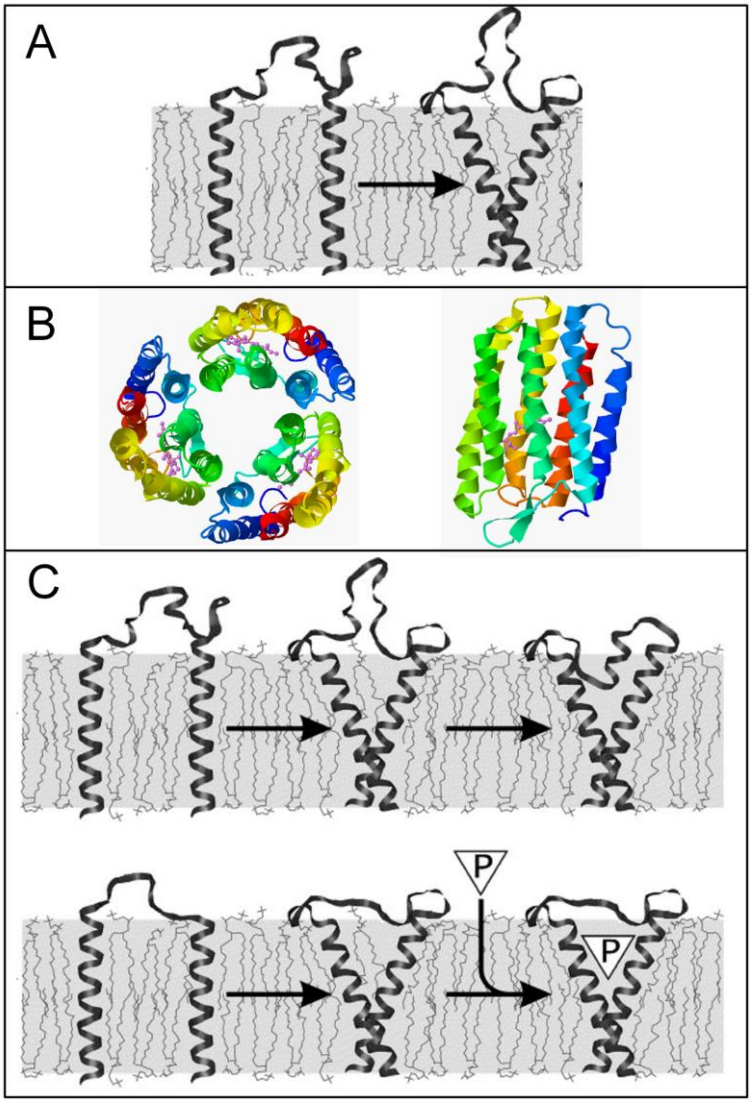

Fig. 1.10 The membrane protein folding model. A. The old two-stage α-helical membrane protein folding model. In this model, each α-helix is folded and inserted into the inner membrane independently. Then higher order folding occurs by helical-helical interactions. **B. The structure of the bacteriorhodopsin (Protein Data Base ID, 1FBB).** Left, the top-down view. BR is a trimer of seven TM helices. Each helix is colored differently. Same TM helices in each monomer are colored same. Each monomer has a retinal molecule (pink) embedded deep inside. Right, the side view of a single monomer from B. The figure is generated by Jmol (http://www.jmol.org/). **C. The three-stage folding model.** Besides the two stages in A, a third folding stage was added, such as the folding of loops between TMDs, and/or its entry into the membrane (top), and/or the binding of prosthetic groups (bottom). P, prosthetic group. Both A and C are adopted and modified from Engelman *et al*. (2003) with permission.

However, the two-stage model does not specify the state when the loops between each α-helix are folded, or when the prosthetic groups bind to the protein. Therefore about a decade later, the same group amended the model by adding a third step, which included steps such as the folding of loops between TMDs, the entry of other regions into the membrane, the binding of prosthetic groups, and the oligomerization of separate polypeptide chains (Engelman *et al.*, 2003) (Fig. 1.10C).

Because the protein backbone and polar side chain groups are hydrophilic, in order to form stable α-helices in the lipid bilayer, this hydrophilicity has to be overcome. There are several ways to accomplish this, such as to have further helical interactions and oligomerizations or insertion of additional polypeptides into the bilayer so as to provide carbonyl hydrogen bond acceptors. One example is the *E. coli* glycerol facilitator (GlpF). GlpF is a transmembrane channel that conducts glycerol, water and small uncharged organic molecules. Fu *et al.* (2000) solved its crystal structure with the substrate glycerol (Fig. 1.11A). In this structure, besides six long transmembrane α-helices, two short ones are also formed, along with coil regions inserted in the membrane. Interestingly, besides other hydrogen bonds formed between long helices, H-bonds are also formed between the long helix M1 (Glu14) and a coil region (His66), and between long helix M4 (Gln93) and a short helix M3 (Thr72) (Fig. 1.11B, C) (Fu *et al.*, 2000, Engelman *et al.*, 2003). The helix association may also facilitate the glycerol (prosthetic group) binding as well, since the single α-helix is convex and has less surface for binding. On the other hand, there is also evidence for the prosthetic groups to stabilize the helix oligomerization, such as the binding of pigments to the light-

harvesting complex (LH2) of purple bacteria *Rhodopseudomonas acidophila* (Prince *et al.*, 1997).

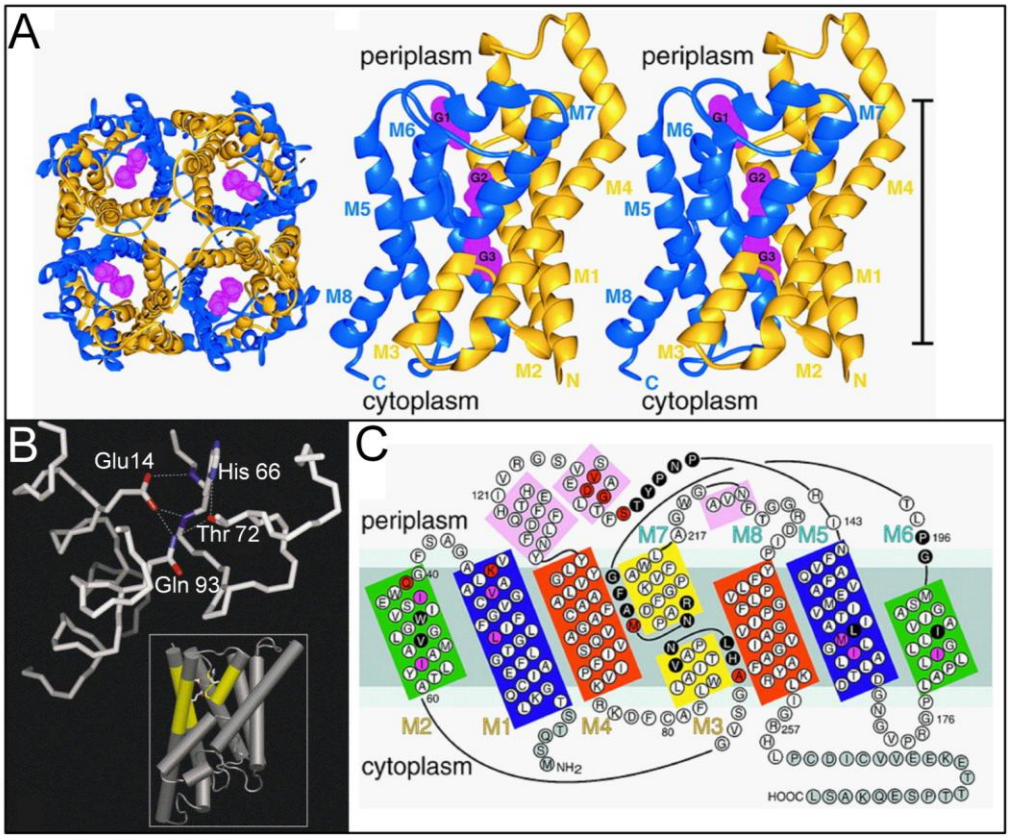

Fig. 1.11 The structure of the *E. coli* glycerol facilitator (GlpF). A. Crystal structure of GlpF with the substrate glycerols (magenta). Left, The top-down view of GlpF tetramer from the periplasm. The quasi two-fold related segments are colored in yellow and blue. The dotted line represents the clipping plane used in the right figure. Right, the side view of two GlpF monomer viewed from the clipping plane of left figure. The vertical bar (35 Å) represents the membrane. α-helices are labeled M1 to M8. **B. Hydrogen bonds are formed to possibly stabilize the short helix and the membrane inserted coil.** The hydrogen bonds (dotted line) are formed between the long helix M1 (Glu14) and a coil region (His66), and between long helix M4 (Gln93) and a short helix M3 (Thr72). Adopted from Engelman *et al*. (2003) with permission. **C. The membrane topology of GlpF with amino acids labeled.** Each domain is arranged according to the crystal structure. Both A and C are adopted from Fu *et al.* (2000) with permission.

Helix-helix interaction in membrane proteins

Many severe diseases are due to the misassembly of α-helical membrane proteins. Mutations in the transmembrane α-helices may abolish their function by disturbing the protein 'active sites' (catalytic or binding sites), or affect the protein folding or trafficking such as accumulation of misfolded proteins in the Endoplasmic Reticulum (ER), or degradation of misfolded proteins (Sanders & Myers, 2004). Thus, the interaction of transmembrane α-helices has become more attractive to researchers because of its significant role in protein folding, assembly, and function. The major factors stabilizing these interactions are thought to be (Popot & Engelman, 2000):

1. Specific interaction with prosthetic groups.

2. The loops in between each α-helix.

3. Lipids. Although lipids usually promote membrane protein folding as a general solvent, sometimes individual or certain classes of lipids may have specific interactions with them, probably as prosthetic groups or regulator ligands, such as in the bovine heart cytochrome c oxidase (Tsukihara *et al.*, 1996).

4. Van der Waals interactions formed by fitting of side chains between helical surfaces.

5. Polar interactions. Although transmembrane helices contains only a small fraction of polar residues (7% threonine and serine, only 1-3% of the other polar amino acids), the polar residues are structurally and functionally important (Curran & Engelman, 2003). Two independent studies, Zhou *et al.* (2001) and Gratkowski *et al.* (2001) both showed that several polar residues (Asn, Asp, Gln, Glu) capable of being

both hydrogen bond donor and acceptor, are able to promote strong oligomerization of hydrophobic model transmembrane helices. Another example is the α-helical homodimeric protein BNip3 (Bcl-2/E1B 19 kDa interacting protein 3, a proapoptotic member of the Bcl-2 family), in which an extensive hydrogen bonding network between Ser and His residues was found to stabilize the tertiary structure (Bocharov *et al.*, 2007) (Fig. 1.12). In fact, polar interactions can also result in the misassembly of membrane proteins, when a nonpolar residue is mutated to a polar one. One example is the mutations in the transmembrane region of the cystic fibrosis conductance regulator (CFTR) associated with the cystic fibrosis. The V232D mutation in helix 4 promotes the formation of hydrogen bond with Q207 in helix 3 (Therien *et al.*, 2001).

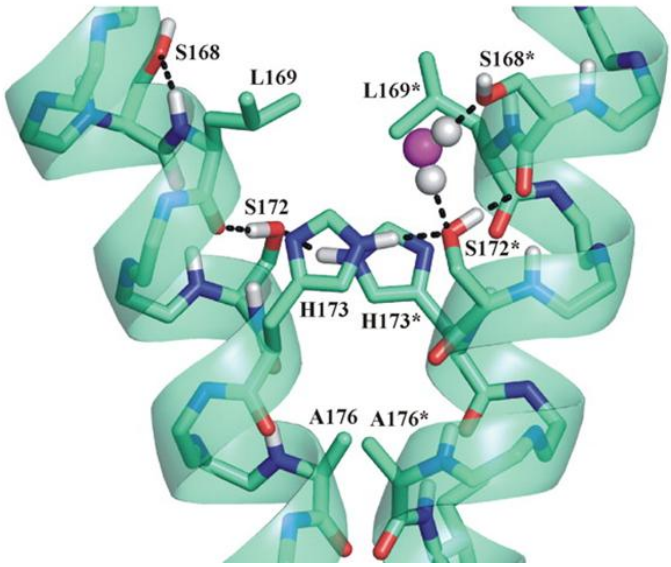

Fig. 1.12 Hydrogen bonds (dotted lines) in the homodimeric protein BNip3. Residues of one monomer are labeled with asterisks. The interhelical hydrogen bonding between His173 of one monomer and Ser172 of the other helps to stabilize the tertiary structure. Adopted from Bocharov *et al.* (2007) with permission.

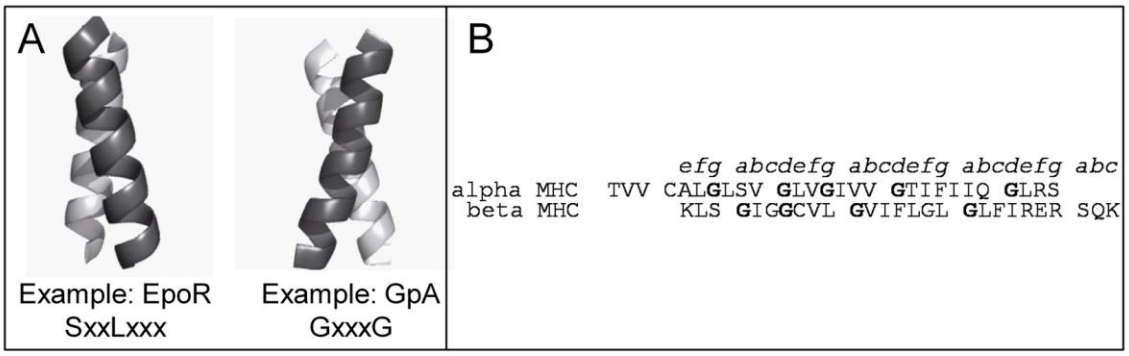

Fig. 1.13 Examples of geometric motifs involved in helical interaction. A. Representatives of the GAS_{Left} (left) and GAS_{Right} (right). Parallel GAS_{Right} pairs have right-handed packing and a 40° crossing angle with a GxxxG-like motif. Parallel GAS_{Left} helices have left-handed packing and a 20° crossing angle with a (G/A/S)xxxxxx(G/A/S) motif. **B. Sequence of the MHC α and β chains.** Both have the GAS_{Left} domains, which also include the GxxxG motif. Gly in each case is in bold. Adapted from Moore *et al.* (2008) with permission.

Geometric motifs involved in helical interaction

Statistical analysis of the three-dimensional (3D) structures of membrane proteins revealed that two thirds of the helical pairs fell within just four tightly clustered motifs (Walters & DeGrado, 2006, Moore *et al.*, 2008). The four largest clusters are the antiparallel helices with GAS_{Left} (29%) and GAS_{Right} (16%) motifs, and the parallel helices with GAS_{Right} (13%) and GAS_{Left} (9%) motifs. The GAS_{Left} motifs have left-handed helical packing with a crossing angle of approximately 20°, and amino acids with small side-chains (Gly, Ala, Ser) located every seven residues. The GAS_{Right} motifs have right-handed packing with a crossing angle of around 40°, and small residues (Gly, Ala, Ser) spaced every four residues, of which the Gly residues give the strongest interaction, also called the GxxxG motif (G, Gly; x, any residues). Figure 1.13A shows

examples of parallel GAS_{Left} and GAS_{Right} motifs. Interestingly, GxxxG motifs are also present in the GAS_{Left} motifs, as in the class II major histocompatibility complex (MHC) α- and β- chains (Cosson & Bonifacino, 1992, Moore *et al.*, 2008) (Fig. 1.13B). The detailed features of this GxxxG motif will be described next.

GxxxG motif

The GxxxG motif was first discovered from studies on the glycophorin A (GpA) protein. GpA forms right-handed dimer in the membrane of the human erythrocytes, solely through the interaction mediated by its single transmembrane domain (Furthmayr & Marchesi, 1976, Lemmon *et al.*, 1992a). Mutagenesis studies on the GpA TM domain identified the sequence LIxxGVxxGVxxT to constitute the dimerization interface (Lemmon *et al.*, 1992b). The interaction between these motifs was confirmed by the 3D structure determined by solution nuclear magnetic resonance (NMR) spectroscopy (MacKenzie *et al.*, 1997) (Fig. 1.14A). A further study identified that the central GxxxG motif by itself is able to induce dimerization (Brosig & Langosch, 1998). The same motif was found to be most frequent from an *in vivo* selection of sequences capable of helix dimerization from a library of randomized transmembrane sequences (Russ & Engelman, 2000). Additional analysis revealed that the GxxxG motif, along with other (G/A/S)xxx(G/A/S) motifs, creates a shallow groove formed by the G/A/S residues that complements the ridge formed by the bulky residues (x of GxxxG) from the neighboring helix, thus stabilizing the helical dimerization by extensive van der Walls interactions (MacKenzie *et al.*, 1997). It has also been suggested that this 'ridge in groove' structure

enables a Cα-H···O hydrogen bond to form between the Cα-H groups of the small residues in one helix and the carbonyls of the other helix backbone, which in turn also enhances the stability of interactions between two helices (Senes *et al.*, 2001) (Fig. 1.14B, C).

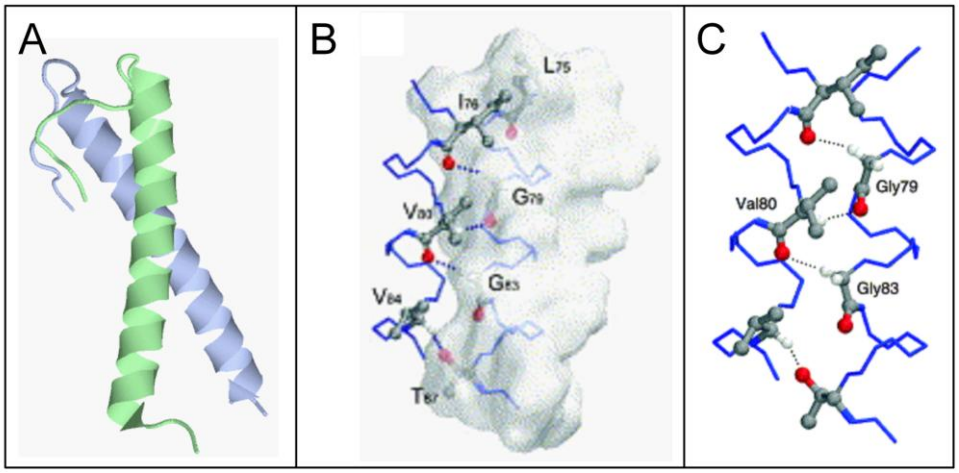

Fig. 1.14 Structure of GpA and the formation of hydrogen bonds. A. Solution NMR structure of the transmembrane domain of human GpA (MacKenzie *et al.*, 1997). Constructed with Jmol (http://www.jmol.org/); PDB ID 1AFO. **B. Stereo view of the the GpA TM domain dimer.** One monomer is shown with surface representation. Only the side chains of the dimerization interface LIxxGVxxGVxxT are shown. The groove formed by GxxxG motif adapts the ridge of V80 and V84. The dots represent the potential Cα-H···O hydrogen bonds formed at the GpA dimer interface. Adopted from Senes *et al*. (2004) with permission. **C. Magnified view of the Cα-H ··O hydrogen bond shown in B.** Adopted from Curran *et al*. (2003) with permission.

Interestingly, the GxxxG motif is not only broadly involved in the homotypic helical dimerization, but also involved in heterotypic helical interactions responsible for the oligomerization of α-helical membrane proteins. This motif is shown to be most

prevalent from statistical analyses either from the 637 membrane protein families of 26 sequenced genomes (Liu *et al.*, 2002), or from the 13,606 analyzed non-homologous TMDs (Senes *et al.*, 2000). However, these proteins or TMDs are not all involved in dimerization. Kim *et al.* (2005) described the presence of GxxxGxxxG-like sequence pattern ("glycine zipper") in the helical packing interface of several homo-oligomeric channel proteins, such as KcsA (bacterial potassium channel), MscL (mechanosensitive channel of large conductance), MscS (mechanosensitive channel of small conductance), and VacA (*Helicobacter pylori* vacuolating toxin A) (Fig. 1.15). In these proteins, the GxxxG motifs do not pack against each other as in the case of GpA and other symmetric dimers. Instead, they pack against a different face of the neighboring helix. These workers also reported that the sequence GxxxGxxxG, the so called glycine zipper motif, is strongly conserved, although small residues (A, S, or T) are able to substitute G with a reduced effect. Like the GxxxG motif, these glycine zippers are also common among membrane proteins. Among the proteins with known structure, all of the glycine zippers present are involved in helical packing. And in many cases, the glycine zipper containing TM helices line membrane pores. For the work described in this dissertation, it is important to note that the glycine zipper-like motif $G_{40}xxxS_{44}xxxG_{48}$ is present in TMD2 of the phage 21 pinholin $S^{21}68$. Thus it is interesting to test if this motif is involved in the heterotypic helical interactions or is facing the lumen of the pinhole.

The prevalence and importance of glycine zippers and GxxxG motifs in the α-helical membrane proteins has been increasingly the focus of more research. A simple search through PubMed (http://www.ncbi.nlm.nih.gov/pubmed/) gives about 90 research

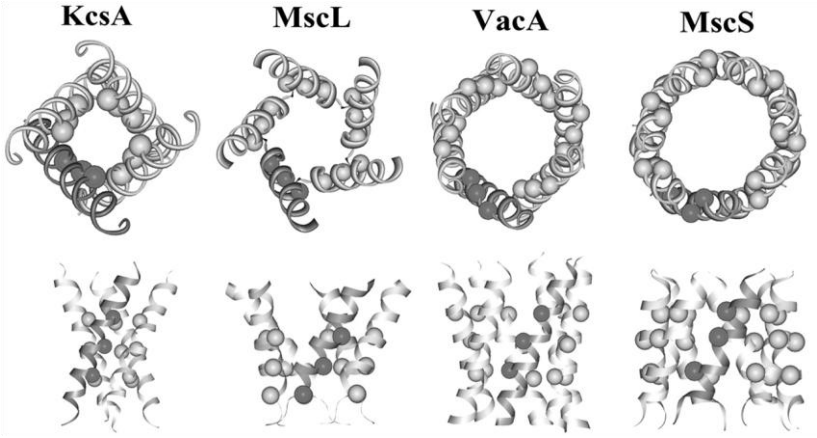

Fig. 1.15 Structures of the homo-oligomeric channel proteins. From left to right, KcsA (pdb 1BL8), MscL (pdb 1MSL), VacA (pdb 1SEW) and MscS (1MXM), see text for detail. The balls represent the Cα of the glycine zipper residues. Below, detailed side view of the glycine zipper regions of each oligomer. Each glycine zipper motif is packed against an opposite face of another helix. Adopted from Kim *et al.* (2005) with permission.

papers on these motifs in only a decade. Importantly, these motifs have also been found in several proteins related to diseases. For example, it is present in the envelope glycoprotein gp41 of the human immunodeficiency virus type-1 (HIV-1). Trimerization of gp41 through its TM domain is crucial for the membrane fusion process between the viral and the target cell plasma membranes and for viral entry (Abad *et al.*, 2009, Lev *et al.*, 2009, Lenz *et al.*, 2005). Mutagenesis studies on the $G_{690}G_{691}xxG_{694}$ sequence present in the TM domain showed that although G_{690} and G_{694} have a somewhat higher tolerance to mutations, additional substitution of the G_{691} severely decreased the fusion activity, indicating the additional stabilization effect of G_{691} (Miyauchi *et al.*, 2006). Hence, the GGxxG motif of gp41 might be a good target in the development of anti-HIV inhibitors. More generally, the glycine zippers or GxxxG motifs involved in these

disease-related proteins may all be brought into attention in pharmaceutical research.

Although the presence of glycine zippers or GxxxG motifs is a useful clue for protein structure prediction, it does not prove the existence of such an interaction in any particular membrane protein. Its involvement in stabilizing helical interactions must be tested in each case. Nevertheless, the identification of these motifs provides a significant foundation for making hypothesis-driven, structure-based experimental design.

Goals and specific aims

As a prototype pinholin, $S^{21}68$ deserves more research attention. The fact that it has only 2 TMDs with 68 amino acids, and forms only small holes, makes it a good candidate for both studies on the mechanism of holins, and on the membrane proteins. Although a small protein, it has a sophisticated mechanism for function. Its TMD1 is a SAR domain, and serves as a negative regulator, or lysis timing controller. Its TMD2 alone lines the pinhole, and has the GxxxSxxxG glycine zipper motif, which might be involved in helical packing. Thus it is an interesting and important subject for further study. The purpose of this dissertation is thus to use both genetic and biochemical methods, as well as computational modeling, and bioinformatics tools to further study the pinholin $S^{21}68$. The specific aims are as follows:

1. To solve the structure of the pinhole.
2. To explore the detail of the pinhole formation pathway.
3. To identify the localization of $S^{21}68$ in the host membrane.

CHAPTER II

THE STRUCTURE OF THE LETHAL PHAGE PINHOLE*

Introduction

The most frequent cytocidal event in the biosphere is the holin-mediated permeabilization of the bacterial membrane that terminates the bacteriophage infection cycle (Young & Wang, 2006). At an allele-specific time, the holin triggers to disrupt the cytoplasmic membrane by the formation of non-specific holes, the first step in a three-step lytic process involving three other phage proteins, the endolysin and Rz-Rz1, the components of the spanin complex (Young & Wang, 2006, Berry *et al.*, 2008). Besides de-energizing the membrane and bringing macromolecular synthesis to a halt, hole-formation allows the destruction of the murein layer by the endolysin, which in turn allows the disruption of the outer membrane by the spanin complex. The entire process is finished within seconds of triggering (Young, 2002). The canonical holins, such as that of phage λ, form very large holes that allow fully-folded endolysins to pass through the membrane to attack the murein. These holes are non-specific, allowing passage of unrelated endolysins (Bläsi & Young, 1996), and large enough for 500 kDa proteins (Wang *et al.*, 2003).

Recently, an alternative and remarkably different class of holin-endolysin systems has emerged (Xu *et al.*, 2004, Park *et al.*, 2006, Park *et al.*, 2007). This class,

---

* Reprinted with permission from "Structure of the lethal phage pinhole" by Pang, T., Savva, C. G., Fleming, K. G., Struck, D. K. & Young, R., 2009. *Proc Natl Acad Sci USA* **106**: 18966-18971.

represented by the lambdoid bacteriophage 21, utilizes endolysins having novel N-terminal secretory signals called SAR (signal-anchor release) domains. SAR sequences initially act as signal-anchor domains and promote the integration of proteins into the cytoplasmic membrane with type II, N-in, C-out topology (Xu *et al.*, 2004, Xu *et al.*, 2005). Importantly, despite the fact that the muralytic domain of the SAR endolysins is secreted to the periplasm, these enzymes are catalytically inactive in their membrane-tethered state, which prevents premature lysis that would curtail the cytoplasmic assembly of progeny virions. Maintenance of the tethered, inactive state of the endolysin depends on the energized state of the bilayer, and release into the periplasm is quantitative when the holin triggers to disrupt the membrane. Thus, for SAR endolysins, the holin protein need only produce lesions large enough to allow the passage of ions through and depolarization of the cytoplasmic membrane. Indeed, unlike lesions formed by the λ holin, lesions formed by the phage 21 holin did not allow the passage of either λ endolysin or a periplasmic marker- tagged GFP protein (Park *et al.*, 2007). The term "pinholin" has been proposed to differentiate the small-hole ("pinhole") forming character of the phage 21 holin from the canonical holins that form large, non-specific holes. A focus on the molecular basis of pinholin function seems warranted, not only because of the intriguing functional differences with the canonical holins but also because a homolog of the S^{21} pinholin has been shown to be involved in the programmed release of the Shiga-like toxin by enterohemorrhagic *E. coli* O157:H7 (Wagner *et al.*, 2002, Wagner & Waldor, 2002).

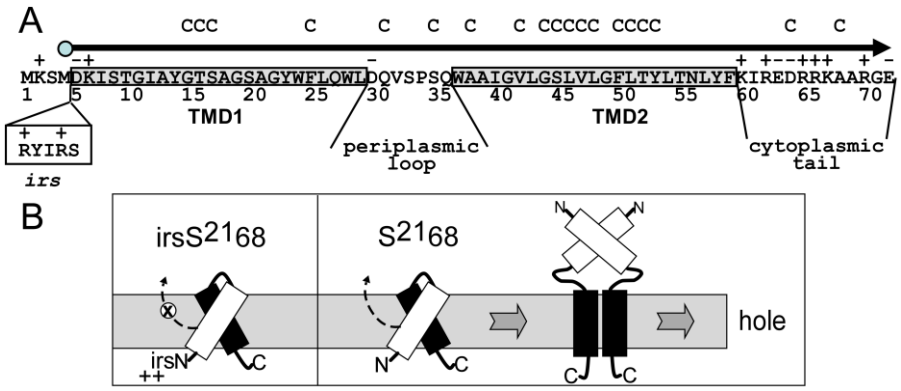

Figure 2.1 Features of $S^{21}68$.
A. Sequence of the S^{21} reading frame. The 71 residues encoded by the *S^{21}* gene are shown, with the $S^{21}68$ reading frame, which begins with Met4, depicted by the arrowhead line. TMD1 and TMD2 are indicated by shaded boxes, and the regions corresponding to the periplasmic loop and cytoplasmic tail are so labeled. Residues altered to Cys for this study are indicated by C above the sequence. The *irs* epitope inserted after Met4 in the irs$S^{21}68$ variant is shown in the clear box.
B. Model for pinhole formation by $S^{21}68$. TMD1 (white) is initially in the membrane, bound to TMD2 (black). When TMD1 exits the membrane, TMD2 is able to dimerize and then oligomerize, in the pathway to pinhole formation. TMD1 undergoes homotypic interactions in the periplasm that facilitate, but are not necessary, for pinhole formation. To the left, the inhibitory effect of the *irs* epitope, with its two positive charges, on the release of TMD1 from the membrane is depicted. Modified from Park *et al*. (2006) with permission.

Like the λ holin gene *S*, the phage 21 holin gene, *S^{21}* encodes two proteins, $S^{21}71$ and $S^{21}68$, by virtue of alternate translational starts (Fig. 2.1A); the longer gene product, like that of lambda, has inhibitory character and is thus an antiholin (Barenboim *et al.*, 1999). Analysis of *$S^{21}68$*, an allele that produces only the holin, has shown that despite its small size of 68 residues, the product has two functional domains corresponding to the two predicted transmembrane domains (TMD) (Fig. 2.1A). TMD1 is not only dispensable for hole-formation and lysis but, in fact, is itself a SAR domain that must

exit the bilayer in order for TMD2 to be competent for hole-formation (Fig. 2.1B) (Park *et al.*, 2006). This is most dramatically illustrated by the properties of a modified allele *irsS*^{21}*68*, which encodes the S^{21}68 with the *irs* epitope, containing 2 positively-charged residues, added to the N-terminus. Because the extra charges prevent TMD1 from exiting the membrane, the irsS^{21}68 protein has an absolute lysis-defective phenotype (Park *et al.*, 2006). In this report, we present biochemical, ultra-structural and computational studies of the elements of S^{21}68 that are involved in the membrane lesion. The results are discussed in terms of a model for the structure of the pinhole and the implications for its temporally-scheduled formation.

Results

Detergent-solubilized S^{21}68 forms channel-like structures

After purification in DDM (n-dodecyl-β-D-Maltopyranoside), S^{21}68 was found to form oligomers with an apparent size of 104 kDa in size-exclusion chromatography (Figs. 2.2A, 2.3). This corresponds to complexes with 4 - 7 S^{21}68 molecules, based on a range of ~100 - 140 for the aggregation number of DDM (Rosevear *et al.*, 1980, VanAken *et al.*, 1986, Aoudia & Zana, 1998, Strop & Brunger, 2005). Electron microscopy of negatively-stained S^{21}68 purified in DDM revealed small doughnut-shaped particles that were reasonably monodisperse (Fig. 2.2B). Reference-free classification of the S^{21}68 oligomers resulted in roughly spherical class averages that measured between 75- and 80 Å in diameter, with a central stain-filled cavity of ~15 Å (Fig. 2.2B, inset, top row). Some of these classes displayed a roughly hexagonal shape,

although no symmetry had been imposed. Examination of structures formed by $S^{21}68_{\Delta TMD1}$ and by lysis-defective $irsS^{21}68$ resulted in particles with similar class averages. This was not surprising for $irsS^{21}68$, since the membrane barrier that restrains the tagged TMD1 is removed by detergent. We suggest that the similarity in the negative-stain images between the oligomer of the full-length holin and that of $S^{21}68_{\Delta TMD1}$ reflects positioning of TMD1 in oligomeric bundles stacked over the pinhole (Fig. 2.1B).

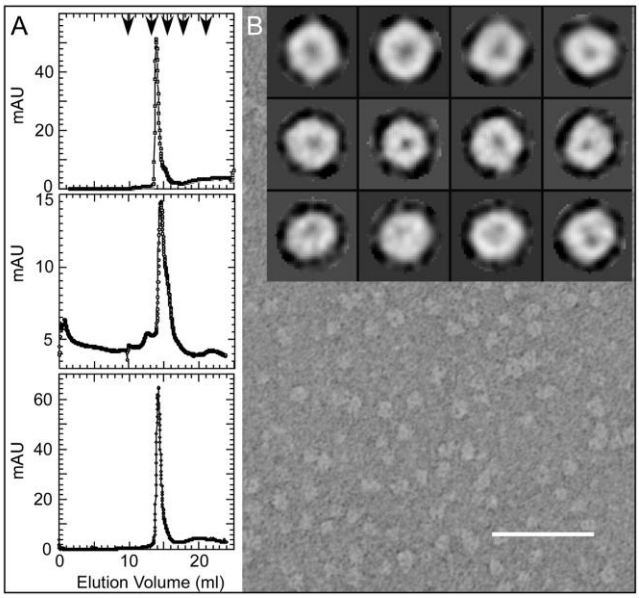

Figure 2.2 *In vitro* characterization of his-tagged $S^{21}68$ and its derivatives.
A. Gel filtration of $S^{21}68^{his}$ and derivatives. Purified protein was applied to a Superdex 200 column and analyzed as described in Materials and Methods. Top panel: $S^{21}68^{his}$; middle: $S^{21}68_{\Delta TMD1}{}^{his}$; bottom: $irsS^{21}68^{his}$. Arrowheads indicate the protein standards, from left to right: 670, 158, 44, 17 and 1.35 kDa.
B. Electron micrograph of negatively stained $S^{21}68^{his}$ purified in DDM. Scale bar =500 Å. Inset: single particle averages for $S^{21}68^{his}$ (top row), $S^{21}68_{\Delta TMD1}{}^{his}$ (middle row), and $irsS^{21}68^{his}$ (bottom row). Each single box is 148 x 148 Å.

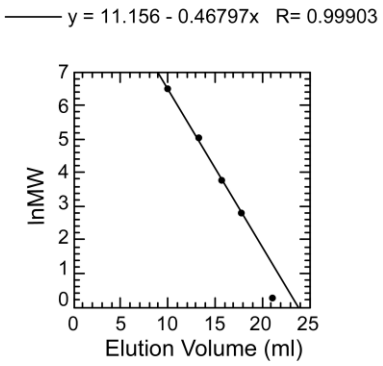

	Elution Vol (ml)	MW (kDa)	lnMW
Thyroglobulin	9.829	670	6.51
Bovine γ-globulin	13.241	158	5.06
Chicken ovalbumin	15.669	44	3.78
Equine myoglobin	17.75	17	2.83
Vitamin B_{12}	20.988	1.35	0.30
$S^{21}68^{his}$	13.907	104	4.65

Figure 2.3 Calculation of the size of the $S^{21}68$ in gel-filtration chromatography. The natural logarithm of the molecular weight of each protein standard was plotted against elution volume on a Superdex 200 gel-filtration column. The elution volume of vitamin B_{12} was close to the bed volume, and ignored in the plot. The apparent molecular weight of $S^{21}68$ was calculated by fitting the equation generated from the protein standard.

Hole-forming ability of *$S^{21}68$* alleles

The negative stain images of the purified pinholin suggest an oligomeric structure with a small channel, consistent with its biological function. To probe the structure of the pinholin in the membrane, we used a variation of cysteine-scanning-accessibility. This approach involves treating whole cells expressing the desired *$S^{21}68$* single-cysteine mutant allele with membrane-impermeant thiol reagent (2-sulfonatoethyl) methanethiosulfonate (MTSES). After quenching the reaction, cells are solubilized with SDS/urea and the extent of MTSES modification is assessed by

derivatizing the remaining free cysteines with a high molecular weight (5 kDa) derivative of methoxy-polyethyleneglycol maleimide (PEG-Mal). For the hole-forming *S*^{21} alleles, residues in both the periplasm and cytoplasm should be modified by MTSES, given a lumenal diameter of at least the 6 Å needed for passage of the reagent through the bilayer (Akabas *et al.*, 1992). We first examined the accessibility of cysteines located in either the periplasmic loop or the cytoplasmic domain of S^{21}68. As can be seen in Fig. 2.4A, positions in the periplasmic loop of S^{21}68 (positions 30 and 34) show partial protection, as can be seen from comparing the unmodified species (asterisk) with or without MTSES, or by comparing the PEGylated species (+PEG), with or without MTSES. (The intensities of the unmodified and PEGylated forms cannot be directly compared to each other because of inherent differences in the efficiency of blot transfer and immuno-staining.) For both irsS^{21}68 and S^{21}68$_{\Delta TMD1}$, the protection is much less efficient, possibly due to a difference in the membrane proximity of these residues in the different contexts. That is, in the wt protein, the periplasmic location of TMD1 may displace the loop residues from the bilayer. Importantly, the protection of the cytoplasmic C-terminal positions (63 and 67) is efficient for both the hole-forming alleles, S^{21}68 and S^{21}68$_{\Delta TMD1}$ but undetectable for the lysis-defective irsS^{21}68. Moreover, membrane depolarization by 2,4-dinitrophenol (DNP) has no effect on the irsS^{21}68 C-terminal inaccessibility to MTSES (Fig. 2.5). Taken together with previous findings, we conclude that (1) the cytoplasmic membrane of cells expressing *irsS*^{21}*68* retains its impermeability to MTSES and (2) the lumen of pinholes formed by both S^{21}68 and S^{21}68$_{\Delta TMD1}$ is large enough to permit the diffusion of MTSES into the cytoplasm.

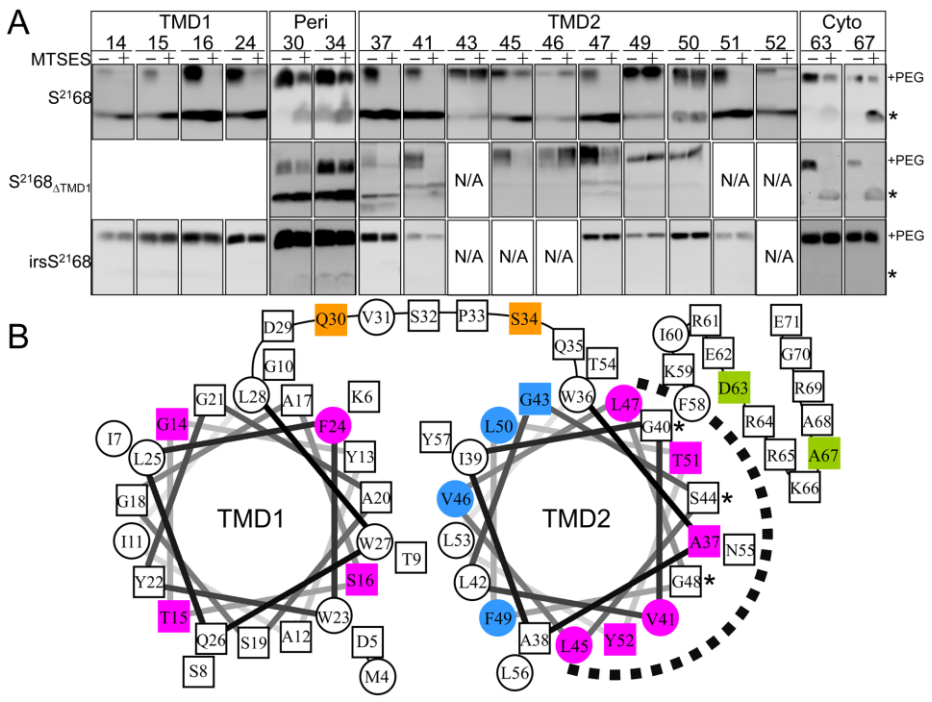

Figure 2.4. MTSES protection analysis of $S^{21}68$.
A. Whole cells carrying plasmids encoding single-Cys substitutions of $S^{21}68$ or its derivatives were induced, treated with the non-permeant thiol reagent MTSES, subjected to organic denaturation and delipidation, treated with PEG-maleimide, and analyzed by immunoblot, as described in Materials and Methods. The asterisk and "+PEG" indicate the position of the unmodified monomer and the PEGylated species, respectively. MTSES protection is indicated by an MTSES-dependent decrease in the PEGylated species and increase in the unmodified species. N/A: data not available. Peri = periplasmic loop. Cyto = cytoplasmic tail.
B. MTSES-protected positions in TMD2 map to its most hydrophilic face. Helical projections of TMD1 and TMD2 are shown, with hydrophobic residues as circles and hydroxylated, and hydrophilic residues, as well as Ala and Gly, as squares. Magenta and blue indicate transmembrane positions of $S^{21}68$ that do or do not show protection by MTSES. Also shown are the positions in the periplasmic loop (orange) and cytoplasmic tail (green) that show MTSES protection. The dashed arc indicates the deduced lumenal face of TMD2. Asterisks: GxxxSxxxG motif in TMD2.

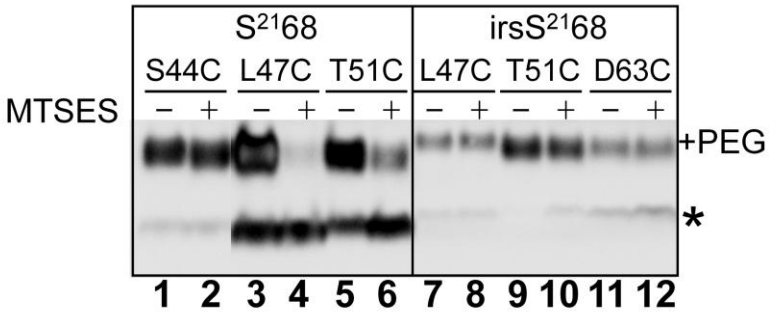

Figure 2.5. Membrane depolarization by DNP treatment does not affect the MTSES protection. Experiment was as described in Fig. 2.4, except that 1mM DNP was added into each culture just before harvesting and into the phosphate buffer used in each step until the L-cysteine quenching reaction. Left panel: $S^{21}68$ carrying the lysis-defective mutation S44C (lanes 1, 2), and cysteine substitutions at the lumen-facing residues L47 (lanes 3, 4) and T51 (lanes 5, 6). Right panel: $irsS^{21}68$ carrying the cysteine substitutions at L47 (lanes 7, 8), T51 (lanes 9, 10), and also at D63, which is located in the cytoplasmic tail (lanes 11, 12).

Identification of the TMD2 residues lining the $S^{21}68$ channel

Since MTSES penetrates the lesion formed by $S^{21}68$, it was feasible to use the cysteine-scanning-accessibility method outlined above to determine which face of the TMD2 helix faces the lumen of the pinhole. Single cysteines were engineered along the length of TMD2 helices encoded by *$S^{21}68$*, *$irsS^{21}68$* and *$S^{21}68_{\Delta TMD1}$* (Fig. 2.1A). With one exception, $S^{21}68_{S44C}$, none of the mutants changed function. MTSES did not react with any of $irsS^{21}68$ proteins carrying cysteine substitutions in TMD2, which is consistent with its inability to form holes in the cytoplasmic membrane (Figs. 2.4A, 2.5). By contrast, in both $S^{21}68$ and $S^{21}68_{\Delta TMD1}$, the same positions lining the hydrophilic face of TMD2 were found to be accessible to MTSES (Fig. 2.4A and B), suggesting that these residues face the lumen of the pinhole. The behavior of the lysis-defective mutant

$S^{21}68_{S44C}$ confirms the linkage between MTSES-sensitivity and lethal pinhole formation. Although located in the hydrophilic face, $S^{21}68_{S44C}$ lost MTSES-accessibility, even when the membrane was depolarized (Figs. 2.5, 2.6). However, when co-expressed with $S^{21}68$, triggering occurred very early and it became MTSES-accessible (Fig. 2.6).

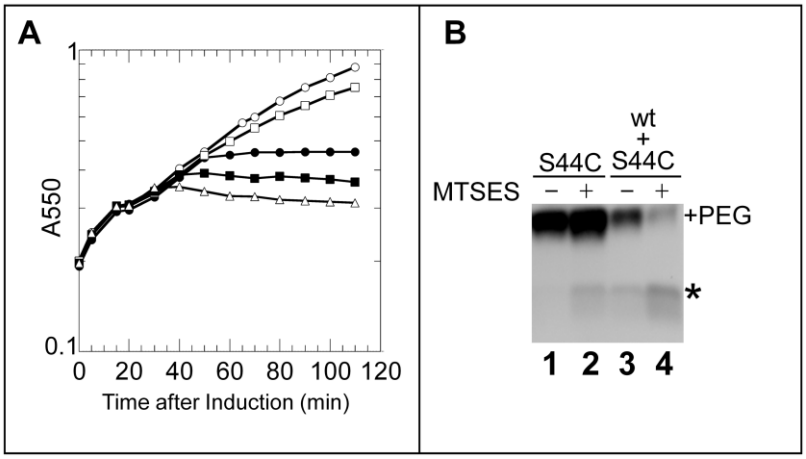

Figure 2.6. $S^{21}68_{S44C}$ is lysis-defective but can participate in pinhole formation with the wt protein.
A. Triggering of *$S^{21}68$* alleles. Cultures carrying indicated plasmids and prophages were induced at t = 0 and monitored for culture growth as A_{550}. Open circles: prophage $\lambda Q^{21}\Delta(SRRzRz1)^{21}$, no plasmid. Closed circles: prophage $\lambda S^{21}68$, no plasmid. Open squares: prophage $\lambda Q^{21}\Delta(SRRzRz1)^{21}$, plasmid $pS^{21}68_{aS44C}$. Closed squares: prophage $\lambda S^{21}68$, plasmid $pS^{21}68_{a}$. Open triangles: prophage $\lambda S^{21}68$, plasmid $pS^{21}68_{aS44C}$.
B. MTSES-protection of position 44. Experiment as described in Fig. 2.4, except that the cells carried $pS^{21}68_{aS44C}$ with either (lanes 1, 2) prophage $\lambda Q^{21}\Delta(SRRzRz1)^{21}$ or (lanes 3, 4) prophage $\lambda S^{21}68$.

The SAR domain of $S^{21}68$ is in the periplasm

Next, cysteine was substituted for four residues which would occupy the different helical faces of TMD1. In the $S^{21}68$ context, all four positions were found to be

accessible to MTSES (Fig. 2.4A). These results extend our previous results, that, during the pathway to pinhole-formation, TMD1 becomes protease-sensitive in spheroplasts (Park *et al.*, 2006), and indicate that it becomes completely relocated to the aqueous milieu of the periplasm, rather than just to the external face of the cytoplasmic membrane. In contrast, the same positions in the non-lethal *irs*-tagged derivative were completely insensitive to MTSES, consistent with its retention in the membrane.

Cross-linking of the pinholin in the membrane and in detergent

In order to identify the oligomeric states of $S^{21}68$ and its derivatives, whole cells expressing *$S^{21}68$* or *irs$S^{21}68$* were treated with the membrane-permeable amine-specific cross-linker, dithiobis[succinimidyl propionate] (DSP) and analyzed by immunoblot using anti-S^{21} antibodies. For $S^{21}68$, a cross-linked ladder up to at least hexameric order was obtained (Fig. 2.7, lane 2). In contrast, oligomerization appeared to be blocked at the dimer stage in cells expressing the non-lethal *irs$S^{21}68$* (lane 3). Moreover, we have previously shown that the presence of the *irs* epitope on $S^{21}68$ not only renders the protein non-functional, but also converts it to an antiholin which blocks the hole-forming activity of $S^{21}68$ (Park *et al.*, 2006). Accordingly, when *$S^{21}68$* and *irs$S^{21}68$* were co-expressed, the formation of cross-linked oligomers of $S^{21}68$ above the dimeric species was inhibited (lane 4). These data demonstrate that the cross-linking ladder generated from treating whole cells can be correlated with the lytic function of the pinholins present. The DSP cross-linking pattern for purified $S^{21}68$ in detergent was similar to that obtained from the membrane-embedded protein, except that, including the monomer,

seven species were clearly identifiable (Fig. 2.7, lane 5), each with an Mr corresponding to an integral multiple of the Mr of the monomer (Fig. 2.8). The same multimer ladder, shifted for the reduced molecular mass of the monomer, was seen for the other lytic allele, $S^{21}68_{\Delta TMD1}$, as well as for the non-lytic $irsS^{21}68$, which, in the absence of the membrane, has no barrier to pinhole formation (Fig. 2.7, lanes 6 and 7).

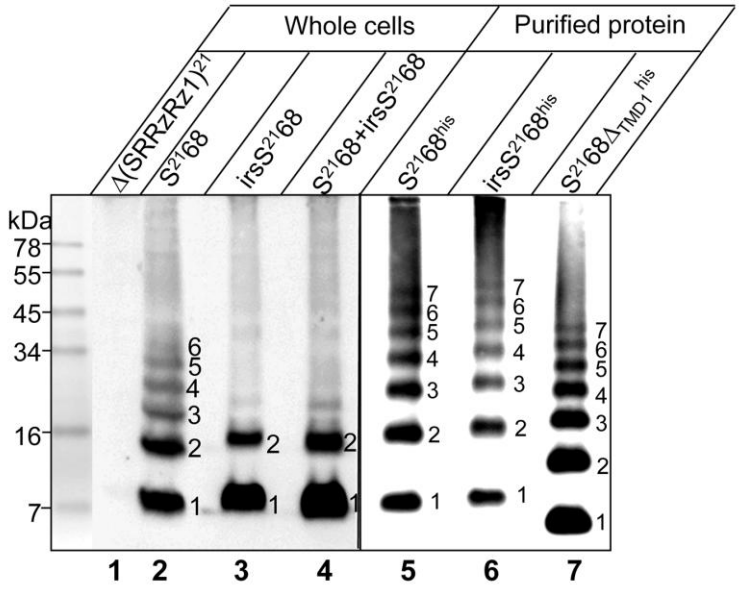

Figure 2.7. DSP cross-linking reveals pinholin oligomerization *in vivo* and *in vitro*. Left section: whole cells carrying prophage $\lambda Q^{21}\Delta(SRRzRz1)^{21}$ only (lane 1), or prophage $\lambda Q^{21}\Delta(SRRzRz1)^{21}$ with either plasmid $pS^{21}68$ (lane 2), or $pirsS^{21}68$* (lane 3), or prophage $\lambda S^{21}68$ with the plasmid $pirsS^{21}68$* (lane 4), as indicated, were induced, treated with the cross-linker DSP, and analyzed by SDS-PAGE and immunoblot, as described in Materials and Methods. Right section: protein purified from expression of alleles encoding his-tagged $S^{21}68$ or its derivatives, as indicated, was treated with DSP and analyzed by immunoblot. Oligomeric state indicated for each cross-linked species.

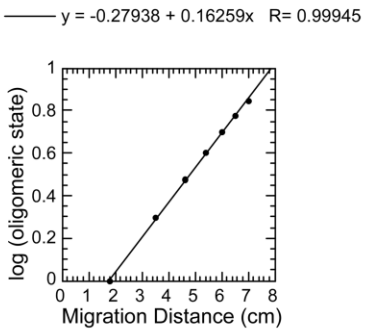

Migration distance (cm)	Oligomeric state	Calc. Oligomeric state
1.8	1	1.03
3.5	2	1.95
4.6	3	2.94
5.4	4	3.97
6	5	4.97
6.5	6	5.99
7	7	7.22

Figure 2.8. The DSP cross-linked $S^{21}68$ bands correspond to their oligomeric states. The decadic logarithm of the apparent oligomeric state of each cross-linked $S^{21}68$ band was plotted against the migration distance of each band on the gel. A linear equation was applied. In the table, the calculated oligomeric state was obtained by putting each migration distance into the equation.

A pinhole arrangement is suggested by computational modeling

Because its lethality drastically limits the level of protein expression, the pinhole is currently not amenable to high-resolution structural analysis by crystallography or NMR. However, the simplicity of $S^{21}68_{\Delta TMD1}$, comprising little more than a single transmembrane helix, and the fact that it forms holes with the same lumen-facing residues as the full-length holin, suggested a computational approach could be used to complement the biochemical and ultrastructural investigations. Therefore, a sequence corresponding to residues 36-58 of TMD2 was used in a simulated annealing search for closed N-mers, varying N from 5 to 7, and the resulting structures evaluated according to two general criteria: first, the distribution of MTSES-insensitive residues (43, 46, 49, and 50), which should be facing the lipid, and MTSES-sensitive residues (37, 41, 45, 47, 51, 52), which should be facing the lumen; second, the size of the predicted transmembrane pore, which must be large enough to allow both passage of MTSES

through the membrane and allow the chemistry of MTSES labeling without steric clash. The structures obtained for N= 5 - 7 all gave lipid-lumen distributions that were compatible with the experimental results, with the exception of Leu47, which, although MTSES-sensitive, was always lipid-exposed, not lumen-facing. However, Leu47 lipid exposure was somewhat attenuated in the heptameric structure (Fig. 2.9), in that only the delta carbons were lipid-exposed in this bundle, and the remaining atoms of the side chain (e.g. C_β and C_γ) were involved in helix-helix interactions that are juxtapositioned to the lumen surface of the pinhole. The pore-size criterion significantly favored the heptamer model, where the diameter of the luminal cavity is approximately 15.3 Å at Val41, constricting to 13.3Å at Leu45 in the center, and opening up to 16.0 Å at Thr51 (Fig. 2.9). These dimensions are significantly larger than in the hexamer (7 - 13Å) and pentamer (~6Å) (Fig. 2.10). Since MTSES occupies an ~12Å by ~6 Å cylindrical space (Kaplan *et al.*, 2000), only the hexamer and heptamer structures are compatible with MTSES permeation, and the hexameric lumen would likely put unacceptable steric constraints on MTSES reactivity towards lumenal thiols. Taken together, the simulated annealing computations favor a model for the functional pinhole based on a heptameric bundle of TMD2 helices, consistent with the results obtained with treating the purified pinholes with the cross-linker DSP (Fig. 2.7).

Using the energy function in CHI, we identified 20 residues involved in helix-helix interactions in the heptamer, which, by occluded surface analysis (Pattabiraman *et al.*, 1995, Fleming & Engelman, 2001) led to the assignment of two interaction surfaces could for each helix: surface A, comprising residues

$W_{36}A_{37}xxG_{40}V_{41}xG_{43}S_{44}xxL_{47}G_{48}xL_{50}T_{51}xxT_{54}$; and surface B, comprising residues $A_{38}xxV_{41}L_{42}xxL_{45}xxxF_{49}xxY_{52}L_{53}xN_{55}L_{56}xF_{58}$ (Fig. 2.9). Val41 plays a unique role in the pinholin since it has significant interactions on the inner surface of the pore in both the A and B faces. Interestingly, the core of surface A is formed by a triplet of small residues, $G_{40}xxxS_{44}xxxG_{48}$, which makes a sterically unhindered pocket accommodating the side chains of the bulky residues L45, F49 and Y52. The heptamer structure also displays three interhelical hydrogen bonds between Ser or Thr side chains and backbone carbonyls on different helices: (i) Ser44 / Leu45; (ii) Thr51 / Tyr52; and (iii) Thr54 / Leu56.

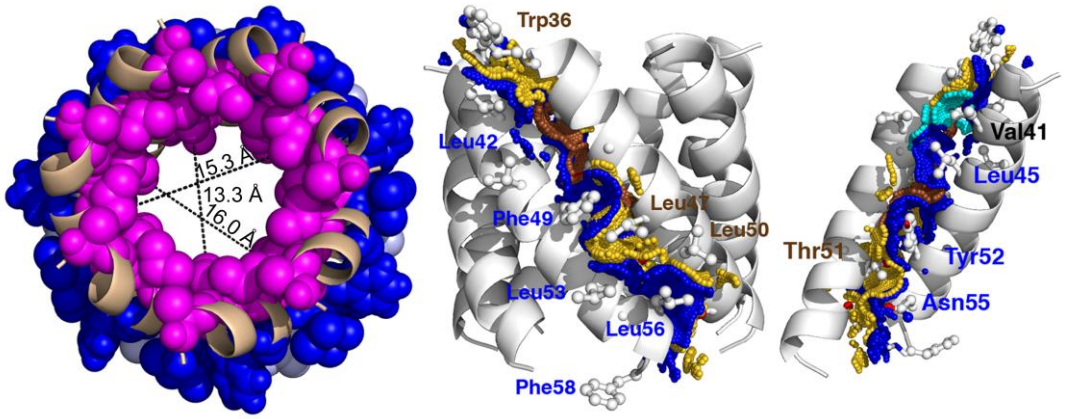

Figure 2.9. Computational model for the heptameric pinhole.
Left: Top down view of N=7 pinhole model with pore distances shown at various depths. MTSES- sensitive and insensitive positions are shown in magenta and blue, respectively.
Middle: Side view of N=7 pinhole model showing the helix-helix interaction contact surface. Contact surface A containing the glycine zipper is shown in gold and labeled in brown; the Gly40, Ser44 and Gly48 contact surface is colored brown. Contact surface B is shown and labeled in blue.
Right: A lumenal view of the contact surface, with 5 helices removed for clarity. Contact surfaces are colored as in the middle figure, except that Val41 is shown in cyan.

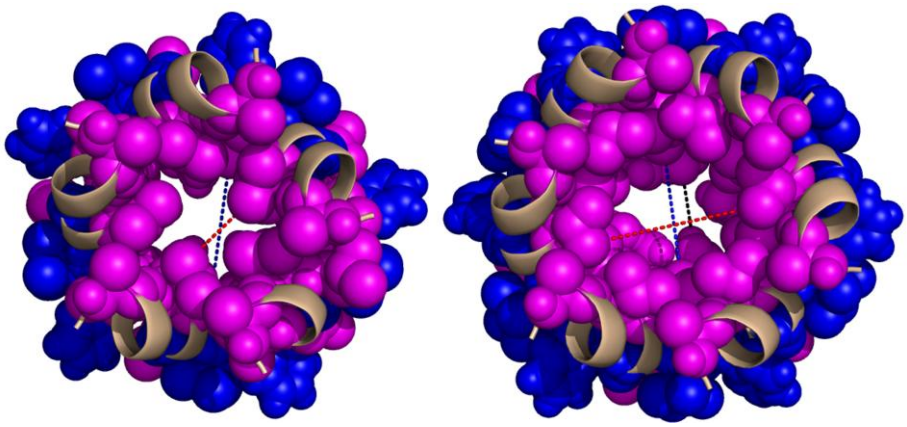

Figure 2.10. Computational models for the pentameric (left) and hexameric (right) pinholes. MTSES sensitive and insensitive positions are shown in magenta and blue, respectively. Colored dashed lines show pore distances at various depths. In the pentamer, red: 6.4 Å at Val41; blue: 11.6 Å at Leu45. In the hexamer, red: 12.6 Å at Val41; blue: 10.5 Å at Leu45; black: 6.7 Å at Tyr52.

Discussion

The pinholins are a new class of holins that forms small holes using only a single TMD (Park *et al.*, 2006). Interest in the prototype pinholin, $S^{21}68$, was piqued by the simplicity of its primary structure, by evidence indicating that its N-terminal TMD was required to exit the bilayer for triggering to occur, and by its near identity with the holin of the prophage 933w, which controls release of Stx toxin during *E. coli* O157:H7 infections (Wagner *et al.*, 2002, Wagner & Waldor, 2002) (Fig. 2.11). Here, we have used structural, biochemical, and computational studies to interrogate the structure of the lethal pinholin lesion, both in the membrane and purified in detergent.

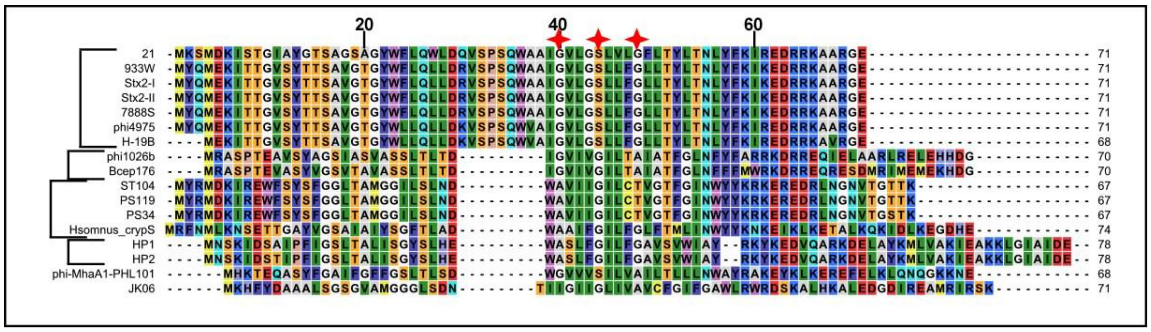

Figure 2.11. Conservation of "glycine-zipper" motif in class II pinholins. The genomes of phages and prophages of Gram-negative bacteria were scanned for annotated holin genes. Among the class II holins (two predicted TMDs), those with putative SAR domains were selected by the presence of a dual start motif, MxxM, or by homology to sequences with dual start motifs. The brackets indicate families of related sequences. The red stars indicate the positions of the "glycine-zipper" motif in S^{21}. Numbering at the top refers to S^{21}, and the length in amino acids, of each sequence is to the right. The Genbank identification numbers of these sequences are: 21 = 215467 ; 933W = 9632510; Stx2-1 =20065950; Stx2-II = 32171159 ; 7888S = 10799915; phi4975 = 30910957; H-19B = 2668771; phi1026b = 38707913 ; Bcep176 = 77864684; ST104 = 46358688; PS119 = 30910957; PS34 =3676080; Hsomnus_crypS = 915370; HP1 = 9628629; HP2 = 17981839; phi-MhaA1-PHL101 = 90110550; JK06 = unannotated holin gene found in phage JK06 genome, GI = 71149512.

Topological dynamics and pinhole formation in the membrane

The picture that TMD1 exits the membrane during the hole-formation pathway has been strongly reinforced here, with the finding that in S^{21}68, which triggers, but not in irsS^{21}68, which does not, residues all around the TMD1 helix become sensitive to MTSES attack in whole cells (Fig. 2.4A). Moreover, it was shown that coupled to this topological change in TMD1, positions along one surface of TMD2 and in the C-terminal cytoplasmic tail become accessible to MTSES (Fig. 2.4A). Not unexpectedly, the surface of S^{21}68 that becomes solvent-exposed is its most hydrophilic surface (Fig. 2.4B). Although the arc of accessibility begins and ends with Leu residues (Leu45,

Leu47), all but one (Val41) of the other residues on that face are either polar (Asn55), hydroxylated (Ser44, Thr51, Tyr52), or of neutral hydrophobicity (Ala37, Gly40, Gly48). Importantly, protection for most of the lumen-facing residues approaches completion (Fig. 2.4A), indicating that essentially all of the $S^{21}68$ protein, which is present in ~6400 copies per cell at the time of triggering, based on quantitative immunoblotting with purified $S^{21}68$ as a standard (Fig. 2.12), is involved in pinholes. In addition, the DSP-crosslinking data clearly indicate that oligomeric complexes of $S^{21}68$ up to at least hexamer order are present in the membrane after triggering (Fig. 2.7). In contrast, if TMD1 is prevented from exiting the membrane by the *irs* tag, thus blocking pinhole formation, DSP-crosslinking indicates that the protein cannot oligomerize beyond a dimer. Thus, the pinhole formation system seems to be set up for an all-or-nothing response that suddenly forms ~900 pinholes. Although we do not know the ion flux the pinholes would support, they must be sufficiently large to permit efficient MTSES reaction with lumenal thiols, which would certainly require at least 1 nm diameter (Kaplan *et al.*, 2000). Since single colicin channels of ~0.8 nm diameter can depolarize an *E. coli* cell in a few minutes (Schein *et al.*, 1978, Davidson *et al.*, 1984), it seems likely that > 900 heptameric pinholes is greatly in excess of what is needed for depolarization within seconds. We suggest this reflects the biological mandate for a pinholin, to effect instantaneous and complete de-energization of the membrane at the programmed time, thus causing quantitative activation of the pre-localized SAR endolysins and rapid lysis. It would be counter-productive to form pinholes gradually,

which would presumably reduce ATP-generation and the biosynthetic capacity of the infected cell in parallel.

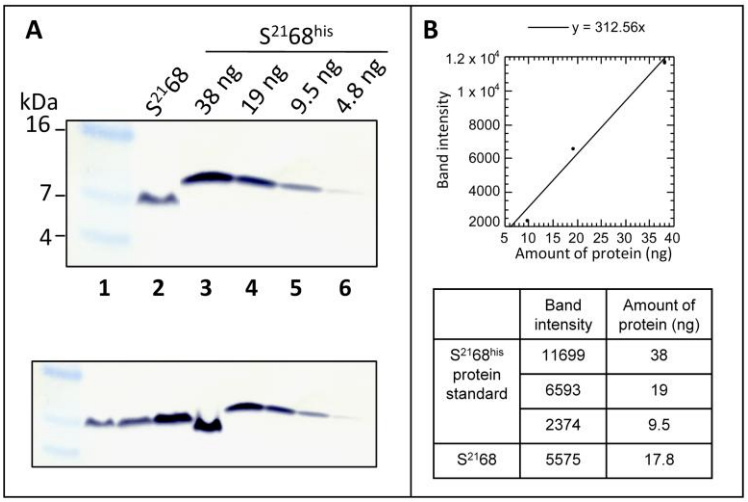

Figure 2.12. Measurement of $S^{21}68$ expression level at the time of triggering.
A. MDS12*ΔtonA*(λ*S*^{21}*68*) was thermally induced and an aliquot of 2.1×10^8 cells was precipitated by trichloroacetic acid immediately after $S^{21}68$ triggering. The sample was subjected to SDS-PAGE and Western blotting in parallel with samples containing a known amount of purified $S^{21}68^{his}$. Lane 1, molecular weight standard; lane 2, $S^{21}68$ from MDS12*ΔtonA*(λ*S*^{21}*68*).; lanes 3-6, purified $S^{21}68^{his}$, amount indicated at the top of each lane. Band intensities were measured using the ImageJ program (http://rsb.info.nih.gov/ij/).
B. The amount of $S^{21}68$ present in the induced cultures was calculated using the standard curve generated from samples containing the purified $S^{21}68^{his}$ protein. Based on 17.8 ng $S^{21}68$ accumulated in 2.1×10^8 cells, approximately 6400 $S^{21}68$ molecules are present at the normal triggering time.

Structure of the pinhole

The pinholes are too small to visualize in membranes where triggering has occurred, so our only direct structural information in the biological context comes from

the thiol accessibility and cross-linking data described above. The pinhole however can be purified in DDM as a holo-heptameric complex (Figs. 2.2 and 2.7). Moreover, searches using simulated annealing of TMD2 generated a heptameric model for the pinhole that is consistent with all of these results. Importantly, one of the two heterotypic interaction surfaces in the heptameric model contains the sequence $G_{40}xxxS_{44}xxxG_{48}$. The motif appears to be critical for pinhole formation, because one of the single Cys substitutions used in this study, S44C, does not trigger. In addition, similar motifs are conserved in TMD2 in other holins likely to be pinholins, some not detectably related to $S^{21}68$ (Fig. 2.11). Such "glycine-zipper" motifs featuring Gly and other residues with small side chains at intervals of 3 amino acids underlie the heterotypic interactions between TMDs in the other well-studied homo-oligomeric channel proteins: KcsA (tetramer), MscL (pentamer), VacA (hexamer) and MscS (heptamer) (Kim *et al.*, 2005). In each of these cases, the homo-oligomerizing helix using this motif is the sole TMD that lines the pore, and, as in our model for the heptameric pinhole, the interaction is heterotypic, with the motif embedded in one face that interacts with a different face of the next helix. Finally it must be noted that the GxxxGxxxG motif was first identified in the homotypic dimer interaction surface between the TMDs of glycophorin (Russ & Engelman, 2000), and has recently been shown to mediate homotypic dimerization of the TMD of myelin protein zero (MPZ), both in membranes and in detergent (Plotkowski *et al.*, 2007).

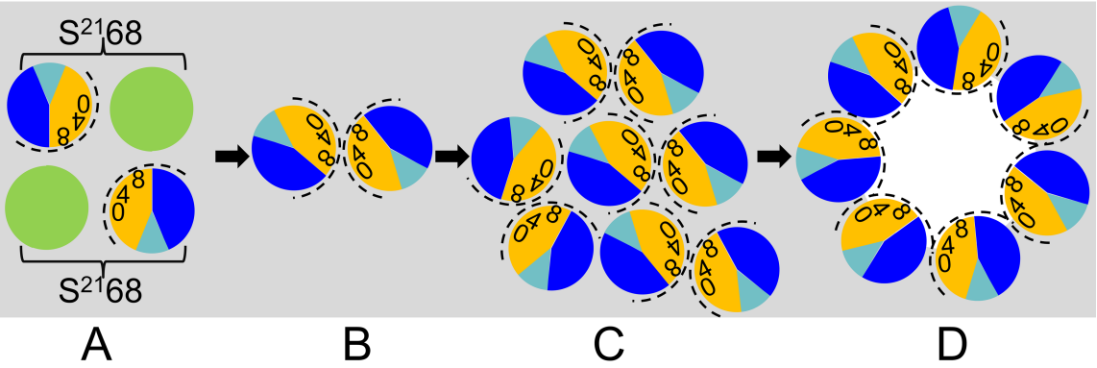

Figure 2.13. Model for the pinhole formation pathway. View is top-down from periplasm; grey = lipid. TMD1 and TMD2 are shown as green and sectored circles, respectively. In TMD2, orange and dark blue represent A and B interaction faces (Fig. 2.9), with 0, 4, and 8 indicating the helical positions of the G_{40}, S_{44} and G_{48} residues. The face accessible to MTSES in the pinhole is indicated by the dashed arc. A. Inactive dimers, with bracket linking cognate TMD1 and TMD2. One possible orientation is shown. B. Active dimers, after escape of TMD1 from membrane; homotypic interface. C. Aggregate of active dimers; actual number of dimers is likely to be much larger. D. Heptameric pinholes after triggering; heterotypic interface.

Implications for the pre-hole state and holin triggering

Taken together, the MTSES-protection patterns, chemical cross-linking data, and computational results suggest a general model for the hole-formation pathway. In this perspective, the pinholins accumulate as dimers, randomly dispersed in the membrane; these dimers are inactive because TMD1 is still in the bilayer (Figs. 2.1B and 2.13). We have shown that, in a population of pinholins, TMD1 gradually exits the membrane, with the proportion increasing as the triggering time approaches (Park *et al.*, 2006). This leads to formation of the active dimers (Figs. 2.1B and 2.13), with only TMD2 in the bilayer; obviously, the ΔTMD1 protein would accumulate directly in this conformation. In the active dimer, we suppose that the hydrophilic face of TMD2 is sequestered against itself

with the $G_{40}xxxS_{44}xxxG_{48}$ motif supporting a homotypic interface. When a critical concentration of active dimers is reached, formation of two-dimensional aggregates begins (Fig. 2.13). There is precedent for this with bacteriorhodopsin (BR). BR accumulates as a monomer in the cytoplasmic membrane until a critical concentration (C_r) is reached, after which the free BR concentration remains constant and the hexagonally-packed BR lattice accumulates. In the pinholin aggregates, triggering would then result from a change in how TMD2 interacts with itself, shifting from the homotypic interaction defining the dimer to the heterotypic A:B interaction, also dependent on the zipper motif. The driving force for this conversion could be hydration of the lumenal-side chains, which, in the heptameric model presented here, are mostly hydrophilic.

In this pathway, the pre-hole conformation is essential for pinhole formation, rather than just an inactive state. It should be noted that the S44C substitution is inactive in hole-formation but can be recruited into pinholes by functional $S^{21}68$ (Fig. 2.6). We suggest that S44C disrupts the pre-hole active dimer by poisoning the homotypic interface, as it should in the central position of the GxxxSxxxG motif, but can be accommodated in the heterotypic interface. Thus the mutant protein would be incorporated into holes by being a proximal monomeric bystander when the concerted triggering event occurs.

This model does not directly address the sensitivity to the energized state of the membrane, which might oppose the hydration step, stabilize the GxxxSxxxG interaction, or destabilize the heterotypic inter-helical interactions in the pinhole. In this regard, the

helices of the modeled heptamer are aligned at an angle of 34° to the normal, a geometry which might be strongly affected by the presence of the membrane potential (Fig. 2.9). The sensitivity to the proton motive force (pmf) is a key component of the biological function of the pinholin, and indeed all holins, because it confers "all or nothing" character. In our rationale, the spontaneous conversion of a single aggregate of pinholin dimers to a pinhole leads immediately to pmf collapse, assuring coordinated holin triggering throughout the whole cell. In any case, the structural and biological model presented here provides a framework for future experiments to examine the working parts of this simple, universal, and ancient biological timing system.

Materials and Methods

Media, culture growth and general DNA manipulations

Cultures were grown in standard Luria-Bertani (LB) media supplemented with ampicillin (100 μg/ml), chloramphenicol (10 μg/ml), and kanamycin (40 μg/ml) as indicated. Isopropyl-β-D-thiogalactopyranoside (IPTG) and arabinose were used for inductions of plasmid-borne promoters at final concentrations of 1 mM and 0.2%, respectively. Lysis profiles were obtained by monitoring A_{550} after thermal or IPTG/ arabinose inductions, as described previously (Smith & Young, 1998, Tran *et al.*, 2005). Site-directed mutagenesis, cloning steps and DNA sequencing have been described (Smith & Young, 1998).

Table 2.1. Bacterial strains, bacteriophages, and plasmids.

	Genotype and relevant features	Source/ reference
phages		
λhy21*Kan*	λ *cI857* hy*(QSRRzRz1)*^{21} *bor*::*kan*	(Barenboim *et al.*, 1999)
λ*Q*^{21}Δ*(SRRzRz1)*^{21}	λ *cI857* hy*(Q*^{21}*Δ(SRRzRz1)* ^{21}::*Cam*^{R}*) bor*::*kan'*	this study
λ*S*^{21}*68*	λhy21*Kan S*^{21}*68*(*R*$_{am}$/*Rz*$_{am}$/*Rz1*$_{am}$)^{21}	this study
E. coli strains		
MG1655	F^{-} *ilvG rfb50 rph1*	(Guyer *et al.*, 1981)
MG1655*lacI*^{q1}*tonA*::Tn*10*		(Park *et al.*, 2006)
MDS12	MG1655 with 12 deletions, totalling 376,180 nt, including cryptic prophages	(Kolisnychenko *et al.*, 2002)
RY 17341	MDS12*ΔtonA*	lab stock
C43(DE3)	derivative of BL21(DE3) [*E. coli* F^{-} *ompT hsdS*$_{B}$ (r$_{B}^{-}$ m$_{B}^{-}$) *gal dcm* λ(DE3)], used for overexpression of membrane proteins.	(Miroux & Walker, 1996)
MDS12Δ*tonA*(λhy21*Kan*)	Lysogen carrying prophage λhy21*Kan*	this study
MDS12*ΔtonA*(λ*Q*^{21}*Δ(SRRzRz1)*^{21})	Lysogen carrying prophage λ*Q*^{21}Δ*(SRRzRz1)*^{21}	this study
MDS12*ΔtonA*(λ*S*^{21}*68*)	Lysogen carrying prophage λ*S*^{21}*68*	this study
plasmids		
pBR121	pBR322::*(Q'SRRzRz1)*^{21}	(Barenboim *et al.*, 1999)
pBR-Cam^{R}	pBR121 with the DNA between the *Eco*RI site upstream of the *S*^{21} gene and the *Cla*I site within the *kan*^{R} gene replaced with a *cam*^{R} cassette	this study
pBP68	pBR121 but *S*^{21}*68* instead of *S*^{21}	(Barenboim *et al.*, 1999)
pS^{21}68	pBP68 (*R*$_{am}$/*Rz*$_{am}$/*Rz1*$_{am}$)^{21}, Shine-Dalgarno sequence of *S*^{21}*68* changed.	this study
pTP2	pBR322 origin, pR′ promoter, *(S68/R/Rz/Rz1)*^{21}	(Park *et al.*, 2006)
pS^{21}68$_{\Delta TMD1}$	pTP2 with the codons encoding TMD1 of *S*^{21}*68* deleted, (*R*$_{am}$/*Rz*$_{am}$/*Rz1*$_{am}$)^{21}	this study
pTP7	pTP2 encoding RYIRS fusion to N terminus of S^{21}68	(Park *et al.*, 2006)

Table 2.1. Continued.

plasmids	Genotype and relevant features	Source/ reference
pirsS^{21}68	pTP7 (R_{am}/Rz_{am}/$Rz1_{am}$)^{21}	this study
pQ	pSC101 origin with modification, $P_{lac/ara-1}$ promoter, *Q* from λ	(Gründling *et al.*, 2001)
pRE	pJF118EH with *lacI*^{Q} and P_{tac} replaced by pR' promoter	(Park *et al.*, 2006)
pS^{21}68$_a$	pRE with pR'^{21}, (*S68*R_{am}/Rz_{am}/$Rz1_{am}$)^{21} *Amp*^{R}, instead of *Kan*^{R}	this study
pirsS^{21}68*	pS^{21}68$_a$ with codons encoding RYIRS fused to N terminus of *S*^{21}*68*	this study
pETS^{21}68^{his}	pET11a carrying *S*^{21}*68* gene, with introduction of codons of GGH_6GG between codons 66 and 67.	(Park *et al.*, 2006)
pETS^{21}68$_{\Delta TMD1}$^{his}	pETS^{21}68^{his} but *S*^{21}*68*$_{\Delta TMD1}$ instead of the *S*^{21}*68*.	this study
pETirsS^{21}68^{his}	pETS^{21}68^{his} with codons encoding RYIRS fused to N terminus of *S*^{21}*68*.	this study
pS^{21}68^{his}	pS^{21}68$_a$ with codons encoding GGH_6GG inserted between codons 66 and 67.	this study
pirsS^{21}68^{his}	pS^{21}68^{his} with codons encoding RYIRS fused to N terminus of *S*^{21}*68*.	this study

Bacterial strains, bacteriophages, and plasmids

The key features of the bacterial strains, bacteriophages and plasmids used in this work are listed in Table 2.1.

For cysteine modification and cross-linking experiments, derivatives of the plasmid pS^{21}68 were used (Fig. 2.14A). The plasmid, pS^{21}68 was derived from pBP121 (Barenboim *et al.*, 1999), which has the entire phage 21 lysis gene cassette, genes (*SRRzRz1*)^{21} (Bonovich & Young, 1991) cloned in pBR322 under its native promoter, the late gene promoter pR'^{21}. In addition, the *S*^{21} gene is modified by deletion of its first

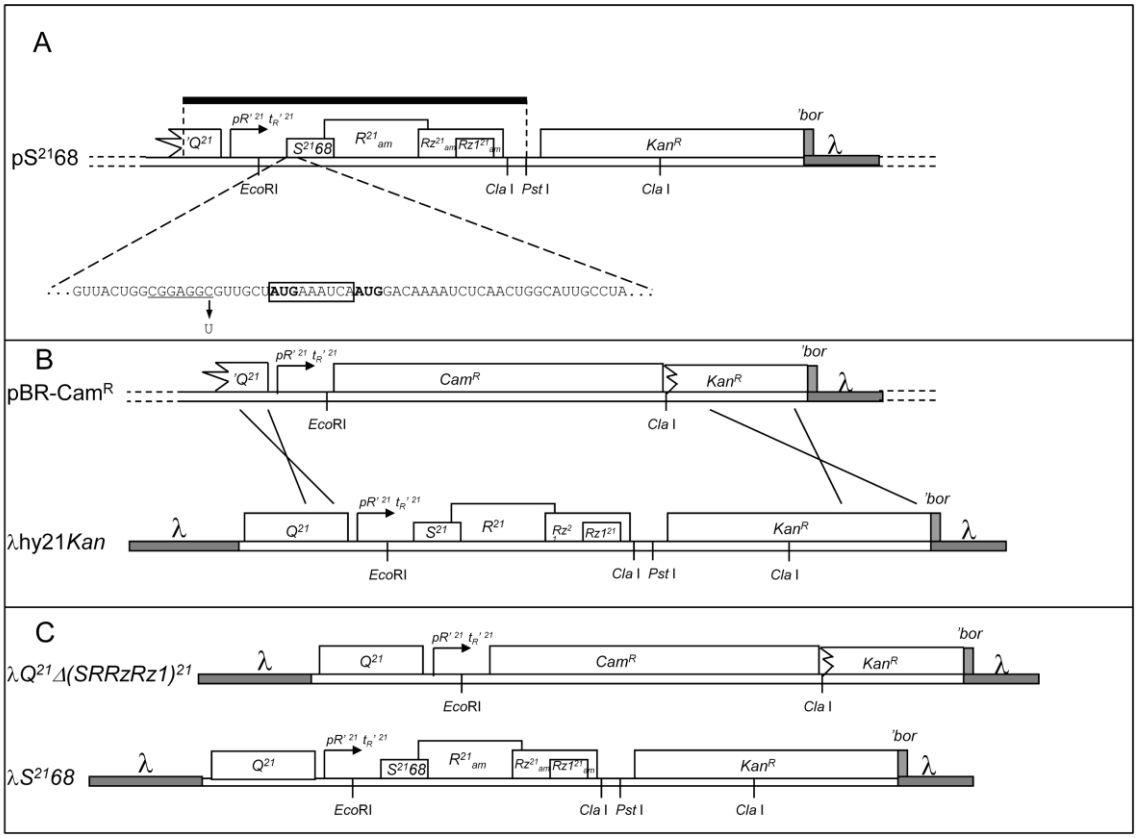

Figure 2.14. Structure of plasmids and phages.

A. Structure of the plasmid pS^{21}68. The black bar above the phage 21 lysis gene cassette represents the DNA fragment inserted between the *Nco*I and *Pst*I sites of plasmid pRE to construct plasmid pS^{21}68$_a$. In this construct, the first three codons (boxed) of S^{21} are deleted, so that the holin S^{21}68, but not the antiholin S^{21}71, is encoded. The Shine-Dalgarno sequence serving the $S^{21}68$ gene is changed from 5'-CGGAGGC-3' to 5'-CGGAGGT-3', and amber nonsense codons were introduced into R^{21} (positions Tyr39 and Tyr42), Rz^{21} (Gln100), and $Rz1^{21}$ (Trp39). See *Materials and Methods* for details of construction.

B. Structures of the plasmid pBR-Cam^R and phage λhy21*Kan*. Crosses between the two constructs indicate the regions of homology.

C. Structures of the phage $\lambda Q^{21}\Delta(SRRzRz1)^{21}$ and the phage $\lambda S^{21}68$. Phage $\lambda Q^{21}\Delta(SRRzRz1)^{21}$ was obtained by homologous recombination between the plasmid pBR-Cam^R and the phage λhy21*Kan*. Phage $\lambda S^{21}68$ was obtained by homologous recombination between the plasmid pS^{21}68 and the phage $\lambda Q^{21}\Delta(SRRzRz1)^{21}$. See *Materials and Methods* for details.

three codons, creating the allele *S*^{21}*68*, the Shine-Dalgarno sequence serving the *S*^{21}*68* gene is changed from 5'-CGGAGGC-3' to 5'-CGGAGGT-3', and the other three lysis genes were inactivated by introducing amber nonsense codons into *R*^{21} (positions Tyr39 and Tyr42), *Rz*^{21} (Gln100), and *Rz1*^{21} (Trp39). All pS^{21}68 based plasmids were transformed into the strain MDS12*ΔtonA* (RY 17341) (Kolisnychenko *et al.*, 2002) carrying the prophage λ*Q*^{21}*Δ(SRRzRz1)*^{21} (Fig. 2.14C), which, by thermal- induction, provides the phage 21 late gene activator, Q^{21}, to trans activate the pS^{21}68. The bacteriophage λ*Q*^{21}*Δ(SRRzRz1)*^{21} was generated by recombination between λhy21*Kan* (Barenboim *et al.*, 1999) and pBR-Cam^{R} (Fig. 2.14B). The plasmid, pBR-Cam^{R}, was derived from pBR121 (Barenboim *et al.*, 1999) by replacing the DNA between the *Eco*RI site upstream of the *S*^{21} gene and the *Cla*I site within the *kan*^{R} gene with a *cam*^{R} cassette (Lutz & Bujard, 1997). MDS12*ΔtonA*(λhy21*Kan*) was transformed with pBR-Cam^{R} and a lysate was obtained by thermal induction. The lysate was used to infect MDS12*ΔtonA* at low multiplicity and the lysogen MDS12*ΔtonA*(λ*Q*^{21}*Δ(SRRzRz1)*^{21}) was recovered by selecting on LB-Cam (10 μg/ml chloramphenicol) and screening for sensitivity to kanamycin.

The *S*^{21}*68*$_{\Delta TMD1}$ and *irsS*^{21}*68* alleles are expressed from plasmids pS^{21}68$_{\Delta TMD1}$ and pirsS^{21}68, respectively. Plasmid pS^{21}68$_{\Delta TMD1}$ is a derivative of pTP2 (Park *et al.*, 2006), with the codons encoding TMD1 of *S*^{21}*68* deleted (Fig. 2.1A), and with the introduction of nonsense codons into the *(RRzRz1)*^{21} lysis genes, as described above. The same nonsense codons were inserted into pTP7 (Park *et al.*, 2006), generating the plasmid pirsS^{21}68, encoding S^{21}68 with the *irs* epitope inserted after the Met4 start codon (Fig.

2.1A). Each plasmid was transformed into the strain MG1655 *lacI*^{q1} *tonA::*Tn*10* (Park *et al.*, 2006, Guyer *et al.*, 1981) carrying pQ, a low copy plasmid carrying the λ gene *Q*, encoding the late gene activator, under an IPTG and arabinose inducible promoter (Gründling *et al.*, 2001).

For experiments requiring co-expression of the wt *S*^{21}*68* with certain derivative alleles, strain MDS12*ΔtonA* carrying the inducible prophage λ*S*^{21}*68* (Fig. 2.14C) was used as the host. The lysogen MDS12*ΔtonA*(λ*S*^{21}*68*) was obtained by infecting MDS12*ΔtonA* with the lysate obtained by thermal induction of MDS12*ΔtonA*(λ*Q*^{21}*Δ(SRRzRz1)*^{21}) carrying pS^{21}68, selecting for lysogens on LB-Kan (40 μg/ml kanamycin) and screening for sensitivity to chloramphenicol. Induction of this prophage results in the production of the Q^{21} late gene activator and S^{21}68 in trans to co-resident plasmids.

The plasmid pS^{21}68$_a$ was used to provide the other *S*^{21}*68* allele in trans to λ*S*^{21}*68*. It was constructed by inserting the DNA between the middle of the *Q*^{21} gene and the *Pst*I site downstream of the 21 lysis cassette of the plasmid pS^{21}68 into the *Nco*I and *Pst*I sites of plasmid pRE (Fig. 2.14A) (Park *et al.*, 2006). Thus the plasmid pS^{21}68$_a$ has the pR'^{21} promoter and the entire lysis gene cassette, identical to pS^{21}68, except that it carries *Amp*^{R}, instead of *Kan*^{R}. The plasmid pirsS^{21}68* was used to provide a copy of *irsS*^{21}*68* allele in trans to λ*S*^{21}*68*. It was derived from plasmid pS^{21}68$_a$, with the codons encoding the *irs* epitope inserted after the Met4 codon of the *S*^{21}*68* gene.

Plasmids pETS^{21}68^{his}, pETS^{21}68$_{\Delta TMD1}{}^{his}$, and pETirsS^{21}68^{his} were used for over-expression of *S*^{21}*68*^{his}, *S*^{21}*68*$_{\Delta TMD1}{}^{his}$, and *irsS*^{21}*68*^{his}, respectively. pETS^{21}68^{his} carries

$S^{21}68$ inserted into the hyper-production plasmid pET11a, with codons encoding the purification tag GGH_6GG inserted between codons 66 and 67 (Park *et al.*, 2006). The plasmids $pETS^{21}68_{\Delta TMD1}{}^{his}$, and $pETirsS^{21}68^{his}$ are isogenic to $pETS^{21}68^{his}$ but encode the ΔTMD1 and *irs*-tagged derivatives, respectively. Each plasmid was transformed into *E. coli* strain C43(DE3) (Miroux & Walker, 1996).

For *in vivo* characterization of *$S^{21}68^{his}$* and *$irsS^{21}68^{his}$*, plasmids $pS^{21}68^{his}$ and $pirsS^{21}68^{his}$ were used, respectively. $pS^{21}68^{his}$ is identical to $pS^{21}68_a$, except that the DNA sequence encoding the his-tag was inserted between codons 66 and 67, as in the plasmid $pETS^{21}68^{his}$. Similarly, the plasmid $pirsS^{21}68^{his}$ was derived from $pirsS^{21}68$*. Each plasmid was transformed into lysogen MDS12*ΔtonA*($\lambda Q^{21}\Delta(SRRzRz1)^{21}$), for thermal induction. Single-cysteine substitutions were inserted in corresponding plasmids by site-directed mutagenesis.

Purification of $S^{21}68^{his}$

For all experiments involving purified protein, alleles encoding his-tagged *S^{21}* gene products were used, with the sequence GGH_6GG inserted between residues 66 and 67 (Park *et al.*, 2006). The presence of the oligohistidine tag had no effect on function or oligomerization (Fig. 2.15). $S^{21}68^{his}$, $S^{21}68_{\Delta TMD1}{}^{his}$, and $irsS^{21}68^{his}$ were purified from an induced culture of *E. coli* C43(DE3)(Miroux & Walker, 1996) carrying the plasmid $pETS^{21}68^{his}$, $pETS^{21}68_{\Delta TMD1}{}^{his}$, and $pETirsS^{21}68^{his}$, respectively. Induction, detergent extraction and purification of the his-tagged proteins were performed according to Savva *et al.* (2008). Briefly, cells over-expressing protein $S^{21}68^{his}$ or its variants were

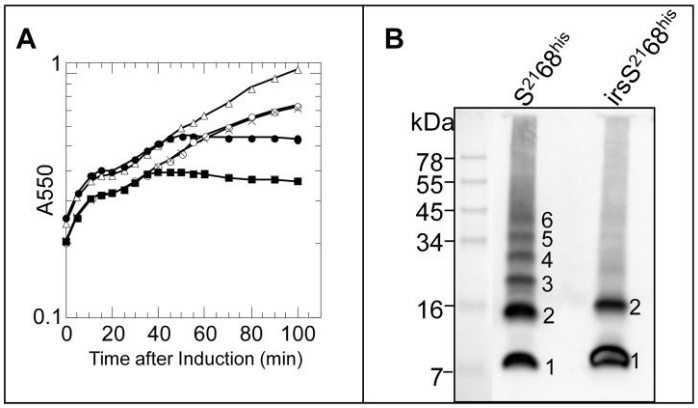

Figure 2.15. The addition of his-tag does not affect the function of $S^{21}68$.
A. Triggering of *$S^{21}68^{his}$* alleles. Cultures carrying the prophage $\lambda Q^{21}\Delta(SRRzRz1)^{21}$ and indicated plasmids were induced at t = 0 and monitored for culture growth as A_{550}. Open triangles: no plasmid. Closed circles: plasmid $pS^{21}68$. Open circles: plasmid $pirsS^{21}68$*. Closed squares: plasmid $pS^{21}68^{his}$. Crosses: $pirsS^{21}68^{his}$.
B. DSP cross-linking of $S^{21}68^{his}$ and $S^{21}68^{his}$ *in vivo*. Experiment was as described in Fig. 2.7, left panel, except that whole cells carrying prophage $\lambda Q^{21}\Delta(SRRzRz1)^{21}$ with either plasmid $pS^{21}68^{his}$ or $pirsS^{21}68^{his}$ were used.

pelleted and resuspended in lysis buffer (20 mM Tris pH7.9, 150 mM NaCl, 1 mM DTT, 1 mM EDTA, 1 mM PMSF) and lysed by passing through an French pressure cell (Spectronic Instruments; Rochester, MY) at 16,000 psi. Whole cells and cell debris were removed by centrifugation at 10,000g in a Sorvall SS-34 rotor for 15 minutes at 4°C. Membranes were harvested by ultracentrifugation at 130,000g for 90 minutes at 4°C in a Beckman Ti50.2 rotor and extracted overnight at 4°C in buffer containing 20 mM Tris pH7.9, 150 mM NaCl, 10 mM $MgCl_2$, 1 mM PMSF, and 1% (w/v) n-dodecyl-β-D-maltopyranoside (DDM; Anatrace). Soluble material was separated from insoluble material by ultracentrifugation in 4°C at 130,000g for 90 minutes, and was applied to Talon Metal Affinity Resin (Clontech) for Immobilized Metal Affinity Chromatography

(IMAC). $S^{21}68^{his}$ or its variants was eluted in buffer containing 20 mM Tris pH7.9, 150 mM NaCl, 500 mM imidazole, 0.1% (w/v) DDM.

Gel filtration chromatography

Gel filtration analysis was performed on an AKTA FPLC workstation (Pharmacia). Briefly, purified protein samples in elution buffer (20 mM Tris pH7.9, 150 mM NaCl, 500 mM imidazole, 0.1% (w/v) DDM) were centrifuged in 4°C at 130,000g for 10 minutes to remove any aggregates. A 300 µl volume of each supernatant was loaded on a Superdex^{TM} 200 10/300 GL column (Pharmacia; bed dimensions 10 × 300 mm, bed volume 24 ml, pre-equilibrated with buffer containing 20 mM Tris pH7.9, 150 mM NaCl, 0.1% (w/v) DDM) with flow rate 0.4 ml/min at room temperature, eluted with the same pre-equilibration buffer and collected in 1 ml fractions.

Electron microscopy

Purified protein at 0.5µM was applied to freshly glow-discharged formvar-carbon coated grids and stained with 2% (w/v) aqueous uranyl acetate according to the method of Valentine *et al.* (1968). Micrographs were recorded on a JEOL 1200EX TEM operating at 100 KV, with a calibrated magnification of 48,600X, and scanned on a Leafscan 45 microdensitometer to a final sampling size of 4.12 Å/pixel at the specimen level. Approximately 900 particles for $S^{21}68^{his}$, 1,100 particles for $S^{21}68_{\Delta TMD1}{}^{his}$ and 710 particles for $irsS^{21}68^{his}$ were selected manually, low-pass filtered to remove high-

frequencies beyond 10 Å, and subjected to iterative, reference-free classification using the refine2d.py command in the EMAN (Ludtke *et al.*, 1999) software package.

Cysteine modification

Cultures were grown to A_{550} = 0.4, induced with IPTG/arabinose or by a thermal shift, as appropriate, and aerated past the time of holin triggering or, in the case of non-lethal *S*^{21}*68* alleles, for 50 min. Cells corresponding to 0.25 A_{550} units were collected by centrifugation, washed twice with 1 ml PB (50 mM phosphate buffer, pH7) and then re-suspended in 0.25 ml of PB. Each sample was divided into two 125 µl aliquots. To one, 10 mM MTSES (Anatrace) was added and to the other, an equivalent amount of water was added. After 30 min at room temperature, 50 mM L-cysteine was added to quench any unreacted MTSES. After 10 minutes, the cells were diluted by the addition of 0.75ml PB, collected by centrifugation, washed twice with 1 ml PB, resuspended in 100 µl PB and extracted with of 750 µl chloroform: methanol: water (1:4:1). After incubation on ice for 30 min, the denatured and delipidated proteins were collected by centrifugation at 13,000g for 5 min at 4℃ . The protein pellets were washed once with 400 µl 95% methanol and resuspended in 100µl PEGylation buffer (10M urea, 1% SDS, 1 mM EDTA, 0.6 M Tris, pH7, adapted from Lu *et al*. (2001)). 50µl of each sample was transferred to a clean tube and treated with 0.2 mM mPEG-maleimide (Creative Biochem) for 30 min at room temperature, and then precipitated with 1 ml cold ethanol. After overnight at -20°C, proteins were collected by centrifugation at 13,000g for 15 minutes at 4°C. The pellets were air-dried and resuspended in sample loading buffer for

analysis by SDS-PAGE (Tran *et al.*, 2007). For experiments involving depolarization of the membrane, 1mM DNP was added into the culture at the time of harvesting and used to supplement PB in each step until quenching with L-cysteine.

Chemical cross-linking

A culture volume corresponding to 1 A_{550} unit was harvested, washed and resuspended in 640 µl of PBS (phosphate buffered saline, containing 0.1 M sodium phosphate, 0.15 M NaCl; pH7.2), and treated with 2 mM DSP (Pierce) at room temperature for 30 min. The reaction was quenched by the addition of 20 mM Tris, pH7.5 and the proteins were collected by precipitation with trichloroacetic acid for analysis by SDS-PAGE. For the DSP cross-linking of purified $S^{21}68^{his}$ or its variants, 1 pmol of each protein in 0.1% DDM was used. The reaction was mixed with 2X sample loading buffer directly after quenching, boiled for 5 min and analyzed by SDS-PAGE.

SDS-PAGE and Western blotting

Sodium dodecyl sulfate-polyacrylamide gel electrophoresis (SDS-PAGE) and Western blotting was performed as described (Park *et al.*, 2006). Briefly, 10% Tris-Tricine gels were used to separate protein samples. Proteins were then transferred to either 0.2 µm PVDF membranes (Pall), for $S^{21}68$ and $irsS^{21}68$ protein variants; or 0.1 µm nitrocellulose membranes (Whatman, NJ) for $S^{21}68_{\Delta TMD1}$ protein variants. An antibody raised in rabbit against the S^{21} C-terminal peptide KIREDRRKAARGE was used as primary antibody to detect S^{21} protein variants (Barenboim *et al.*, 1999), at a

dilution of 1:1,000, and pre-incubated with *E. coli* strain MG1655 *lacI*^{q1} *tonA::*Tn*10* or RY17341 cell lysates to reduce background. Horseradish peroxidase-conjugated goat-anti-rabbit secondary antibody (Pierce) was used at a dilution of 1:4,000. Except Fig. 2.12, blots were developed by using the Supersignal West Femto maximum sensitivity substrate kit (Thermo Scientific) according to the manufacturer's instructions. Images were obtained by using the Molecular Imager Gel Doc XR system (Bio-Rad) and analyzed by software Quantity One (Bio-Rad). The blot in Fig. 2.12 was developed by the chromogenic substrate 4-chloro-1-naphthol (Sigma).

Computational methods

A 24-residue sequence corresponding to residues 36-58 of the S^{21} TMD2 (WAAIGVLGSLVLGFLTYLTNLYF; Fig. 2.1A) was used to compute oligomeric pinholin structures using CHI. The simulated annealing search calculation protocols have previously been described in detail (Adams *et al.*, 1995, Adams *et al.*, 1996), except that the CHI suite of scripts uses CNS to implement the molecular dynamics. The OPLS topology and parameter sets were used with all polar hydrogens included (Jorgensen & Tirado-Rives, 1988). CHI uses an implicit membrane solvent with a dielectric constant = 2.

Conformations of TMD2 oligomers ranging from n=4-7 were independently generated in different computational searches. Each oligomeric state was symmetrically searched with a helix rotation angle, α, ranging from 0-360˚ and a sampling step size of 5˚, starting with both left- (Ω =45˚) and right-handed crossing angles (Ω =-45˚). For

each oligomer, four trials were carried out for each rotation and crossing angle conformation using simulated annealing of all atomic coordinates during which rotation- and crossing-angles were free to vary. The resulting 576 structures were analyzed to determine the final rotation and crossing angles. Clusters of low-energy structures were calculated by determining the frequency of structures appearing in a particular region of interaction space using a cutoff of 1.0 Å root mean square deviation and a minimum requirement of ten structures to define a cluster. An average structure for each cluster was calculated and evaluated for consistency with the experimental data on the MTSES sensitivity and pore size from permeability.

The A- and B- helix-helix interaction surfaces were identified for the experimentally compatible oligomeric structures by calculating the distribution of inter-chain interactions using the occluded surface algorithm (Pattabiraman *et al.*, 1995, Fleming & Engelman, 2001). The occluded surface can be thought of as the contacting molecular surface between two helices and is represented in Fig 2.9 as a dot surface. Hydrogen bonding interactions were calculated using HBPLUS (McDonald & Thornton, 1994).

CHAPTER III

MUTATIONAL ANALYSIS OF THE S^{21} PINHOLIN*

Introduction

In phage lysis, canonical holins, like the lambda S105 and T4 T proteins, terminate the infection cycle by suddenly "triggering" to form very large holes in the cytoplasmic membrane at the end of an allele-specific period of accumulation in the bilayer (Young & White, 2008, Dewey *et al.*, 2010). These lesions allow the non-specific escape of the phage endolysin, fully folded and enzymatically functional, across the bilayer, leading to lysis within seconds. Recently, a second type of holin, designated as a pinholin, has been discovered (Park *et al.*, 2007). Pinholins get their name from the fact that they form small holes that simply depolarize the membrane, rather than allowing the non-specific escape of a folded protein. To effect lysis, pinholins require SAR endolysins, which have an N-terminal transmembrane domain (TMD) that engages the *sec* translocon and results in export of the endolysin in an inactive, membrane-tethered form (Xu *et al.*, 2004, Sun *et al.*, 2009). When the pinholins trigger to depolarize the membrane, these membrane-tethered enzymes are released from the bilayer and re-fold to the active state, resulting in destruction of the murein and lysis. For both pinholins and canonical holins, the molecular basis for the allele-specific timing of the triggering event is unknown. However, they share a common characteristic: they

---

* Reprinted with permission from "Mutational analysis of the S^{21} pinholin" by Pang, T., Park, T. & Young, R., 2010. *Mol Microbiol.* **(In Press.)**

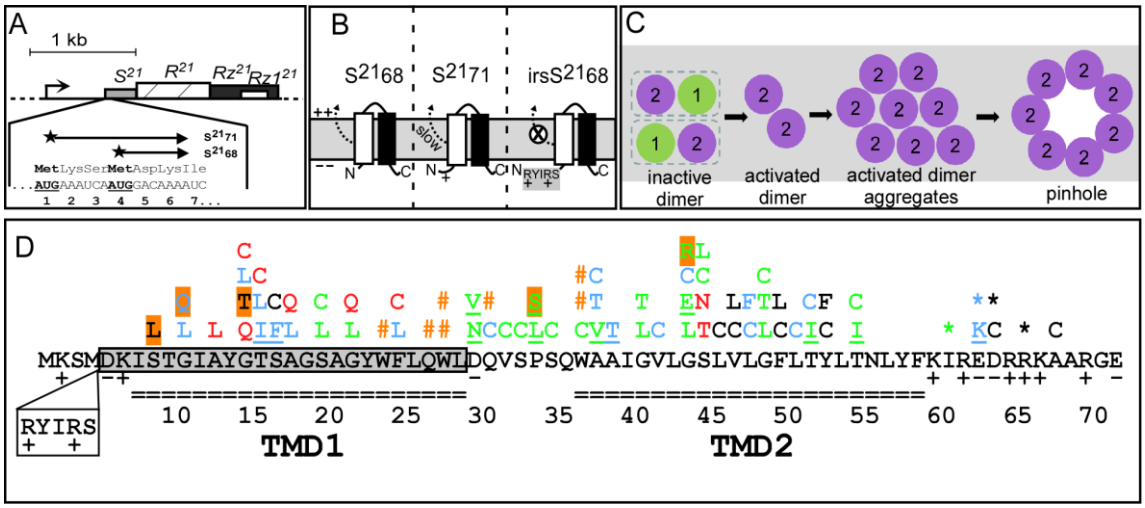

Figure 3.1. Features of the phage 21 holin. A. Phage 21 lysis cassette. Phage 21 lysis genes *S*, *R*, *Rz*, *Rz1* are located downstream of the late gene promoter, indicated by the arrow. S^{21} gene has a dual-start motif, which encodes both a holin $S^{21}68$ (translated from the Met4 start codon), and an antiholin $S^{21}71$ (translated from codon Met1) (Barenboim *et al.*, 1999, Park *et al.*, 2006). Both start codons are bold and underlined.

B. The membrane topology of $S^{21}68$ (left), $S^{21}71$ (middle), and $irsS^{21}68$ (right). TMD1: white box; TMD2: black box. The TMD1 of $S^{21}68$ is initially inserted in the membrane but later released into the periplasm (Park *et al.*, 2006) (see panel C). The externalization of TMD1 is delayed in the context of $S^{21}71$ and completely blocked in the context of $irsS^{21}68$, which has the *irs*-tag (RYIRS) fused to the N-terminus of $S^{21}68$.

C. Model of $S^{21}68$ hole formation pathway (top-down view from periplasm). The two TMDs (green: TMD1; purple: TMD2) in a single $S^{21}68$ molecule are boxed. Initially, both TMDs of $S^{21}68$ are inserted in the membrane in an inactive dimer form. When TMD1 is released, the inactive dimer is converted into an activated dimer form. Activated dimers then aggregate and nucleate to form heptameric pinholes. (Modified from Pang *et al*. (2009), with permission.)

D. The distribution of mutations on the S^{21} reading frame. The S^{21} reading frame is shown, with TMD1 and TMD2 indicated by the double-line underscore. The residues deleted in $S^{21}68_{\Delta TMD1}$ are shaded in gray. The position and sequence of the *irs* epitope in $irsS^{21}68$ is shown as a box below the sequence. Individual $S^{21}68$ mutants in the collection are shown above the amino acid sequence. Pound signs and underlined mutations represent nonsense and missense mutations obtained by EMS mutagenesis and selection, respectively; all others were obtained by site-directed mutagenesis. Asterisks mark the position of ochre nonsense mutations, Color code: black, no significant change in triggering time compared to the parental; red, accelerating triggering time by >15 m; blue, delayed triggering by >10 m; green, triggering abolished. Highlighted mutants have reduced or undetectable level of protein.

both can be prematurely triggered to lethal hole-formation by artificial depolarization of the membrane with energy poisons and uncouplers (Xu *et al.*, 2004, Park *et al.*, 2006).

The prototype pinholin is $S^{21}68$, the holin of the lambdoid phage 21. $S^{21}68$ is one of two products of S^{21}, the first gene in the phage 21 lysis cassette (Fig. 3.1A). The pathway to pinhole formation begins with the holin protein in an inactive form, with both of its two transmembrane domains (TMDs) in the bilayer (Fig. 3.1B, C) (Park *et al.*, 2006). To proceed towards pinhole formation, TMD1 (Fig. 3.1C, D) must exit from the membrane, an event which happens spontaneously in a time-dependent fashion after insertion of $S^{21}68$ into the membrane. This change in membrane topology can be accelerated if the membrane is artificially depolarized with an uncoupler. In contrast, the topology change is completely blocked for a lysis-defective allele, $irsS^{21}68$, which has the *irs* epitope, containing two positively charged residues, at the N-terminus of its protein product (Fig. 3.1B, D). The $irsS^{21}68$ allele is dominant and cross-linking studies indicate that its product dimerizes with $S^{21}68$ protein (Pang *et al.*, 2009). Thus it has the properties of an antiholin, a heterogeneous class of holin-specific inhibitors encoded by many bacteriophages (Wang *et al.*, 2000, Young & Wang, 2006), either as alternate product of the holin gene (Bläsi *et al.*, 1990) or an unlinked gene (Ramanculov & Young, 2001a, Tran *et al.*, 2005). In fact, S^{21} produces a second polypeptide, $S^{21}71$, by virtue of translational starts three codons upstream of the start used for the $S^{21}68$ holin (Fig. 3.1A) (Barenboim *et al.*, 1999). $S^{21}71$ has weak antiholin character, in that membrane escape of TMD1 is delayed but not blocked, presumably because it has only a single positively charged residue at its N-terminus (Fig. 3.1A, B, D). Taken together,

these results suggested a model in which the products of *S*^{21} first populate an inactive dimer stage, where TMD1 is retained in the membrane (Fig. 3.1C). In the subsequent pathway to pinhole formation, the pinholins in the inactive dimer are first converted to an "activated" state, with TMD1 externalized, ultimately leading to an oligomer within which the heptameric pinhole forms. Evidence for the activated dimer is indirect, in that cysteine substitutions in TMD1 can lead to the periplasmic formation of intermolecular disulfide linkages in an orientation-specific manner (Park *et al.*, 2006). Periplasmic interaction of TMD1 is not required for pinhole formation, because a mutant in which all of TMD1 has been deleted retains robust triggering ability.

The structure of the pinhole in the membrane has been interrogated with cysteine-accessibility studies, using a library of cysteine-substitutions at positions throughout the pinholin sequence, with cross-linking experiments using the amine-specific reagent DSP (dithiobis[succinimidyl propionate]), and with computational approaches using coarse-grained simulated annealing of the TMD2 sequence (Pang *et al.*, 2009). These efforts led to a heptameric model for the minimal pinhole, in which seven TMD2 domains oriented at 31° to the plane of the membrane form a left-handed helical bundle around a channel of ~1.5 nm diameter.

These recent results provide a much more comprehensive picture of the functional and structural aspects of the S^{21} pinholin than is available for any of the previously studied holins. Here we report an extensive mutational analysis of *S*^{21}and discuss the results in terms of the model for the structure of the inactive dimer that is proposed to be the first significant intermediate in the pinhole formation pathway.

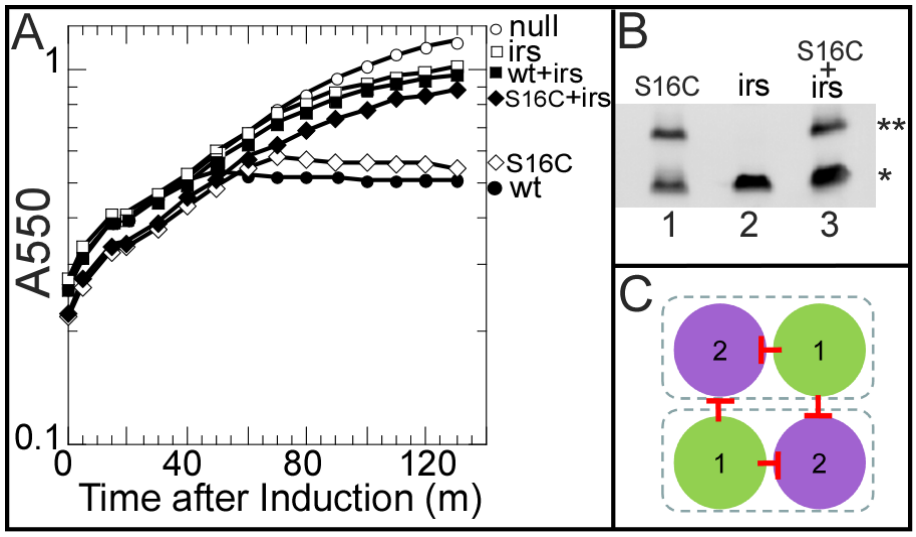

Figure 3.2. irsS^{21}68 does not inhibit the externalization of S^{21}68 TMD1.
A. Triggering of *S^{21}68* alleles. Cultures were induced at t=0 and monitored for growth as A_{550}. Open circles, prophage λ*Q^{21}Δ(SRRzRz1)^{21}*, no plasmid. Closed circles, prophage λ*S^{21}68*, no plasmid. Open squares, prophage λ*Q^{21}Δ(SRRzRz1)^{21}*, plasmid pirsS^{21}68*. Closed squares, prophage λ*S^{21}68*, plasmid pirsS^{21}68*. Open diamond, prophage λ*S^{21}68$_{S16C}$*, no plasmid. Closed diamond, prophage λ*S^{21}68$_{S16C}$*, plasmid pirsS^{21}68*.
B. Periplasmic disulfide-bond formation with S^{21}68$_{S16C}$. Cultures were induced and precipitated by TCA at 1 h after induction. Samples were resuspended in sample loading buffer without reducing agent and analyzed by SDS-PAGE and Western blotting. The primary antibody detects both the S^{21}68 variants and irsS^{21}68 since the epitope is at the S^{21} C-terminus. Double and single asterisks indicate the position of dimer and monomer, individually. Lane 1, prophage λ*S^{21}68$_{S16C}$*, no plasmid. Lane 2, prophage λ*Q^{21}Δ(SRRzRz1)^{21}*, plasmid pirsS^{21}68*. Lane 3, prophage λ*S^{21}68$_{S16C}$*, plasmid pirsS^{21}68*.
C. Top-down view of the inactive dimer. Same scheme as Fig. 3.1C. TMD1 interacts with TMD2 both inter- and intra- molecularly, depicted by the red stop arrows.

Results

TMD1 inhibits TMD2 pinhole formation in both cis and trans

Previously, we provided evidence that TMD1 is externalized to the periplasm by showing that the cysteine-substitution protein, S^{21}68$_{S16C}$, forms disulfide-linked dimers

during the pathway to pinhole formation (Park *et al.*, 2006). We wondered whether the functional inhibition exerted by irsS^{21}68 also extended to the topological change of the inhibited pinholin. To answer this question, we assessed disulfide-dimer formation by S^{21}68$_{S16C}$ in the presence of the antiholin allele (Fig. 3.2A, B). No change in dimer formation was observed, although the lethal function of the cysteine-substitution protein was completely inhibited by irsS^{21}68. This indicates that irsS^{21}68 does not inhibit the externalization of S^{21}68 TMD1 and suggests that the inhibition effect must be due to the interaction of the membrane-embedded *irs*-tagged TMD1 of irsS^{21}68 with TMD2 of S^{21}68. Coupled with the previous results (Park *et al.*, 2006), these data indicate that membrane-embedded TMD1 could interact with TMD2 both intermolecularly and intramolecularly (Fig. 3.2C). The strong lysis-timing and survival phenotypes available in this system suggested that a genetic analysis could identify the helix-helix interfaces involved.

Mutants in each topological domain of S^{21}68 have altered triggering phenotypes

An extensive library of *S^{21}68* missense alleles was generated by two methods (Table 3.1). First, loss of function mutants were obtained by selecting for a defect in the lethal pinhole formation after EMS mutagenesis (Table 3.2). In this selection, 39 mutants were isolated with missense or nonsense mutations in the *S^{21}68* gene, which resolved into 7 unique nonsense and 13 unique missense mutations (Table 3.1, asterisk entries; Table 3.2; Fig. 3.1D). There are 10 nonsense mutations accessible by transition mutation from the parental *S^{21}68* base sequence. The most distal of these, R65op, is likely to

Table 3.1. *S[21]68* mutants.

loc[1]	allele[2]	full-length[3]		Δ(TMD1)[4]		irsS[21]68[5]	
		T[6]	Prot[7]	T[6]	Prot[7]	alone[8]	+wt[9]
	wt	0	1	0	1	NL	NL
TMD1	S8L	0	0.2			NL	NL
	G10L	+40					
	G10Q	+40	0.2				
	A12L	-35				NL	70
	G14Q	-35				30	70
	G14T	0					
	G14L	+40					
	G14C	-35				NL	NL
	T15I*	+40					
	T15L	+40					
	T15C	-35				NL	NL
	S16F*	+30					
	S16C	0					
	A17L	+60					
	A17Q	-35				60	40
	S19L	NL					
	S19C	NL					
	G21L	NL					
	G21Q	-35				110	80
	F24L	+40					
	F24C	-20					
Loop	D29N*	NL		0			
	D29V*	NL		+40			
	Q30C	+40		+20	0.4		
	V31C	NL		+10			
	S32C	NL		-40			
	P33L*	NL		NL			
	P33S*	NL	0				
	S34C	NL		+10			
TMD2	W36C	NL		NL	0.01		
	A37V*	NL		NL			
	A37T	+30		-30			
	A37C	+40		+30			
	A38T*	+50		-20			
	G40L	NL		NL	0.4		
	G40T	NL		NL			
	V41C	+40		-10			
	G43L	NL		NL			
	G43E*	NL		NL	0.2		
	G43R*	NL	0				
	G43C	+40		+50			
	S44L	NL		+30	0.3		
	S44T	-35		NL		90	NL
	S44N	-35		-45		NL	NL
	S44C	NL		NL	0.4		

Table 3.1.Continued.

loc[1]	allele[2]	full-length[3]		Δ(TMD1)[4]		irsS^{21}68[5]	
		T[6]	Prot[7]	T[6]	Prot[7]	alone[8]	+wt[9]
	L45C	+10		+30	0.2		
	V46C	0		-10			
	V46L	+10		0			
	L47C	+60		+20			
	L47F	+50		0			
	G48L	NL		NL			
	G48T	NL		+20			
	G48C	NL		NL			
TMD2	F49C	-10		-10			
	F49L	0		0			
	L50C	+30		+30	0.2		
	T51I*	NL		NL			
	T51C	+20		NL			
	Y52C	0		NL	0.4		
	Y52F	+10		-10			
	T54I*	NL		NL			
	T54C	NL		NL			
	I60$_{och}$[10]	NL	nt	NL	nt		
	E62$_{och}$	+40	nt	+60	nt		
	E62K*	+40		NL			
tail	D63$_{och}$	0	nt	+30	nt		
	D63C	0		0			
	R65$_{och}$	0	nt	+30	nt		
	A67C	0		0			

[1] Topological domain
[2] Mutant alleles. Asterisk: mutants generated by EMS mutagenesis.
[3]relative to parental S^{21}68
[4]relative to parental S^{21}68$_{\Delta TMD1}$
[5]relative to parental irsS^{21}68
[6]change in triggering time of each mutant (m) relative to the parental allele (50 m after induction for both S^{21}68 and S^{21}68$_{\Delta TMD1}$). NL: non-lethal.
[7]The protein accumulation level of each mutant. Only mutants with significantly lower amount of protein accumulated than wildtype are shown. The number indicates the protein amount as a ratio to the wildtype. nt, not tested.
[8]The triggering time of each irsS^{21}68 mutant (m). The parental irsS^{21}68 is NL (non-lethal).
[9]The triggering time of each irsS^{21}68 mutant in the presence of S^{21}68 expressed from prophage λ*S^{21}68*. The wt irsS^{21}68 inhibits the triggering of S^{21}68 and is thus labeled as NL.
[10] Ochre stop codon substitution of that residue.

Table 3.2. Independent $S^{21}68$ lysis-defective alleles recovered from EMS mutagenesis.

codon	amino acid change		codon change		isolates
15	Thr	Ile	ACA	ATA	4
16	Ser	Phe	TCT	TTT	1
23	Trp	End	TGG	TGA	2
26	Gln	End	CAG	TAG	1
27	Trp	End	TGG	TAG	1
27	Trp	End	TGG	TGA	3
29	Asp	Asn	GAT	AAT	4
29	Asp	Val	GAT	GTT	1
30	Gln	End	CAG	TAG	1
33	Pro	Leu	CCG	CTG	1
33	Pro	Ser	CCG	TCG	1
36	Trp	End	TGG	TAG	1
36	Trp	End	TGG	TGA	2
37	Ala	Val	GCT	GTT	1
38	Ala	Thr	GCG	ACG	3
43	Gly	Glu	GGA	GAA	4
43	Gly	Arg	GGA	AGA	1
51	Thr	Ile	ACT	ATT	5
54	Thr	Ile	ACA	ATA	1
62	Glu	Lys	GAA	AAA	1

retain lethality, based on the analysis of the C-terminal mutations (see below). Thus 7 of 9 (78%) possible nonsense mutations were recovered in the selection for loss of lethality. These considerations and the degree of repeats of the missense alleles isolated (Table 3.2) indicate that the selection was near saturation, in terms of mutations accessible by a single base change. Other than the extremely short N-terminal cytoplasmic domain, which in $S^{21}68$ consists of only 3 residues, each of the other four topological domains (TMD1, loop, TMD2 and C-terminal cytoplasmic tail) had at least one position where

non-lethal mutations were selected (Table 3.2; Fig. 3.1D). It should be noted that the plasmid context used for the selection was a hybrid, with S^{21} inserted in the place of *S* in the λ lysis cassette, but the phenotypic analysis was done with these alleles re-created in the context of the complete phage 21 lysis cassette. In a few cases (T15I, S16F, A38T, E62K), the mutant alleles recovered lethal function, albeit significantly delayed, as observed for lambda *S* mutants selected in a similar plasmid-based system (Raab *et al.*, 1986). As before, this is likely because the expression level in the selection for loss of lethality was somewhat lower than that attained in the induced prophage and the cognate late gene expression context.

Many other mutants were obtained by site-directed mutagenesis, including a number constructed for Cys-substitution experiments aimed at probing the lumenal residues of the pinhole (Pang *et al.*, 2009). The mutant alleles were subjected to phenotypic analysis, including triggering time and accumulation of the mutant protein (Table 3.1).

In overview, three mutant triggering phenotypes were observed: non-lethal (no triggering after induction), delayed, and early, summarized in Table 3.1 and Fig. 3.1D. For delayed or non-lethal mutants, only those with normal levels of protein accumulation are included in the analysis below.

TMD1 mutants suggest its orientation in the inactive dimer

Since TMD1 is not required for lethal function but must be removed from the bilayer to allow fruitful oligomerization by TMD2, any mutation in TMD1 affecting the

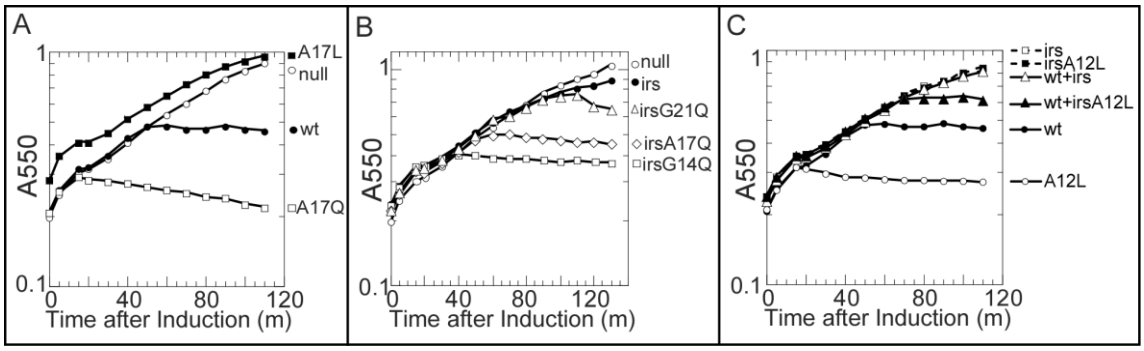

Figure 3.3. Triggering phenotypes of TMD1 mutants. Same procedure as in Fig. 3.2A.

A. A17 mutant phenotypes mirror hydrophobicity. Each culture contained prophage $\lambda Q^{21}\Delta(SRRzRz1)^{21}$, with no plasmid (open circles), or plasmids $pS^{21}68$ (closed circles), $pS^{21}68_{A17Q}$ (open squares), or $pS^{21}68_{A17L}$ (closed squares).

B. Hydrophilic changes suppress the triggering defect of $irsS^{21}68$. Each culture contained prophage $\lambda Q^{21}\Delta(SRRzRz1)^{21}$ with no plasmid (open circles), or plasmids: $pirsS^{21}68^*$ (closed circles), $pirsS^{21}68^*_{G14Q}$ (open squares), $pirsS^{21}68^*_{A17Q}$ (open diamonds), or $pS^{21}68_{G21Q}$ (open triangles).

C. A12L confers early triggering and reduces trans inhibition by $irsS^{21}68$. Circles, prophage $\lambda Q^{21}\Delta(SRRzRz1)^{21}$ with either $pS^{21}68$ (closed), or $pS^{21}68_{A12L}$ (open). Dashed line with squares, prophage $\lambda Q^{21}\Delta(SRRzRz1)^{21}$ with either $pirsS^{21}68^*$ (open), or $pirsS^{21}68^*_{A12L}$ (closed). Triangles, prophage $\lambda S^{21}68$ with either $pirsS^{21}68^*$ (open), or $pirsS^{21}68^*_{A12L}$ (closed).

triggering time is most likely affecting its ability to exit the membrane. Presumably, such changes would be due either to changing its inter- or intramolecular affinity for TMD2, or changing its hydrophobicity, or both. The clearest example of such effects comes from mutations at Ala17, where changes to the more hydrophilic Gln and the more hydrophobic Leu had the expected opposite effects on triggering time (Fig. 3.3A, Table 3.1): dramatically early triggering for the former and drastically delayed for the latter. Similar patterns were observed at Gly14 and Gly21 (Table 3.1). The simplest interpretation is that these positions face the lipid (Fig. 3.4A), a notion supported by the

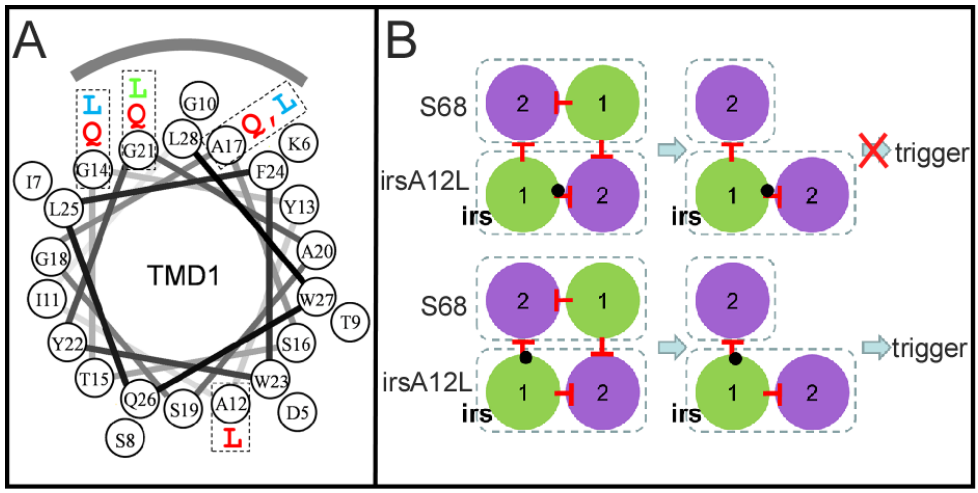

Figure 3.4. Mapping TMD1 mutations.
A. Helical wheel projection of S^{21}68 TMD1. Mutations used to analyze the orientation of TMD1 in the inactive dimer are labeled with the same color code as Fig. 3.1D. The shaded arc indicates the face interacting with lipid in the inactive dimer.
B. The effect of the position of A12L on the antiholin function of irsS^{21}68. Upper, A12L mutation (black dot) in the context of irsS^{21}68 is shown either affecting the cis (intramolecular; upper diagram) or the trans (intermolecular; lower diagram) interaction with TMD1. In the former, inhibition of triggering should be maintained, but not in the latter.

fact that the early-triggering mutants G14Q, A17Q and G21Q all restored lytic function in the context of irsS^{21}68 (Fig. 3.3B, Table 3.1).

In contrast, an Ala →Leu change at position 12 on the opposite face of TMD1, although increasing hydrophobicity, dramatically advanced triggering (Fig. 3.3C, 4A), suggesting that the A12L mutation destabilizes a TMD1- TMD2 interaction. We reasoned that if it was the cis (intramolecular) interaction that was affected, then A12L would not affect the negative dominance in the context of irsS^{21}68 (Fig. 3.4B, upper). However, the opposite was observed, with irsS^{21}68$_{A12L}$ clearly compromised in its

antiholin character (Fig. 3.3C). This suggests that A12L disrupts the trans (intermolecular) TMD1-TMD2 interface (Fig. 3.4B, lower).

Substitutions with cysteine at five positions in TMD1 generated a wide range of phenotypes: dramatic advance of the triggering time (G14C, T15C), small advance or no change (S16C, F24C), and abolition of triggering (S19C) (Table 3.1). These changes clearly cannot be interpreted in terms of a significant alteration in hydrophobic character. The phenotypes are complicated by the fact that, after extraction from the bilayer, TMD1 undergoes homotypic interactions that, in the case of S16C, can lead to disulfide-bond-linked homodimer formation (Park *et al.*, 2006). To assess the degree of covalent dimerization, cells were harvested by TCA (trichloroacetic acid) precipitation at the time of triggering (or at 60 m for the non-triggering allele S19C). Western blot analysis of these samples prepared in the absence of reducing agent revealed that the two very early lysis mutants, G14C and T15C, and the S16C mutant have a substantial fraction of the pinholin in covalently linked dimer state at the time of triggering (Fig. 3.5A). When DTT (dithiothreitol) was added to the cultures immediately after induction, disulfide bond formation was reduced or eliminated and the triggering times of all three mutants were significantly delayed, indicating that in all three cases disulfide bond formation contributes positively to pinhole formation.

Mutations in the periplasmic loop

The periplasmic loop was significantly over-represented among the mutants selected for loss of lethality after EMS mutagenesis (Fig. 3.1D, Tables 3.1, 3.2). At

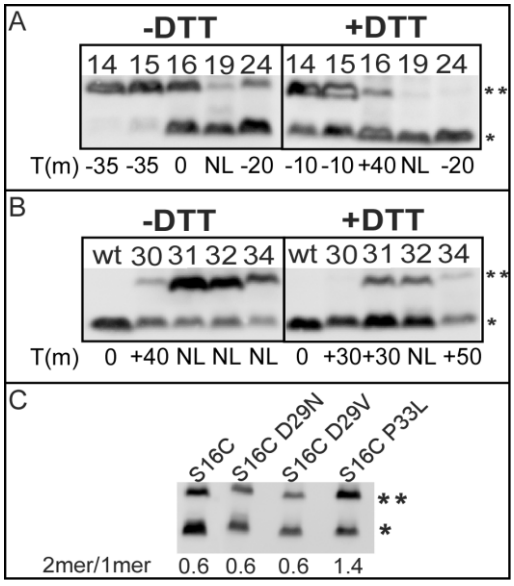

Figure 3.5. Western blots.

A, B. The effect of DTT on the disulfide-bond formation of $S^{21}68$ cysteine mutants.

Cultures carrying prophage $\lambda Q^{21}\Delta(SRRzRz1)^{21}$ and derivatives of plasmid $pS^{21}68$ were thermally induced and precipitated by TCA either at the time of triggering or, for the delayed or non-lethal mutants, at the time when $S^{21}68_{S16C}$ triggers. Samples were analyzed by SDS-PAGE and Western blotting without reducing agent. Right panels show samples from cultures treated with 1 mM DTT at the time of induction. Numbers on each lane indicate residue positions of Cys substitutions. Asterisks indicate the position of monomer and dimers, as in Fig 3.2B. The triggering time of each mutant relative to that of wt $S^{21}68$, in minutes, is indicated at the bottom. **A,** Cys substitutions in TMD1. **B,** Cys substitutions in the connecting loop.

C. The effect of each mutation on the externalization of $S^{21}68$ TMD1.

Same procedure as in Fig 3.2B, except that cells carried prophage $\lambda Q^{21}\Delta(SRRzRz1)^{21}$ with derivatives of plasmid $pS^{21}68$ encoding mutations on the $S^{21}68$ gene as indicated on top of each lane. Asterisks indicate the position of monomer and dimers, as in Fig 3.2B. The dimer to monomer ratio of each mutant is illustrated on the bottom.

D29, the only possible G to A transition, resulting in D29N, was among the non-lethal isolates selected, as well as the presumably much rarer D29V, which requires an A to T transversion. Both of the missense mutations accessible by a C to T transition mutation from P33 (P33L, P33S) were also selected. Moreover, every site-directed change made

in the loop residues, all of which resulted in Cys substitutions, caused a non-lethal or severely delayed lysis phenotype (Fig. 3.1D, Table 3.1). However, in these cases, the formation of the disulfide bond appears to be irrelevant to the triggering defect, since DTT treatment reduced or eliminated the formation of the linkages but did not affect the triggering time significantly (Fig. 3.5B). The simplest explanation for these defects would be that changes in the loop would compromise externalization of TMD1, in which case the defective alleles should regain lethality in the ΔTMD1 context. However, neither of the D29 mutants nor P33L had a detectable defect in terms of externalization of TMD1, as indicated by the effect of mutation on the dimer to monomer ratio of $S^{21}68_{S16C}$ (Fig. 3.5C). Moreover, D29V significantly delayed the triggering and P33L retained the non-lethal character in the $S^{21}68_{\Delta TMD1}$ context (Table 3.1). These results suggest that these mutations exerted their effects at stages beyond TMD1 export.

Analysis of mutants in TMD2 suggests faces for TMD1 interaction

Phenotypic analysis of mutations in TMD2 (Fig. 3.1D, Table 3.1) is more difficult because each change could affect the release of TMD1, by interfering with the TMD1-TMD2 interaction or TMD2-TMD2 interactions downstream in the pathway to pinhole formation. To identify the residues involved in the TMD1- TMD2 interface in the inactive dimer form, the effect of each mutation was tested both in the context of the full-length and TMD1 deletion alleles. Mutations in five positions (A37T, A38T, V41C, L47F, G48T; Fig. 3.6A; Table 3.1) were found to affect the triggering time of $S^{21}68$ and $S^{21}68_{\Delta TMD1}$ differently, without affecting accumulation of either, and in each case, the

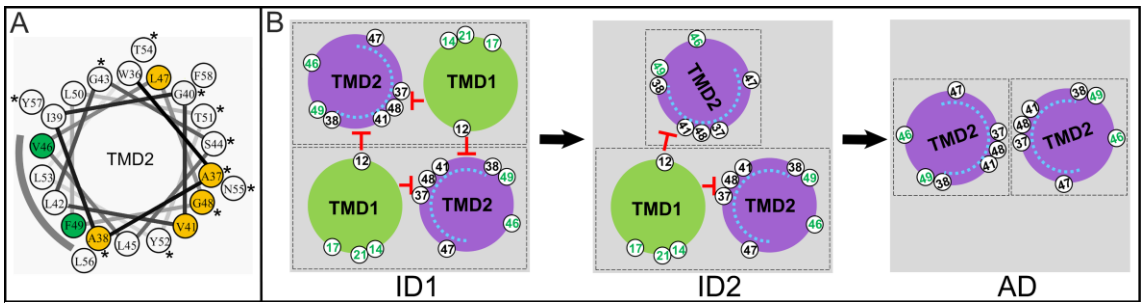

Figure 3.6. Orientation map of the inactive dimer.
A. Helical wheel projection of TMD2. Positions where mutations exhibit accelerated lethal function in the ΔTMD1 context, and thus predicted to interact with TMD1, are colored in orange. V46 and F49, colored in green, exhibit phenotypic insensitivity and thus are likely to be facing the lipid, indicated by the shaded arc. Hydrophilic and weakly hydrophobic residues are indicated by asterisk.
B. The orientations of TMD1 and TMD2 in the inactive dimer. Same scheme as in Fig. 3.1C, but, in addition, residue positions are indicated in white circles. Residues predicted to face lipid and involved in TMD1-TMD2 interactions are colored green and black, respectively. The blue arc inside TMD2 represents the extent of the hydrophilic and weakly hydrophobic residues that eventually face the lumen of the pinhole. ID1, 2 = inactive forms 1 and 2; AD = putative activated dimer.

lethal function was improved, either recovering lethality or triggering earlier, in the ΔTMD1 context (Table 3.1). This indicates that the original defect in each case was due to the retention of TMD1 in the bilayer. It follows that these positions, occupying a wide arc on the helical surface of TMD2, are likely to be involved in a TMD1-TMD2 interface (Fig. 3.6A), either intramolecular or intermolecular, and that the mutations increase the affinity of TMD2 for TMD1.

In comparison with the analysis of TMD1 mutations (see above), there is less clear evidence specifying a lipid-interacting face of TMD2. However, replacing residues V46 or F49 with either C or L has no effect on the triggering time of either $S^{21}68$ or $S^{21}68_{\Delta TMD1}$ (Table 3.1). The tolerance of these two positions to major changes in side

chain architecture suggests that they may not be involved in protein- protein interactions and may thus face the lipid (Fig. 3.6A).

Mutations in the C-terminal cytoplasmic domain

A nearly universal feature of class I and II holins is the presence of a short cytoplasmic C-terminus, usually very hydrophilic and carrying predominantly positively charged residues (Young & Wang, 2006). $S^{21}68$ is no exception, with a 13 residue cytoplasmic tail bearing 9 charged residues, six of which are Arg or Lys (Fig. 3.1D). Table 3.1 shows that most of this domain is dispensable, since a stop codon at D63, eliminating 9 of the 13 residues, has no effect on lysis timing. Stops earlier in the reading frame severely damage or ablate lethal function, but, since the antibody used is specific for the C-terminal oligopeptide sequence, it is not known whether protein localization or accumulation is compromised. Finally, E62K, which increases the number of basic residues by one and the overall predicted positive charge by two, is a lysis-delay allele in the full-length context and is non-lethal in the deletion context (Table 3.1). Similar inhibitory phenotypes have been observed for analogous mutants in the C-terminal cytoplasmic domain of the canonical class I holin, lambda S105 (Bläsi *et al.*, 1999), suggesting a regulatory role for this domain in both types of holin.

Discussion

The temporally-regulated lethal function of phage holins is not only an important fundamental process in its own right, as the most common cytocidal event in the

biosphere, but is also arguably one of the simplest temporally scheduled processes in biology. Holin triggering occurs with remarkable precision at an allele-specific time on a 10 – 100 minute time scale after the onset of holin gene expression (Young & Wang, 2006). The recently discovered pinholin class of holins is a particularly attractive system for dissecting this fundamental process, because of the small size of the pinholin, only 68 residues, the interesting dynamic membrane topology of its TMD1, and the rather simple nature of the lethal pinhole, a heptamer of TMD2 (Pang *et al.*, 2009). Here we analyze the cellular and molecular phenotypes of an extensive collection of S^{21} mutants in an effort to dissect the pathway to pinhole formation and to provide a genetic basis for future biochemical, biophysical and structural investigation.

The results presented here allow two specific advances in our understanding of the S^{21} pathway, allowing us to discern the orientations of the two TMDs in the inactive dimer and revealing the existence of a second class of inactive dimer, with only 1 TMD1 in the membrane. The findings also suggest refinements of the model for S^{21} that may apply to holin function in general.

The structure of the inactive dimer

Previously, we demonstrated that TMD1 is non-essential for pinhole formation and, in the growing population of pinholin proteins, is progressively externalized during the pathway to triggering (Park *et al.*, 2006). Moreover, triggering induced by addition of energy poisons is associated with quantitative release of TMD1s from the bilayer. In contrast, the irsS^{21}68 variant, which cannot externalize its TMD1, is non-lethal, does not

oligomerize beyond the dimer stage (Pang *et al.*, 2009), and is negative-dominant, hetero-dimerizing with and blocking the lethal function of the parental pinholin. These observations indicated that TMD1 is an intrinsic inhibitor of TMD2 oligomerization and suggested that an inactive dimer, with TMD1 still in the membrane, is part of the normal pathway to triggering. Here we further show that the irsS^{21}68 dominance is imposed without preventing the externalization of TMD1 of the functional pinholin with which it dimerizes (Fig. 3.2A, B). This result has several implications. First, mutations in TMD1 that affect lysis timing are likely to do so by affecting the release of TMD1 from the bilayer, either by altering interactions with TMD2 or by altering the intrinsic hydrophobicity of TMD1 and thus its stability in the membrane. Second, TMD1 can externalize spontaneously without coordinating its topological change with its sister TMD1 in the inactive dimer (see below). Finally, and most importantly, the fact that dimers with only one TMD1 in the membrane do not oligomerize or progress to pinhole formation indicates that TMD1 must make trans (i.e., intermolecular) inhibitory contacts with TMD2 in the inactive dimer. Moreover, careful examination of the patterns of phenotypic variance in the three possible contexts (the full-length holin form (S^{21}68), the strong antiholin form (irsS^{21}68) and the ΔTMD1 form (S^{21}68$_{\Delta TMD1}$)) has allowed us to establish an orientation map for the TMDs in the inactive dimer (Fig. 3.6B). Residues important for assigning the orientation are: residues G14, A17 and G21 in TMD1, suggested to face the lipid; A12 in TMD1, suggested to face TMD2 in trans, and residues A37T, A38T, V41C, L47F, and G48T, which are indicated to interact with TMD1. Actually, we do not have direct evidence for a cis (intramolecular) interaction

between TMD1 and TMD2, although $S^{21}68$ protein must start as a monomer in the membrane, during which time presumably a cis interaction would maintain the holin in an inactive form. Moreover, the length of the arc defined by the five TMD2 mutations that have TMD1-sensitive phenotypes suggests that at least some of them, likely including positions 37 and 47, must occupy the intramolecular interface.

Although the orientation model is low resolution, it should be testable experimentally, either with biochemistry, using cysteine-scanning and copper-phenanthroline-mediated disulfide bond formation (Gründling *et al.*, 2000b, Sun & Kaback, 1997), with genetics, by isolating intragenic suppressors of the lethal and/or lytic phenotypes, or, perhaps, with structural studies, if the TMD1-TMD2 interaction can be covalently locked with disulfide bonds and thus survive the removal of the membrane by detergent.

The role of dimer formation in holin function

Both the λ holin S105, and the prototype pinholin $S^{21}68$, have an antiholin form with a short N-terminal extension carrying an extra positively charged residue that affects topology of TMD1. In the case of λ, the TMD1 of the antiholin form S107 is inhibited from entering the bilayer, whereas that of $S^{21}71$ is retarded in its ability to escape from it. In both cases, the properties of the antiholin form have been made discernible by studying mutant alleles more strongly blocked from making the topological transition than the native antiholin; i.e., a deletion of TMD1 in λ *S* (White *et al.*, 2010), and the *irs*-tag allele in S^{21}. In both of these cases, the enhanced antiholins are

capable of an absolute block in the lethal function and in the formation of dimers with the holin form. It is critical to note that in neither case is antiholin inhibition the fundamental basis of the temporal regulation of triggering. Even in the absence of the antiholin form, holin-mediated timing retains its fundamental characteristics: long-term accumulation of the holin without affect on membrane integrity, sudden triggering associated with lethality and depolarization of the membrane, and sensitivity to premature triggering by energy poisons (Gründling *et al.*, 2001, Park *et al.*, 2006). The simplest notion, by inference, is that antiholin-mediated inhibition or retardation of triggering reflects the stabilization of a normal dimer intermediate in the pathway to lethal function. Support for this idea is provided by the existence of multiple *S* lysis-defective alleles that are blocked at the dimer stage (Gründling *et al.*, 2000b). Similarly, many S^{21} non-lethal mutants are blocked at the dimer stage (T. Pang and R. Young, unpublished). However, until kinetic evidence from *in vivo* or *in vitro* experiments demonstrating a precursor-product relationship between dimers and the lethal holes is available, alternative scenarios in which both antiholin inhibition and mutational inactivation lead to off-pathway, "dead-end" dimers are also possible. Nevertheless, a potential rationale for the existence of dimers as a normal intermediate in hole formation may be inferred from consideration of $S^{21}68$. According to the orientation map of the inactive dimer generated here, the relatively hydrophilic residues of TMD2 that ultimately face the lumen of the pinhole are sequestered against TMD1 in both cis and trans (Fig. 3.6A, B). Moreover, evidence provided here suggests that, in the normal pathway, there is a second form of the inactive dimer, in which only one TMD1 remains

in the bilayer. The proposed orientation map would require the least rotational re-arrangement to allow continued sequestration of the future lumenal face, in this case by sequestration against the remaining embedded TMD1 and the other TMD2 (Fig. 3.6B). By this reasoning, the putative "activated" dimer, produced by the externalization of both TMD1s, would be much less able to sequester the lumenal residues, thus providing a driving force for oligomerization.

Influence of covalent dimers on pinholin timing

For the mutants G14C, T15C and S16C, inhibiting disulfide bond formation in the periplasm with DTT retards triggering. Three interpretations are possible, keeping in perspective the fact that TMD1 is non-essential for hole formation. One possibility is that TMD1 externalization is reversible and thus formation of the disulfide bond traps TMD1 in the periplasm. This seems unlikely, since the *sec* localization machinery, especially SRP (Signal Recognition Particle), is not available from the periplasm (Luirink *et al.*, 2005). A simpler interpretation is that the covalent linkage stabilizes the activated dimer by simply eliminating potential dissociation of the TMD2s. Alternatively, the disulfide linkage between the perplasmic TMD1s might indirectly simply favor an orientation of TMD2 that facilitates progress down the pathway. Distinguishing between these general rationales will require an *in vitro* system to assess the monomer-dimer partition in a lipid bilayer.

Materials and Methods

Bacterial strains, plasmids, media and culture growth

Mutant selections and constructions were done in *E. coli* XL1-Blue cells (Smith & Young, 1998) carrying plasmid pS^{21}68(RRzRz1)$^{\lambda}$, which has the λ *S* gene and its Shine-Dalgarno sequence of the plasmid pS105 replaced by the *S^{21}68* gene and its upstream Shine-Dalgarno sequence. *E. coli* strain MG1655*lacI^{q1}tonA*::Tn*10* (Guyer *et al.*, 1981) carrying plasmid pQ, which carries the gene for the λ late gene activator, Q, under Plac/ara-1 control, has been described (Gründling *et al.*, 2001). Other *E. coli* strains, and plasmids bearing wildtype *S^{21}68*, *S^{21}68$_{\Delta TMD1}$* and *irsS^{21}68* alleles have also been described previously (Pang *et al.*, 2009). These plasmids have the entire phage 21 lysis cassette under its native late promoter. In each case, the phage 21 lysis genes *R^{21}*, *Rz^{21}* and *Rz1^{21}* are inactivated by nonsense mutations. The lysogen MDS12*ΔtonA*(λ*Q^{21}Δ(SRRzRz1)^{21}*) carrying plasmid pS^{21}68 or its derivatives was used for phenotypic analysis of the wildtype or mutant *S^{21}68* alleles. For *S^{21}68$_{\Delta TMD1}$* alleles, the *E. coli* strain MG1655*lacI^{q1}tonA*::Tn*10* carrying the compatible plasmids pQ and pS^{21}68$_{\Delta TMD1}$ or its derivatives were used to express the wildtype or mutant *S^{21}68$_{\Delta TMD1}$* alleles. To test the function of *irsS^{21}68* mutant alleles, derivatives of plasmid pirsS^{21}68* were used, which has the promoter and the entire lysis cassette region identical to pS^{21}68, except that it has codons encoding the *irs*-epitope (RYIRS) fused to the N-terminus of *S^{21}68* gene, and it carries *Amp^{R}*, instead of *Kan^{R}*. They were transformed into either the lysogen MDS12*ΔtonA*(λ*Q^{21}Δ(SRRzRz1)^{21}*), or MDS12*ΔtonA*(λ*S^{21}68*) which provides a chromosomal copy of *S^{21}68*.

Cultures were grown in standard Luria- Bertani (LB) media supplemented with antibiotics where needed: kanamycin (40 μg/ml), ampicillin (100 μg/ml), and chloramphenicol (10 μg/ml).

Plasmids carried by lysogens were induced by shifting the culture into 42°C for 15 m. Plasmid pQ was induced by 1 mM isopropyl-β-D-thiogalactopyranoside (IPTG) and 0.2% arabinose. Lysis profiles were obtained by monitoring A_{550} after thermal or IPTG/ arabinose inductions, as described previously (Smith & Young, 1998, Tran *et al.*, 2005). When needed, 1mM DTT was added into the culture at the time of induction.

EMS mutagenesis and screen for the $S^{21}68$ lysis defective mutants

EMS mutagenesis was performed by the procedure of Miller (1992) using the *recA*$^-$ strain XL1-blue carrying monomeric $pS^{21}68(RRzRz1)^{\lambda}$. After exposure to EMS, cells were washed and plated on LB agar to measure cell viability.The degree of mutagenesis was estimated by the frequency of rifampicin-resistance mutants after outgrowth of the EMS-treated cells, as described by Miller (1992).

After overnight growth of the EMS-treated cells, plasmid DNA was recovered and transformed into MG1655*lacI*^{q1}*tonA*::Tn*10* (Guyer *et al.*, 1981) carrying the plasmid pQ. A portion of the transformant pool was inoculated into 25 ml LB medium supplemented with Amp and the culture was grown to A_{550} ~0.2 and induced with IPTG and arabinose for 2 h. After induction, the cells were collected by centrifugation and plated on LB-Amp plates without inducer. Surviving colonies were inoculated into individual cultures, induced as above and then treated with 1% chloroform. Cultures that

continued to grow after induction but underwent lysis after chloroform addition were presumed to have expressed the downstream λ*R* endolysin gene and were likely to harbor a lysis-defective $S^{21}68$ allele. The $pS^{21}68(RRzRz1)^{\lambda}$ plasmid was recovered from these cultures and was re-transformed into fresh MG1655*lacI*^{q1}*tonA*::Tn*10* cells to confirm that the lysis defective phenotype segregated with the plasmid. All the candidate plasmids that passed this final test were subjected to DNA sequence analysis.

Each of the EMS mutations was re-created in plasmid $pS^{21}68$. Each plasmid was transformed into lysogen MDS12*ΔtonA*($\lambda Q^{21}\Delta(SRRzRz1)^{21}$), and the effect on the triggering time of $S^{21}68$ was tested.

Site-directed mutagenesis, and general DNA manipulations

Procedures for plasmid DNA isolation, QuikChange (Stratagene) mutagenesis, cloning steps and DNA sequencing have been described (Smith *et al.*, 1998). Oligonucleotides were obtained from Integrated DNA Technologies, Coralville, IA, and were used without further purification. All enzymes were purchased from New England Biolabs, with the exception of *Pfu* polymerase, which was from Stratagene. Automated fluorescent sequencing was performed at the Laboratory for Plant Genomic Technologies at Texas A&M University.

TCA precipitation, SDS-PAGE and Western blotting

Ten percent TCA was used to immediately stop cell growth and precipitate protein as previously described (Park *et al.*, 2006). Precipitates were resuspended in

sample loading buffer with the addition of 5% β-mercaptoethanol, unless for the purpose of detecting the disulfide-bond linked dimer. SDS-PAGE and Western blotting were performed as described (Pang *et al.*, 2009). Proteins were separated on 10% Tris-Tricine gels and transferred to 0.1 μm nitrocellulose membrane (Whatman, NJ). Antiserum against the S^{21} C-terminal peptide KIREDRRKAARGE was used as primary antibody (Barenboim *et al.*, 1999). Blots were developed by using the Supersignal West Femto maximum sensitivity substrate kit (Thermo Scientific) according to the manufacturer's instructions. Images were obtained by using the Molecular Imager Gel Doc DR system (Bio-Rad) and analyzed by software Quantity One (Bio-Rad).

CHAPTER IV

OLIGOMERIC INTERACTIONS OF THE S^{21} PINHOLIN

Introduction

Pinholins and SAR endolysins are recently discovered classes of phage lysis proteins. Pinholins differ from canonical holins, which form large non-specific holes in the cytoplasmic membrane that allow release of the phage endolysin, resulting in degradation of the cell wall (Young & White, 2008). Instead, pinholins merely depolarize the membrane by forming small holes ("pinholes") incapable of allowing protein transit. This is effective in terms of lysis because of the properties of the SAR endolysin, which is secreted and accumulates in the periplasm, tethered to the membrane in an enzymatically-inactive form. When depolarization occurs, the SAR endolysin is released from the membrane and refolds to an active form, leading immediately to destruction of the murein. For both canonical holins and pinholins, hole-formation occurs suddenly, after a period of harmless accumulation in the membrane, during which time membrane energization, macromolecular synthesis and virion assembly continues undisturbed. Although the molecular basis of the temporal scheduling of this event, called "triggering", is unknown, it is dependent on the energized state of the membrane. For example, even a 50% depletion of the proton motive force (pmf) will prematurely trigger the λ holin, resulting in release of endolysin and lysis within seconds (Gründling *et al.*, 2001). Thus for both canonical holins and pinholins, triggering determines the timing of lysis, although the molecular strategies are completely different.

The prototype pinholin is the $S^{21}68$ protein of the lambdoid phage 21. Genetic, biochemical, structural and modeling studies indicate that $S^{21}68$ triggers to form heptameric channels of approximately 1.5 nm diameter (Pang *et al.*, 2009). $S^{21}68$ has two transmembrane domains (TMDs) (Fig. 3.1D), but only TMD2 is required for the pinhole (Park *et al.*, 2006). A structure has been proposed for the pinhole, based on coarse-grained simulated annealing of TMD2 (Fig. 2.9) (Pang *et al.*, 2009). In this model, heterotypic TMD2-TMD2 interactions occur through two interfaces, A and B. The A interface contains a motif, $G_{40}xxxS_{44}xxxG_{48}$ that resembles glycine-zipper motifs important for both homotypic and heterotypic interactions between transmembrane helices.

Although TMD1 is not required for the pinhole structure, it has a role in temporal regulation as an inhibitor of the lethal function of TMD2. Genetic and molecular evidence has been presented indicating TMD1 binds to and inhibits TMD2 in both cis and trans in an inactive dimer, which is proposed to be the first kinetically important intermediate in the pinhole formation pathway (Fig. 4.1) (Pang *et al.*, 2010). Progress towards hole formation requires a dramatic topological change, with TMD1 exiting the bilayer (Fig. 3.1B, 4.1). Both TMD1s must be externalized before TMD2 can proceed towards oligomeric status and pinhole formation.

$S^{21}68$ is just one of two proteins produced from S^{21} (Fig. 3.1A). The other, $S^{21}71$, a product of a translational start three codons upstream, exhibits retarded externalization of TMD1, presumably because of the extra positively charged residue at its N-terminus (Fig. 3.1B). Taken together, these observations indicate that $S^{21}71$, with its retarded

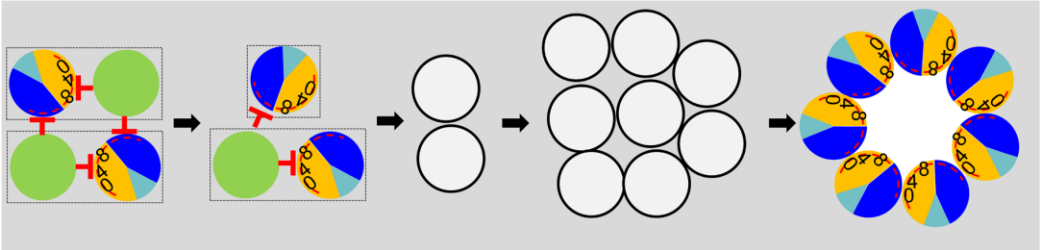

Figure 4.1. Model of $S^{21}68$ hole formation pathway (top-down view from periplasm). The two TMDs (green: TMD1; sectored: TMD2) in a single $S^{21}68$ molecule are boxed. Initially, both TMDs are inserted in the membrane in an inactive dimer form, with TMD1 inhibiting TMD2 both in cis and in trans. Then one of the two TMD1s is released, and finally both TMD1s are released, which converts the inactive dimer into an activated dimer form. Activated dimers then aggregate, and nucleate to form heptameric pinholes. In TMD2, orange and dark blue represent A and B interaction faces (Fig. 2.9), with 0, 4, and 8 indicating the helical positions of the G40, S44, and G48 residues, respectively. The red stop arrows indicate the cis and trans inhibition of TMD1 to TMD2. The interaction face(s) of TMD2 in both the activated dimer and aggregates are not known, thus TMD2 is depicted as clear circle in both cases. The hydrophilic residues of TMD2 that eventually face the lumen of the pinhole are represented by red arc. Grey, lipid.

topological dynamics, is an antiholin, albeit a weak one. Antiholins are phage-encoded proteins that bind specifically to and inhibit holins, allowing fine-tuning of the holin triggering time. Dual translational starts encoding holin-antiholin pairs are not uncommon in holin genes, and, in several cases (λ, P22, phi29), differences in topological dynamics have been invoked for the inhibitory character of the antiholins (Young & Bläsi, 1995, Bläsi & Young, 1996). A stronger inhibitory phenotype can be obtained by fusing an epitope, *irs*, containing two positively charged residues, to the N-terminus of $S^{21}68$ (Fig. 3.1D). The resultant construct, $irsS^{21}68$ is completely blocked from the topological change of TMD1, does not support pinhole formation, and exhibits strong dominant negative, or antiholin, character (Fig. 3.1B).

Despite its intrinsic inhibitory capacity, TMD1 is not essential for lysis timing, as shown by the fact that an $S^{21}68_{\Delta TMD1}$ allele exhibits scheduled triggering and can be prematurely triggered by artificial collapse of the pmf by treatment of induced cells with an uncoupler (Park *et al.*, 2006). This suggests that there is a kinetically distinct pathway downstream of the activated dimer, with only TMD2 in the membrane, ultimately terminating in the sudden formation of the lethal pinholes. Recently, an extensive library of mutant alleles of $S^{21}68$ was assembled, both by selections for loss of lethal function and by site-directed mutagenesis (Pang *et al.*, 2010). Phenotypic and molecular analysis of this mutant collection, coupled with earlier biochemical and physiological studies, has suggested a multi-step pathway for pinhole formation (Fig. 4.1). In particular, mutations in TMD1 that affected lysis timing could be correlated with the ability of TMD1 to escape the membrane, either by changing intrinsic hydrophobic character or by altering interactions with TMD2. A model for the orientations of TMD1 and TMD2 in the initial inactive dimer was generated (Fig. 4.1). Here we report additional phenotypic and molecular analyses of this mutant collection. The results are discussed in terms of a scheme for the pinhole formation pathway.

Results

Early lysis mutants outside of TMD1

Early lysis phenotypes are common in TMD1; 5 of the 20 residues give rise to 6 mutants with triggering times ~35 m earlier than wt (Table 4.1). These mutants are straightforward to interpret: any mutation that dramatically reduces the dwell-time of

Table 4.1. Triggering time of the early mutant.

loc[1]	allele[2]	full-length[3]	Δ(TMD1)[4]
	wt	0	0
TMD1	A12L	-35	
	G14Q	-35	
	G14C	-35	
	T15C	-35	
	A17Q	-35	
	G21Q	-35	
loop	S32C	NL	-40
TMD2	A37T	+30	-30
	A38T	+50	-20
	S44T	-35	NL
	S44N	-35	-45

[1]Localization of each mutant in the topological domains.
[2]Mutant alleles.
[3]Effect of each mutation on the triggering time (m) of the full length holin $S^{21}68$ (wt triggers at 50 m). NL, nonlethal.
[4]Effect of each mutation on the triggering time (m) of the truncated holin $S^{21}68_{\Delta TMD1}$ (wt 50 m). NL, nonlethal.

TMD1 in the membrane, either by reducing hydrophobicity or disrupting interactions with TMD2, can be expected to advance the triggering time. In the remaining 48 residues, only one position, S44, gives rise to mutants with dramatically early triggering: S44T and S44N (Table 4.1, Fig. 4.2A). S44 is not only the central residue of the GxxxSxxxG homotypic interaction motif but, in the structure proposed for the TMD2 heptamer, it is part of the heterotypic interaction surface A and also exposed to the pinhole lumen. Interestingly, only one of these two mutants, S44N, also exhibits early lysis in the context of ΔTMD1, while the other, S44T, is completely non-functional (Table 4.1, Fig. 4.2B). In contrast, three other mutations, S32C in the connecting loop

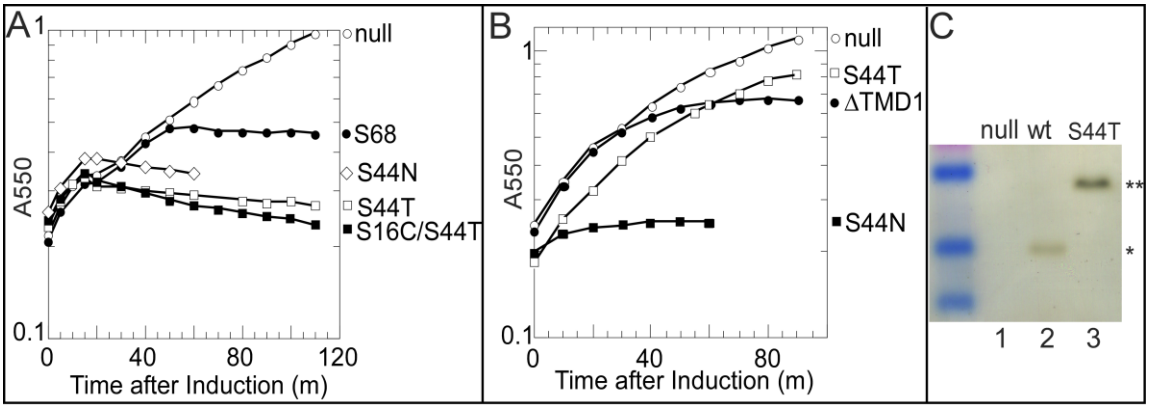

Figure 4.2. Phenotypes of the S44T and S44N.

A. Growth curve of *S[21]68* alleles. Lysogen carrying prophage $\lambda Q^{21}\Delta(SRRzRz1)^{21}$ and indicated plasmids were induced at t=0 and monitored for growth as A_{550}. Open circles, no plasmid; closed circles, $pS^{21}68$; open diamonds, $pS^{21}68_{S44N}$; open squares $pS^{21}68_{S44T}$; closed squares, $pS^{21}68_{S16C/S44T}$.

B. Growth curve of *S[21]68$_{\Delta TMD1}$* alleles. Culture growth was monitored as in A, except that each culture carries plasmids pQ and the indicated plasmids: open circles, plasmid vector pRE (Gründling *et al.*, 2001); closed circles, $pS^{21}68_{\Delta TMD1}$; open squares, $pS^{21}68_{\Delta TMD1S44T}$; closed squares, $pS^{21}68_{\Delta TMD1S44N}$.

C. Disulfide-bond formation of $S^{21}68_{S16C}$ alleles. Cultures carrying prophage $\lambda Q^{21}\Delta(SRRzRz1)^{21}$ and indicated plasmids were induced and precipitated by TCA at 15 m after induction. Samples were resuspended in sample loading buffer without reducing agent and analyzed by SDS-PAGE and Western blotting. Double and single asterisks indicate the position of dimer and monomer, individually. Lane 1, no plasmid; lane 2, plasmid $pS^{21}68_{S16C}$; lane 3, plasmid $pS^{21}68_{S16C/S44T}$.

and A37T and A38T in TMD2, exhibit radically early triggering in the deletion allele but are either severely delayed (A37T, A38T) or non-lethal (S32C) in the full length context (Table 4.1). While these phenotypes cannot yet be interpreted with confidence, the simplest notion is that the S32C, A37T, and A38T changes, while intrinsically more biased towards completion of the TMD2 oligomerization-hole formation pathway, all increase affinity for TMD1 and thus retard its release to the periplasm. In contrast, the TMD1 of S44T and S44N are released remarkably early from the membrane, as assessed

by the disulfide-bond formation of the S16C mutation in TMD1 (Park *et al.*, 2006) (Fig. 4.2C). In addition with the remarkable contrast between the S44T and S44N phenotypes in the deletion context, it indicates that S44 is involved in at least three different interactions in the pinhole pathway.

Oligomerization defects of non-lethal $S^{21}68$ mutants

In total from a nearly saturated selection for loss of lethality and from site-directed mutagenesis experiments, 26 non-lethal mutant alleles of $S^{21}68$ were obtained, among which 23 encoded $S^{21}68$ proteins that accumulated to normal levels and thus likely did not owe their lysis defect to improper localization or gross misfolding in the membrane (Table 4.2). Lethal pinholes can be detected *in vivo* by the formation of covalent $S^{21}68$ oligomers after treatment of induced cells with the membrane-permeant crosslinker, DSP. These oligomers can be visualized as a ladder of immuno-reactive bands in non-reducing SDS-PAGE (Pang *et al.*, 2009) (Fig. 4.3). In contrast, the irs$S^{21}68$ protein cannot be crosslinked to species higher than the dimer and can block oligomer formation by $S^{21}68$, consistent with its negative-dominant, antiholin character. When the non-lethal but proteolytically stable mutants of full-length $S^{21}68$ were subjected to the same DSP-crosslinking treatment, both patterns were observed (Fig. 4.3, Table 4.2). All three non-lethal mutants of TMD1 resembled irs$S^{21}68$ in being blocked at the dimer stage, consistent with the notion that defects in TMD1 that block externalization prevent the formation of activated dimers, either due to increased hydrophobicity or increased affinity for TMD2 (Pang *et al.*, 2010). Some non-lethal

Table 4.2. Properties of *S[21]68* nonlethal mutant alleles.

loc[1]	allele[2]	Olig[3]	TMD1 externalization[4]	Oligo+wt[5]	D/R[6]
	wt	+	0.6		
TMD1	S19L	-			
	S19C	-			
	G21L	-			
Loop	D29N	-	0.6	+	D
	D29V	-	0.6	+	D
	V31C	+			
	S32C	+			
	P33L	+			R
	S34C	-	NT		
TMD2	W36C	-	NT	+	D
	A37V	+			aD
	G40L	+			aD
	G40T	+			aD
	G43L	-	0.8	+	D
	S44L	-	IF		aD
	S44C	-	0.6		aD
	G48L	-	0.8	-	D
	G48T	+		+	D
	G48C	-	0.3	-	D
	T51I	-	0.6		aD
	T54I	-	0.7	-	D
	T54C	+		+	D
tail	$I60_{och}$ [7]				

[1]Localization of each mutant in the topological domains.
[2]Mutant alleles.
[3]Oligomerization of each mutant as indicated by DSP crosslinking *in vivo*. + indicates the formation of oligomer. – indicates the formation of dimer.
[4]Effect of each mutation on the externalization of TMD1.
[5]Oligomerization of each mutant in the presence of wt $S^{21}68$. Labeled same as in 3.
[6]The dominance/recessiveness test. D: dominant. R: recessive. aD: antidominant.
[7]Ochre stop codon substitution of that residue.

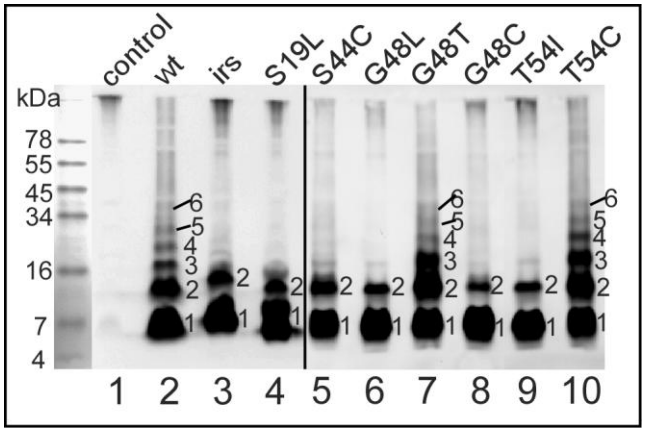

Figure 4.3. Representatives of DSP crosslinking of S^{21}68 varients *in vivo*. Whole cells carrying prophage λ*Q*^{21}*Δ(SRRzRz1)*^{21} only (lane 1) or with each indicated plasmid were induced and, treated with the cross-linker DSP, and analyzed by SDS-PAGE and Western blotting, as described in the Materials and Methods. Plasmid carried in each sample: pS^{21}68 (lane 2), pirsS^{21}68* (lane 3), lane 4-10, derivatives of pS^{21}68, encoding single mutation of *S*^{21}*68* as indicated on top of each lane. Numbers at the right side of each lane indicate the crosslinked oligomers.

mutations in the connecting loop (D29N, D29V, S34C) and in TMD2 (W36C, G43L, S44L, S44C, G48L, G48C, T51I, and T54I) are also blocked at the dimer stage. We wanted to know whether these alleles, like the TMD1 alleles, were defective in oligomerization because of a defect in externalization of TMD1, or could be potentially assigned to a blockage at the activated dimer stage. Previously, we have shown that TMD1, once externalized to the periplasm, can undergo homotypic interactions detectable by assessing spontaneous disulfide bond formation using the S16C substitution allele (Park *et al.*, 2006). Incorporating this change into each of the non-lethal alleles had no effect on the lytic defect [not shown] or the level of protein accumulation (Fig. 4.4). Only one TMD2 mutant, G48C, exhibited reduced disulfide

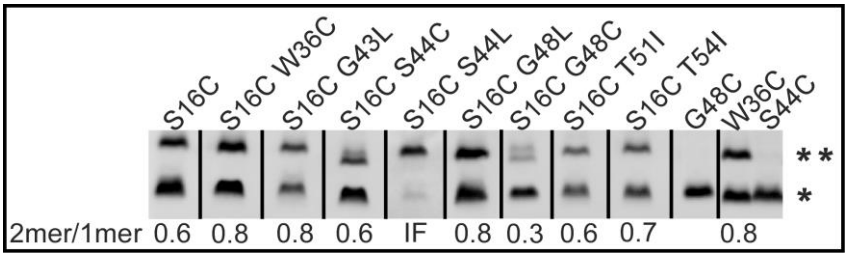

Figure 4.4. The effect of each mutation on the externalization of $S^{21}68$ TMD1. Experiment as described in Fig 4.2C, except that cells carried prophage $\lambda Q^{21}\Delta(SRRzRz1)^{21}$ with derivatives of plasmid $pS^{21}68$ encoding mutations on the $S^{21}68$ gene as indicated on top of each lane. Asterisks indicate the position of monomer and dimers, as in Fig 4.2C. The dimer to monomer ratio of each mutant is illustrated on the bottom. IF, infinite.

bond formation, suggesting that the mutation caused retention of TMD1 in the bilayer. Consistent with this notion, G48 is on the A face of TMD2 (Fig. 2.9) and, according to the orientation map for the inactive dimer (Fig. 4.1), would interact with TMD1 in cis. The other dimer-limited mutants show no defect in the S16C disulfide bond formation assay, and, in fact, one, S44L, appears to be much more efficient than the parental. Ser44 is also on the A face, and, like G48, is part of the $G_{40}xxxS_{44}xxxG_{48}$ zipper motif, so the altered externalization phenotypes of these two alleles, although opposite, support the idea that the zipper motif is important in the cis interaction with TMD1. Moreover, externalization-proficient, oligomerization-defective phenotypes of G43L, S44L, S44C, G48L, T51I, and T54I, all mutants in the A face of TMD2, suggest that these proteins are blocked at the activated dimer stage (Fig. 4.1).

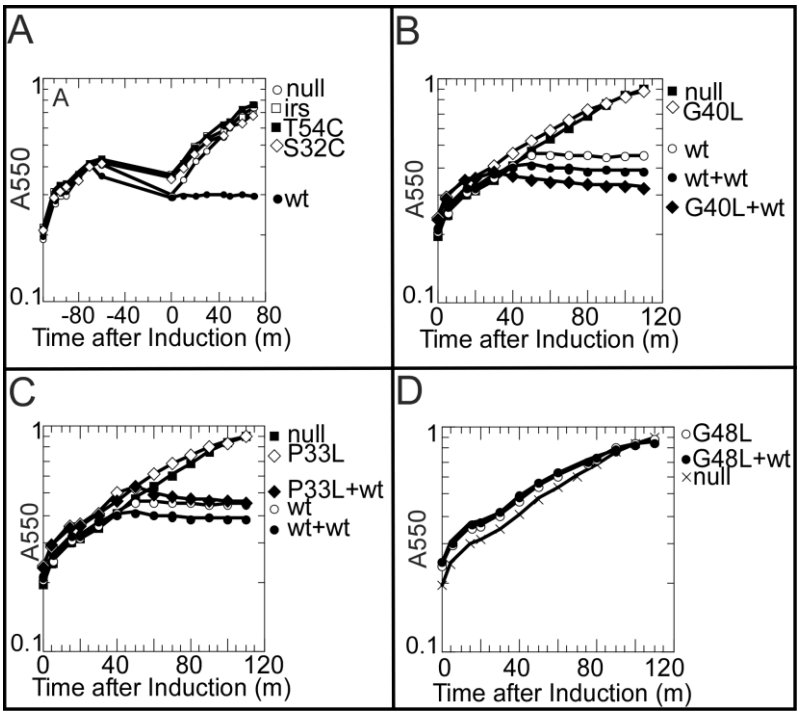

Figure 4.5. Growth curves. Except A, cultures carrying the indicated prophages and plasmids were induced at T=0, and their growth were monitored as A_{550}.

A. The effect of DNP on the triggering of $S^{21}68$ variants (representatives). Prophage $\lambda Q^{21}\Delta(SRRzRz1)^{21}$ with no plasmid (open circles), or plasmid $pS^{21}68$ (closed circles), $pirsS^{21}68$* (open squares), $pS^{21}68_{T54C}$ (closed squares), $pS^{21}68_{S32C}$ (open diamonds) was induced at T=-110. 2mM DNP was added to each culture at T=-70, at which time the $S^{21}68$ triggers. At T=-80, cultures were taken out and LB media containing DNP was replaced by fresh media as described in Materials and Methods. At T=0, growth of each culture was monitored again.

B, C, D. The dominance/recessiveness test of $S^{21}68$ mutants.

B. Representative of the recessive mutants. Closed squares, prophage $\lambda Q^{21}\Delta(SRRzRz1)^{21}$, no plasmid; open circles, prophage $\lambda S^{21}68$, no plasmid; closed circles, prophage $\lambda S^{21}68$, plasmid $pS^{21}68_{a}$; open diamonds, prophage $\lambda Q^{21}\Delta(SRRzRz1)^{21}$, plasmid $pS^{21}68_{aG40L}$; closed diamonds, prophage $\lambda S^{21}68$, plasmid $pS^{21}68_{aG40L}$.

C. Representative of the anti-dominant mutants. Closed squares, open and closed circles represent the same culture as in B. Open diamonds, prophage $\lambda Q^{21}\Delta(SRRzRz1)^{21}$, plasmid $pS^{21}68_{aP33L}$; closed diamonds, prophage $\lambda S^{21}68$, plasmid $pS^{21}68_{aP33L}$.

D. Representative of the dominant-negative mutants. Cross, prophage $\lambda Q^{21}\Delta(SRRzRz1)^{21}$, no plasmid; open circles, prophage $\lambda Q^{21}\Delta(SRRzRz1)^{21}$, plasmid $pS^{21}68_{aG48L}$; closed circles, prophage $\lambda S^{21}68$, plasmid $pS^{21}68_{aG48L}$.

Oligomerization proficient non-lethal mutants

Other mutants in both the loop and TMD2 (V31C, S32C, P33L in the loop; A37V, G40L, G40T, G48T, T54C in the TMD2) exhibited DSP crosslinking ladders indistinguishable from the lethal parental (Fig. 4.3). To test whether lethal function could be rescued by artificially depolarizing the membrane, cells induced for these alleles were treated with DNP. After washing out DNP, these cells resumed growth (Fig. 4.5A), indicating that the mutant oligomers formed are non-lethal and cannot be triggered to form pinholes. The simplest interpretation is that these mutants are blocked at an oligomeric stage, detectable by DSP cross-linking, before the formation of the pinholes. A similar model has been suggested for the canonical holin S105 of phage lambda, also based on the existence of wt DSP-cross-linking phenotypes in mutants that have lost lethal function, although in the case of λ *S*, only one of the non-lethal alleles tested exhibited an oligomeric ladder(Gründling *et al.*, 2000a).

Reversed triggering phenotypes in dominance-recessiveness tests

The 16 non-lethal loop and TMD2 alleles were also tested for dominant-recessive character by inducing in the presence, in trans, of the parental $S^{21}68$ allele borne on a prophage (Table 4.2; Fig. 4.5B, C, D). Under these conditions, only one allele, P33L, was recessive (Fig. 4.5C). All of the other 16 non-lethal mutants were *sensu stricto* dominant, in that their presence in trans to wt resulted in a phenotype different from that observed with the wt allele in both cis and trans positions. Nine of these alleles (D29N, D29V, W36C, G43L, G48L, G48T, G48C, T54C and T54I) had dominant-negative

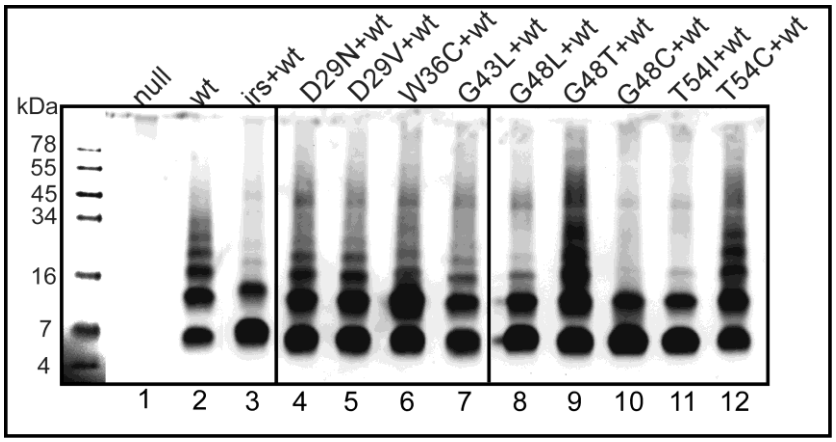

Figure 4.6. DSP crosslinking of $S^{21}68$ wildtype in the presence of $S^{21}68$ mutants *in vivo*. Experiment was performed as in Fig. 4.3. Prophage and plasmid carried in each sample: $\lambda Q^{21}\Delta(SRRzRz1)^{21}$, no plasmid (lane 1); prophage $\lambda S^{21}68$ (lane 2); prophage $\lambda S^{21}68$, plasmid pirs$S^{21}68$* (lane 3); lane 4-12, prophage $\lambda S^{21}68$ with derivatives of p$S^{21}68_a$, encoding single mutation of $S^{21}68$ as indicated on top of each lane.

phenotypes, blocking the triggering of the wt allele in trans (Fig. 4.5D). Among them, seven mutants (D29N, D29V, W36C, G43L, G48L, G48C, and T54I) were blocked at dimer stage. However, only three (G48L, G48C, T54I) were able to prevent oligomerization of the wt protein (Fig. 4.6). This was expected for G48C, since it is defective in TMD1 externalization and thus presumably would function with antiholin character, like irs$S^{21}68$. For the other dominant-negatives, however, there was no correlation with oligomerization proficiency.

The other six non-lethals tested, despite their intrinsic triggering defect, exhibited an early triggering phenotype in trans to the parental, compared to the double-parental control (Fig. 4.5B). Similar unexpected phenotypic reversal was previously observed in

recessiveness-dominance testing of non-lethal mutants of the λ holin (Raab *et al.*, 1988). For clarity, these alleles are designated as "anti-dominant" (aD) in Table 4.2.

Discussion

Lambdoid phage 21 *S^{21}68* is the prototype of a recently discovered class of holins. It is a particularly attractive subject for genetic analysis, because of its small size, only 68 codons, and its malleability to mutagenesis. Previous study on the extensive collection of *S^{21}68* mutants suggests the orientation of both TMDs in the inactive dimer, the first kinetically important stage in the pinhole formation pathway (Pang *et al.*, 2010). Here we provide additional analysis of this mutant collection and suggest a refined pinhole formation model, predicting the orientation of TMD2s in the intermediate stages and suggesting several roles for the glycine zipper motif in TMD2.

A refined pinhole pathway

Previously, we proposed the pinhole formation model for S^{21}68 (Pang *et al.*, 2009) (Fig. 4.1). Initially, the two TMDs are inserted in the membrane as an inactive dimer (Pang *et al.*, 2010). Once TMD1 is released into the periplasm, S^{21}68 forms an activated dimer form, followed by the aggregation of the dimer into oligomers. Finally, the heptameric pinhole forms, possibly driven by the hydration of the lumenal-side chains. Although models for the inactive dimer and the final pinhole with the helical-helical interaction surfaces A and B are suggested by genetic and biochemical methods (Pang *et al.*, 2010, Pang *et al.*, 2009), structures of TMD2s in the intermediate stages are

not clear. Here from analysis of the oligomeric states of $S^{21}68$ non-lethal mutants, we provide evidence for the existence of the intermediate stages and a low-resolution model for each one.

All the non-lethal mutants in TMD2 are in the interface A, suggesting its importance in the pinhole formation pathway. Among all these non-lethal mutants, eight (W36C, G43L, S44L, S44C, G48L, G48C, T51I, and T54I) are blocked in the dimer stage, with only one (G48C) delaying the externalization of TMD1. Thus it suggests the existence of the activated dimer, with the seven mutants blocked in this stage and G48C delayed the transition from the inactive dimer to it. Moreover, three of these mutants (S44L, S44C, and T51I) exhibited an anti-dominant phenotype in the presence of wild-type $S^{21}68$. This suggests that the homotypic interfaces A:A interaction must be involved in the activated dimer, since the blockage of these three interface A mutants at the activated dimer stage can be rescued by providing a copy of the wild-type interface A.

Secondly, five other non-lethal mutants in TMD2 (A37V, G40L, G40T, G48T, T54C) were crosslinked into oligomers indistinguishable from the $S^{21}68$, suggesting the existence of the oligomer state before the pinhole forms. The orientation of TMD2s in this stage is not clear, although helical interactions between interfaces A and B might be involved, since the A:A interaction is involved in the activated dimer stage, and mutations in the same residue of interface A (G48 and T54) can be blocked in either the dimer or the oligomer stage, suggesting the different interactions involved at these residues. Two of these five mutants (G48T and T54C) are dominant-negative, suggesting

that the defect of transition to the pinhole at this stage cannot be rescued by the wild-type $S^{21}68$, whereas it can be rescued in the anti-dominant mutants (A37V, G40L, and G40T). In addition, among the five dominant-negative mutants blocked at the activated dimer stage, two (W36C and G43L) were crosslinked into oligomers in the presence of wt $S^{21}68$, indicating that their blockage of the A:A to A:B transition can be accommodated by the wild-type, but not the transition from the oligomer stage to the pinhole. Ultimately, resolution of the intermediate states in the pathway will require a kinetic analysis that shows the population of these states occurs in a sequential manner. Technically, such a study may prove challenging because of the exquisite sensitivity of holins to the proton-motive force, a characteristic that imposes severe restrictions on the experimental manipulation of growing cells.

Nevertheless, the comprehensive phenotypic analysis of the mutant collection leads us to further refinement of the pinhole formation pathway (Fig. 4.7). The first stage obviously must be the monomer, although no *S*^{21} mutants have been identified that are blocked at the monomer stage. It is possible that a dimerization defect might lead to proteolysis and thus low protein accumulation, as has been shown for at least one mutant in the class I λ holin S105 (Gründling *et al.*, 2000a). In this model, the first kinetically important stage would be the inactive dimer ID1, with membrane-inserted TMD1 inhibits TMD2 both in cis and in trans, the persistence of which defines the lysis time. At genetically encoded time, the TMD1 externalizes into the periplasm. For the wild-type *S*^{21} allele, a second stage of the inactive dimer (ID2) formed between $S^{21}68$ and $S^{21}71$ might exist, with only TMD1 of $S^{21}68$ externalized. In both ID stages, the

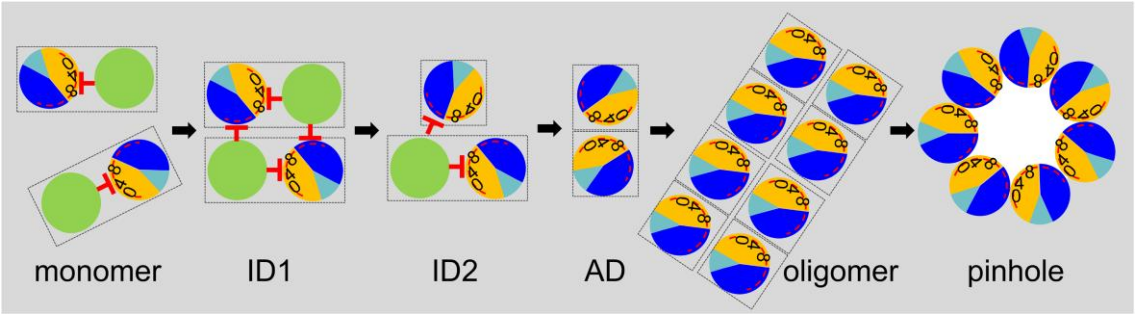

Figure 4.7. Model for the S^{21} pinhole formation pathway. Same scheme as in Fig. 4.1. S^{21} molecules are first inserted as monomers. ID1, 2, the inactive dimer 1, 2; AD, the activated dimer, with the homotypic helical-helical interaction of the glycine zipper containing interface A. In the oligomer state, the A:A interaction transits to A:B heterotypic helical interaction. Finally, the heptameric pinhole forms.

interface A of TMD2, composed of most of the hydrophilic residues, is packed inside the protein clusters and away from lipid. In the activated dimer stage, with both TMD1s released, the interface A is packed against itself from the other pinholin molecule. This state might not be kinetically stable, and may yield to more favored packing, the A:B interaction, which would potentiate transition to an oligomer state. In this state, the helices might align perpendicularly to the lipid bilayer. Finally, the hydration of the lumenal-side chains might drive the helices to rearrange at an angle of 34° to the normal, and the heptameric pinholes to form (Pang *et al.*, 2009). It is likely that this would lead to a local depolarization of the membrane. If the depolarized state favors any of these transitions, the entire pathway would have a fundamentally "all or nothing" character. As noted previously (Wang *et al.*, 2000), holin function should be all or nothing, to avoid poisoning macromolecular metabolism, and thus virion assembly, before triggering.

Mutations on the GxxxSxxxG motif

The interface A of the $S^{21}68$ TMD2 contains a $G_{40}xxxS_{44}xxxG_{48}$ motif, also known as the glycine zipper. The glycine zipper is found to be strongly involved in helical packing against a neighboring helix, as seen in several channel forming proteins MscL, VacA, KcsA (Kim *et al.*, 2005). It also contains the GxxxG motif, which plays a significant role in homotypic helices interaction through hydrogen bonding, as in the dimeric protein glycophorin A (Curran & Engelman, 2003). From analysis of the lysis phenotypes of mutants in these residues, we suggested that this motif is involved in both the homotypic TMD2 interaction in the activated dimer form, and the heterotypic TMD2 interaction in the pinhole structure. Moreover, the structure of the inactive dimer predicted by the mutagenesis analysis also suggests that this motif interacts with TMD1 in cis (Pang *et al.*, 2010).

Mutations were introduced in the G40, S44, and G48 residues. As this motif is likely involved in three interactions in the pathway, it is difficult to explain the phenotype of these mutants at the molecular level. However, the completely opposite phenotypes of $S^{21}68$ mutants on S44 caught our attention. The two non-lethal mutants, S44L and S44C are both TMD1-externalization proficient, dimerization-proficient, oligomerization-deficient, and anti-dominant, indicating the involvement of S44 in the TMD2-TMD2 interaction in the activated dimer. Moreover, the TMD1 of S44L is released much more efficiently than the parental allele or the S44C. This supports the idea that S44 interacts with TMD1, and the S44L mutation must reduce this interaction and accelerate the release of TMD1, possibly because Leu is bulkier than both Ser and

Cys. Two other mutants, S44T and S44N trigger extremely early in the context of full length protein. However, they have a remarkably different phenotype in the TMD1-deleted context. S44T completely abolished the function of $S^{21}68_{\Delta TMD1}$, while S44N accelerates its triggering drastically (Fig. 4.2A, B). This extreme difference supports our model that, in addition to the cis interaction with TMD1, S44 is also involved in both the homotypic and heterotypic interaction of TMD2 in the pinhole pathway. In this model, at some point the activated dimer, which we propose is based on the A:A interaction, has to undergo a shift to the A:B interaction that defines the heptamer. Thus although both S44N and S44T weaken the cis interaction with TMD1, S44N could weaken the homotypic interaction but strengthen the heterotypic interaction, whereas S44T could strengthen both or weaken both. The presence of TMD1 in the periplasm might help S44T-containing TMD2 to overcome this defect and thus S44T exerts an early lysis phenotype only in the full length context.

Materials and Methods

Bacterial strains, prophages, plasmids, media and culture growth

E. coli strains, prophages, and plasmids used in this study have been described previously (Pang *et al.*, 2009, Pang *et al.*, 2010). In each case, the phage 21 lysis cassette has been mutated so that only the *$S^{21}68$* gene or its derivatives are expressed. Briefly, lysogen MDS12*ΔtonA*(λ*Q^{21}Δ(SRRzRz1)^{21}*) carrying the plasmid pS^{21}68 or its derivatives were used to express the wildtype or mutant *$S^{21}68$* alleles. The same lysogen carrying plasmid pirsS^{21}68* was used to express *irs$S^{21}68$*, which has codons encoding the *irs*-

epitope (RYIRS) fused to the N-terminus of *$S^{21}68$* gene in the plasmid $pS^{21}68_a$. Plasmid $pS^{21}68_a$ has the entire lysis cassette region identical to $pS^{21}68$, except that it carries *Amp^R*, instead of *Kan^R*. *E. coli* strain MG1655*lacI*^{q1}*tonA*::Tn*10* (Guyer *et al.*, 1981) carrying plasmids pQ and $pS^{21}68_{\Delta TMD1}$ or its derivatives were used to express the wildtype or mutant *$S^{21}68_{\Delta TMD1}$* alleles. For the dominance/ recessiveness tests, derivatives of plasmid $pS^{21}68_a$ were used. They were induced by the phage 21 late gene activator Q^{21} expressed from either the lysogen MDS12*ΔtonA*(λ*Q^{21}Δ(SRRzRz1)^{21}*), or MDS12*ΔtonA*(λ*$S^{21}68$*) which provides a chromosomal copy of *$S^{21}68$*.

Media, culture growth, and induction of the lysis have been described previously (Pang *et al.*, 2009). Briefly, plasmids carried by lysogens were induced by shifting the culture into 42℃ for 15 minutes. Plasmid pQ was induced by 1 mM Isopropyl-β-D-thiogalactopyranoside (IPTG) and 0.2% arabinose. Lysis profiles were obtained by monitoring A_{550} after induction, as described previously (Smith & Young, 1998, Tran *et al.*, 2005). To assess the effect of DNP to the triggering of holin mutants, at the time when the wildtype holin triggers, 2mM DNP was added into each culture. Culture growth was monitored for additional 10 minutes, then cultures were spun down and the media containing DNP was poured away. Cell pellets were rinsed with LB media twice, and then resuspended in fresh LB media supplemented with corresponding antibiotics. Culture growth was monitored again.

Site-directed mutagenesis, and general DNA manipulations

Procedures for QuikChange (Stratagene) mutagenesis, cloning steps and DNA

sequencing have been described (Smith & Young, 1998). Oligonucleotides were obtained from Integrated DNA Technologies (Coralville, IA). All enzymes were purchased from Promega, except the *Pfu* polymerase, which was from Stratagene.

Chemical crosslinking *in vivo*

DSP crosslinking of $S^{21}68$ and its variants *in vivo* was described previously (Pang *et al.*, 2009). Briefly, 1 A_{550} unit of cells were harvested when wildtype $S^{21}68$ triggers (50 m after induction), washed and resuspended into 640 μl PBS (phosphate buffered saline). The samples were treated with 2mM DSP (Pierce) for 30 m at 25°C and then quenched with 20 mM Tris pH7.5. Proteins were precipitated by trichloroacetic acid (TCA) and analyzed by SDS-PAGE and Western blotting.

TCA precipitation, SDS-PAGE and Western blotting

TCA precipitation, SDS-PAGE and Western blotting were performed as described (Pang *et al.*, 2009). Briefly, 10% TCA was used to immediately stop cell growth and precipitate protein. Precipitates were resuspended in sample loading buffer with the addition of 5% β-mercaptoethanol, unless for the purpose of detecting the disulfide-bond linked dimer of $S^{21}68_{S16C}$ and its variants, or for analyzing the DSP-crosslinked oligomers. Samples were separated on 10% Tris-Tricine gels and transferred to 0.1 μm nitrocellulose membrane (Whatman, NJ). Antisera against the S^{21} C-terminal peptide KIREDRRKAARGE was used as primary antibody (Barenboim *et al.*, 1999).

CHAPTER V

LOCALIZATION OF THE PHAGE 21 PINHOLES

Introduction

Double-stranded DNA phage lysis strategies can be divided into at least two types by the differences in the solubility of endolysins. One is the 'large-hole' holins with soluble endolysins. The soluble endolysins like lambda R and T4 E accumulate in the cytosol in their active form but can only reach their target cell wall through the large holes formed by the holins, such as the canonical holins lambda S105 and T4 T (Young & White, 2008). Another type of endolysin is the SAR (signal anchor-release)-endolysins, such as the phage 21 R^{21}. These endolysins have an N-terminal TMD, the SAR domain, which serves as a signal sequence. Consequently, they are secreted by the host *sec* system. Thus initially they are anchored in the membrane by the SAR domain in an enzymatically inactive form. SAR endolysins are able to spontaneously release into the periplasm at a low rate, depending on the particular protein. Once released, the SAR endolysins fold into their active form to degrade the cell wall (Sun *et al.*, 2009). Thus the SAR-endolysins do not absolutely require the holes formed by holins for function. However, lysis caused by induction of a SAR-endolysin R^{21} alone is delayed and gradual, compared with the saltatory and earlier lysis effected by the holin $S^{21}68$ and R^{21} together (Park *et al.*, 2007). The effect of the holin is due to the fact that maintenance of the SAR domain in the bilayer requires the membrane to be energized; when the holin triggers, the membrane is depolarized and the SAR domains are quantitatively released.

Thus while the large-hole holins control lysis timing by the formation of holes large enough to allow release of the cytoplasmic endolysins, the holins working with the SAR-endolysins control it only by depolarizing the membrane, and are not required to form large holes. In fact, through biochemical and computational studies, the proposed hole formed by the holin $S^{21}68$ from phage 21 is about 1.5 nm in diameter, thus named pinholin (Pang *et al.*, 2009). Although the large-hole holins are interchangeable, and work for the SAR-endolysins, they cannot be replaced by the pinholins (Ramanculov & Young, 2001b, Park *et al.*, 2007).

The pinholin $S^{21}68$ is the shorter translational product of the S^{21} gene (Fig. 3.1A) (Barenboim *et al.*, 1999). The longer product, $S^{21}71$, having three residues (Met1-Lys2-Ser3) in addition to the N-terminus of $S^{21}68$, is a weak antiholin, which is able to delay but not completely block the function of holin $S^{21}68$. Both $S^{21}68$ and $S^{21}71$ have two transmembrane domains (TMDs) (Fig. 3.1D). The TMD1of $S^{21}68$ is a SAR domain, and dispensable, although its release from the membrane is required for the holin function (Park *et al.*, 2006) (Fig. 3.1B,C). The three N-terminal residues delay the release of the TMD1 of $S^{21}71$ (Fig. 3.1B). Fusing an *irs*-tag (sequence RYIRS) to the N-terminus of $S^{21}68$ completely blocks the release of TMD1 as well as its holin function (Fig. 3.1B, D). The fused protein $irsS^{21}68$ is not only non-lethal, but also exhibits a negative dominant phenotype (Park *et al.*, 2006). Thus it behaves as a strong antiholin against $S^{21}68$. Although $S^{21}68$ can be crosslinked into oligomers by the crosslinker DSP, the $irsS^{21}68$ can only be crosslinked into dimers, and it blocks the oligomerization of $S^{21}68$ as well (Pang *et al.*, 2009). The TMD2s alone line the heptameric pinhole in both the context of

$S^{21}68$ and the TMD1-deleted pinholin $S^{21}68_{\Delta TMD1}$(Pang *et al.*, 2009) (Fig. 3.1C, D). Considering the presence of >6,000 $S^{21}68$ molecules per cell at the time of triggering, there must be ~900 pinholes suddenly formed when triggering occurs (Pang *et al.*, 2009).

In Chapters III and IV, a thorough mutagenesis analysis on *S*^{21} gene was performed and a detailed pinhole formation pathway has been suggested. However, one interesting question raised for this pathway is whether the 900 $S^{21}68$ pinholes are dispersed in the membrane evenly, or are aggregated into certain loci. Certainly the individual heptameric pinholes themselves are small enough to maintain significant mobility in the membrane. Previously, White (2008) monitored the localization of a GFP-tagged version of the λ holin, S105, using fluorescent microscopy. Here, a similar technique was used to observe the localization of $S^{21}68$ and its variants and to correlate the subcellular distribution with the lethal function.

Results

GFP tag does not affect the function of $S^{21}68$ or its variants

To observe the localization of $S^{21}68$ and its variants, the GFP protein was fused to the extreme C-terminus of each protein. The fusion alleles were placed into the normal transcriptional context of the lambda lysis cassette, in the presence of a low copy plasmid that is inducible for the λ late gene activator, Q. The function of each fusion protein was verified by monitoring the culture density after induction of each construct (Fig. 5.1A, B). An abrupt cessation of culture growth, indicative of pinholin triggering

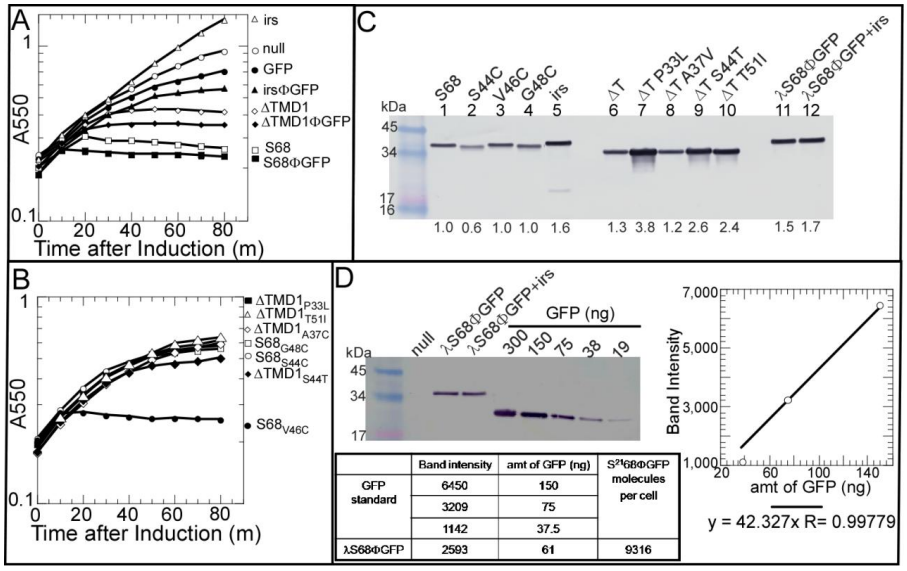

Fig. 5.1 GFP tag does not affect the function of $S^{21}68$ and its variants. A. Triggering of *$S^{21}68ΦGFP$* alleles. Cultures were induced at t=0 and monitored for growth at A_{550}. Each culture contained plasmid pQ and plasmid: pRE (open circles), pR'$S^{21}68$ (open squares), p$S^{21}68_{\Delta TMD1}$ (open diamonds), pirs$S^{21}68$ (open triangles), p$S^{21}68^{GFP}$ (closed squares), p$S^{21}68_{\Delta TMD1}{}^{GFP}$ (closed diamonds), pirs$S^{21}68^{GFP}$ (closed triangles), or pGFP (closed circles). **B. Triggering of the GFP-fused pinholin mutants.** Same as in A, except that each culture expressed: $S^{21}68_{S44C}$ (open circles), $S^{21}68_{V46C}$ (closed circles), $S^{21}68_{G48C}$ (open squares), $S^{21}68_{\Delta TMD1\text{-}P33L}$ (closed squares), $S^{21}68_{\Delta TMD1\text{-}A37C}$ (open diamonds), $S^{21}68_{\Delta TMD1\text{-}S44T}$ (closed diamonds), $S^{21}68_{\Delta TMD1\text{-}T51I}$ (open triangles). **C. Protein accumulation level of the *$S^{21}68ΦGFP$* alleles.** Each culture was induced and samples subjected to TCA precipitation at the time of triggering, or at 60 m after induction for the *irs$S^{21}68ΦGFP$* allele, or at the time when wt triggers for the other non-lethal alleles. Cultures in lanes 1-4 expressed $S^{21}68$ΦGFP (1) and its mutants S44C (2), V46C (3), G48C (4), respectively. Lane 5 has irs$S^{21}68$ΦGFP. Cultures in lanes 6-10 expressed $S^{21}68_{\Delta TMD1}$ΦGFP (6) and its mutants P33L (7), A37V (8), S44T (9), T51I (10), respectively. Cultures in lanes 11 and 12 carried phage λ*Cam*(*$S68^{GFP}R_{am}RzRz1$*)[21] and plasmid pRE (11) or pirs$S^{21}68$ (12). Western blotting was performed using antibodies against the GFP. The relative protein accumulation level normalized to the plasmid expressed $S^{21}68$ΦGFP is indicated at the bottom of each lane. **D. Measurement of $S^{21}68$ΦGFP expression level at the time of triggering.** Cultures were thermally induced and an aliquot of 1.5×10^8 cells was precipitated by TCA immediately after $S^{21}68$ΦGFP triggering. Samples were subjected to SDS-PAGE and Western blotting in parallel with samples containing a known amount of purified GFP. Lane 1, molecular weight standard; lane 2, MDS12*tonA::Tn10*[λ*Cam*Δ(*SR*)]; cultures in lanes 3 and 4 were the same as in lane 11 and 12 of C; lanes 5-9, purified GFP, amount indicated at the top of each lane. The relationship between the band intensities and the amount of GFP were listed in the table and analyzed in the curve. See *Materials and Methods*.

(Park *et al.*, 2006) was observed at ~10 min after induction for the $S^{21}68$ fusion, actually a few minutes earlier than the parental $S^{21}68$. Thus the GFP fusion had no deleterious effect on the holin function. The protein accumulation level of each construct was also measured by comparing it with the purified GFP protein (Fig. 5.1C, D). This revealed that at the time of triggering, ~7 x 10^3 $S^{21}68\Phi$GFP molecules were accumulated in this double-plasmid expression system. Similarly, the ΔTMD1 protein, and the functional mutant $S^{21}68_{V46C}$ also functioned equivalently well with the GFP fusion. Finally, the negative controls, the fusion of GFP to the non-functional, untriggerable irs$S^{21}68$ protein, as well as to the non-lethal mutant alleles of $S^{21}68$ (S44C, G48C) and $S^{21}68_{\Delta TMD1}$ (P33L, A37C, S44T, T51I) did not trigger. Thus, the addition of GFP tag did not affect either the function or the protein accumulation level of $S^{21}68$ or its variants.

Pinholins trigger to form small rafts in the membrane

The localization of GFP-fused pinholins after triggering was observed by the fluorescence microscopy (Fig. 5.2, 5.3A, B). All the functional pinholins, $S^{21}68$, $S^{21}68_{V46C}$ and $S^{21}68_{\Delta TMD1}$ were found in numerous small patches, which we designate as rafts, in the membrane. In contrast, the antiholin irs$S^{21}68$-GFP fusion was distributed evenly in the membrane, although the overall density appeared in some cells to be increased at the cell poles. The negative controls, the nonlethal mutants of $S^{21}68$ (S44C, G48C) and $S^{21}68_{\Delta TMD1}$ (P33L, A37C, S44T, T51I) were distributed evenly as well. To test if the formation of patches is an artifact of cell death or membrane depolarization, the uncoupler dinitrophenol (DNP) was added to the induced cultures before harvesting

for the fluorescence microscopy observation. The addition of DNP had no effect on the localization of either protein. Thus formation of the rafts is perfectly correlated with lethal pinhole formation ability.

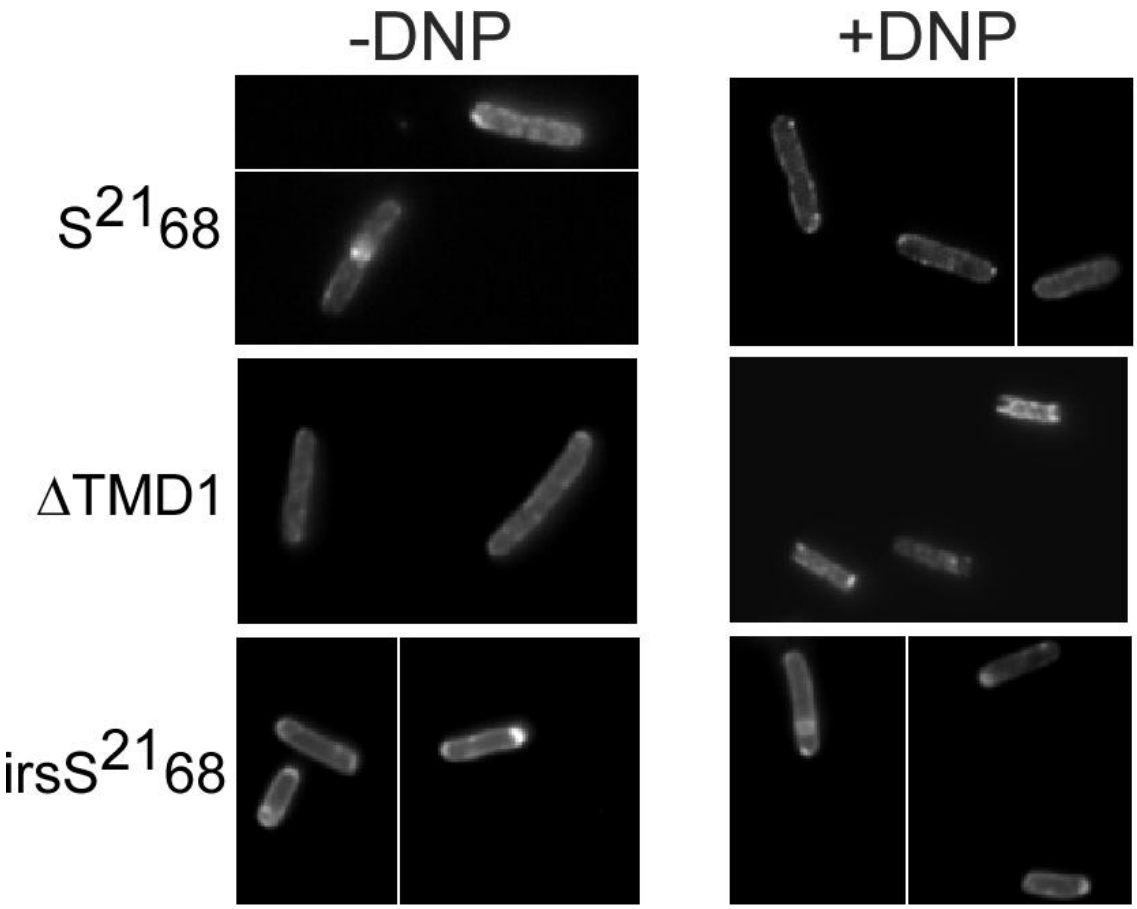

Fig. 5.2 Fluorescent images of cultures expressing $S^{21}68\Phi GFP$ and its variants. Each culture was induced and harvested at the time of triggering, or, in the case of $irsS^{21}68\Phi GFP$, at 60 m after induction. The right side panels for each construct are cultures treated with 2mM dinitrophenol (DNP) 10 m before harvesting. Each single box is 15μm × 10μm.

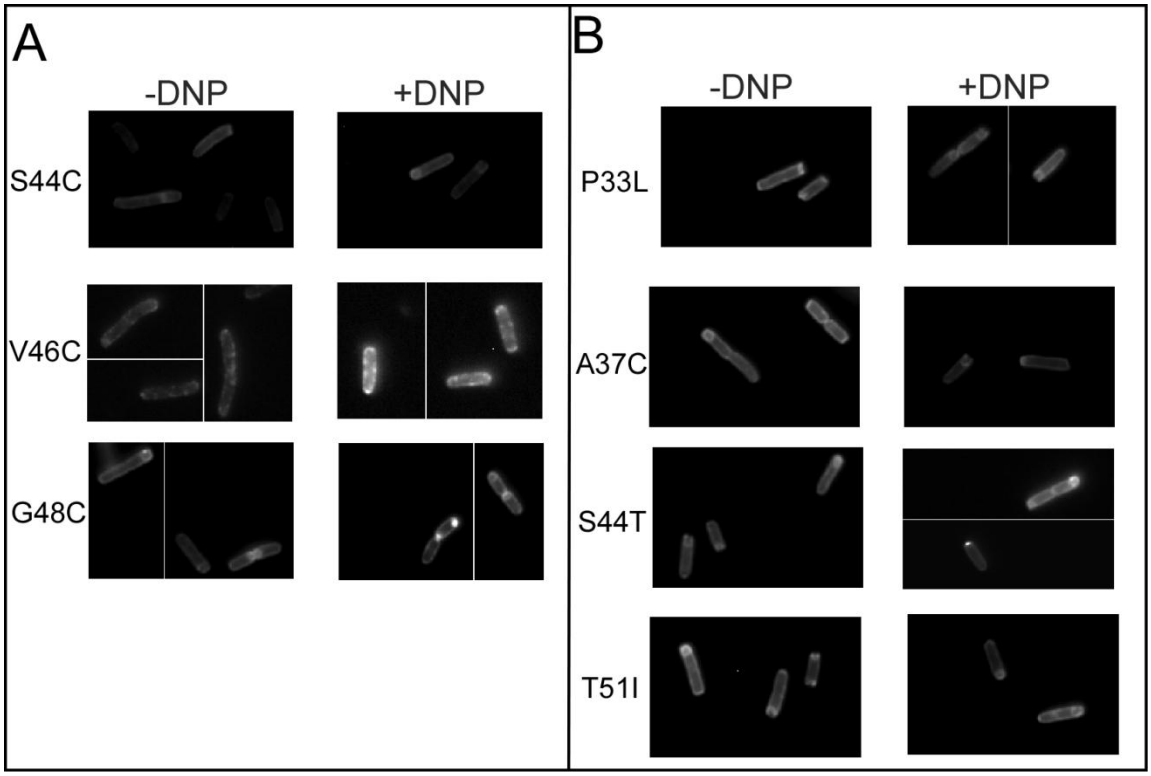

Fig. 5.3 Fluorescent images of cultures expressing $S^{21}68\Phi GFP$ mutants. Samples were prepared as in Fig. 5.2. For each mutant, the left panels and right panels are samples without or with the addition of 2mM DNP, respectively. Each single box is 15μm × 10μm.

Antiholin inhibits the rafts formation of pinholin

The antiholin $irsS^{21}68$ not only inhibits the function of $S^{21}68$, but also blocks its oligomerization by dimerizing with it. Thus, it was important to test if $irsS^{21}68$ would inhibit the raft formation of $S^{21}68$. To observe this effect, the lysogen MDS12*ΔtonA*[λ*Cam*($S68^{GFP}R_{am}RzRz1$)^{21}] was used to express the GFP-tagged $S^{21}68$, while the $irsS^{21}68$ was expressed in trans from plasmid $pirsS^{21}68$. The $S^{21}68\Phi GFP$ expressed from this construct reaches ~9 x 10^3 molecules per cell at the time of

triggering (Fig. 5.1B, C), still at the physiological level. The expression of irsS^{21}68 had no effect on the protein accumulation of S^{21}68ΦGFP (Fig. 5.1B) but completely inhibited its function (Fig. 5.4A) and its raft formation as well (Fig. 5.4B). Thus in every respect accessible to genetic, cytological, physiological and molecular testing, raft formation can be correlated with the lethal function of the pinholin. This strongly indicates that raft formation is a step on the pathway toward the pinhole formation.

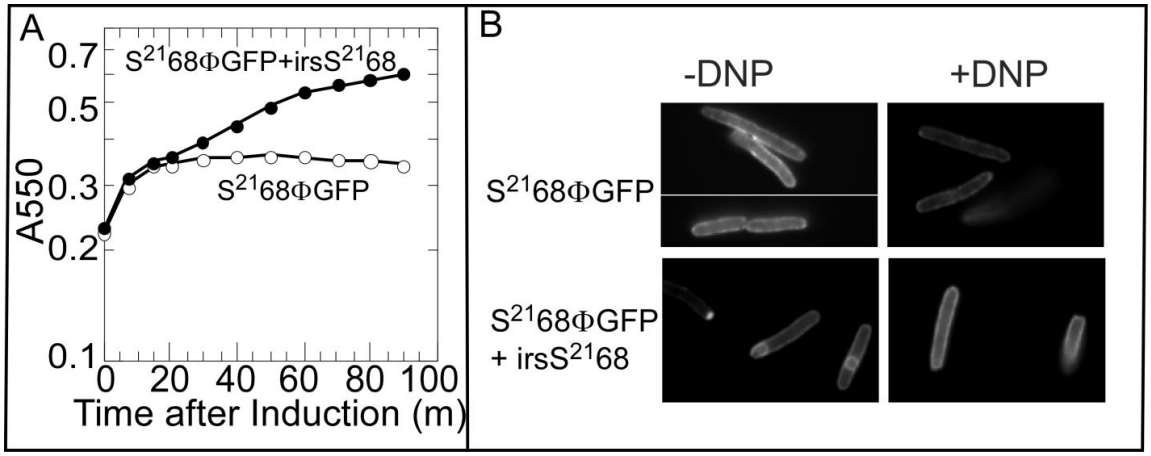

Fig. 5.4 The antiholin irsS^{21}68 inhibits both the triggering and rafts formation of the S^{21}68ΦGFP. A. irsS^{21}68 inhibits the triggering of S^{21}68ΦGFP. Lysogen MDS12*ΔtonA*[λ*Cam*(*S68*^{GFP}*R*$_{am}$*RzRz1*)^{21}] carrying plasmid pRE (open circle) or pirsS^{21}68 (filled circle) was induced at t=0. The culture growth was monitored as in Fig. 5.1A. **B. irsS^{21}68 inhibits the rafts formation of S^{21}68ΦGFP.** Cultures in Fig. 5.4A were harvested at 20 m after induction. Fluorescent images of each sample were taken and arranged as in Fig. 5.3. Each single box is 15μm × 10μm.

Discussion

Although much is known about the pinhole formation pathway of $S^{21}68$, the localization of these pinholes still remains unknown. A direct way of solving this question is to visualize the GFP-fused pinholins using fluorescence microscopy. The GFP fusion technology has been successful in localization studies of membrane proteins in general (Wahome *et al.*, 2009, Giorno *et al.*, 2009, Eberhardt *et al.*, 2009). In a recent study on lambda holin S105, White (2008) used the same technique and have found that S105 forms large rafts at the time or within 1 minute of the time of triggering, and the raft formation is correlated with the S105 function. However, there were problems in this study. First, a very large linker of 30 aa was required to achieve holin-like lysis kinetics. The shorter the linker is, the slower the holin-GFP lysis kinetics was. Secondly, even with the 30 aa linker, the S105ΦGFP still triggered much later than S105. The linker dependence and the slow kinetics suggest that GFP is sterically obstructing the formation of the large rafts or the rearrangement into large holes. Moreover, the number of large rafts was rather high, ranging from 0 to 9, with average 3. This does not correlate well with the large holes observed by Dewey *et al*. (2010), ranging from 0 to 3 per cell. This discrepancy might be due to the higher S105ΦGFP accumulation. Despite these problems, the major qualitative conclusion is that raft formation could be completely correlated with triggering. And, because these observations were done in real-time and using deconvolution confocal fluorescence microscopy, the dynamics and sudden nature of the triggering event could be observed. Although the latter was not possible in this project, due to lack of the technology, it was still of interest to test

whether, in the case of pinhole formation, lethal triggering could be associated with raft formation.

GFP-fusion is not deleterious to holin function or its regulation

In this work, the localization of $S^{21}68$ and its variants were visualized by the GFP fusion at the C-terminus of each protein with a 2 aa linker. A comparable physiological amount of GFP-fusion proteins were accumulated. In addition, the GFP-fusion faithfully maintained allele-specific triggering ability, and the ability to be regulated by antiholin $irsS^{21}68$. The fact that a much shorter linker was needed may reflect the simple radial symmetry of the heptameric pinhole, where the added 30 KDa C-terminal GFP would be displayed away from the lumen of the pinhole, without causing steric effect. Whereas the much larger S105 holes may not afford geometry that can easily allow the adjacency of so many GFP domains.

Rafts formation correlates with pinholin function

Visualization of the GFP-fusions has revealed that pinholin $S^{21}68$ aggregated into numerous small rafts. The formation of rafts is only related with the pinhole formation because: (1). All the lethal GFP-fused pinholins, $S^{21}68$, $S^{21}68_{\Delta TMD1}$, as well as $S^{21}68_{V46C}$ formed rafts. (2). Nonlethal mutants of $S^{21}68$ (S44C, G48C) and $S^{21}68_{\Delta TMD1}$ (P33L, A37C, S44T, T51I) as well as the antiholin $irsS^{21}68$ are all distributed evenly, without rafts formation. (3). Antiholin $irsS^{21}68$ not only inhibited the triggering of the GFP fused $S^{21}68$, but also blocked its rafts formation.

This is in parallel with S105ΦGFP, although pinholins formed much smaller and more rafts. This indicates a common molecular feature of holins and pinholins, the terminal phenotype is raft formation. Depolarizing the membrane by the triggering event is not a cause of raft formation, because the uncoupler DNP collapses the pmf same as the pinholin but did not rescue raft formation (or lethality) for either of the nonlethal mutants.

However, currently we do not know whether the rafts form after triggering or whether they occur at the same time as triggering. Future study will focus on using real-time observation of pinholin-GFP fusions to establish kinetics of raft formation and triggering. In addition, the FRAP (Fluoresence Recovery After Photobleaching) technique can be incorporated to test whether the pinholin rafts are mobile.

Materials and Methods

Bacterial strains and plasmids

The bacterial strains, prophages, and plasmids used in this work are described in Table 5.1. Briefly, *E. coli* strain MG1655*lacI*^{q1}*tonA*::Tn*10* (Guyer *et al.*, 1981) carrying plasmids pQ (Gründling *et al.*, 2001) and pR'S^{21}68, or pS^{21}68$_{\Delta TMD1}$, or pirsS^{21}68 was used to express the gene *S*^{21}*68*, or *S*^{21}*68*$_{\Delta TMD1}$, or *irsS*^{21}*68*, individually. Plasmid pR'S^{21}68 is identical to pTP2 (Park *et al.*, 2006), except for the introduction of amber nonsense codons into *R*^{21} (positions Tyr39 and Tyr42), *Rz*^{21} (Gln100), and *Rz1*^{21} (Trp39). Plasmid pS^{21}68$_{\Delta TMD1}$ and pirsS^{21}68 were described elsewhere (Pang *et al.*, 2009). The same *E. coli* strain carrying pQ and plasmids pGFP, pS^{21}68^{GFP},

Table 5.1. Strains, phage and plasmids.

	Genotype and relevant features	Source/ reference
phages		
λ*Cam*Δ(*SR*)	λb*515* b*519 att*::Tn*903 cI857 nin5* Δ(*SR*) *bor*::Cam^r	lab stock
λ*Cam*(*S68^{GFP}R$_{am}$RzRz1*)^{21}	λb*515* b*519 att*::Tn*903 cI857 nin5* Δ(*SRRzRz1*):: (*S68^{GFP}R$_{am}$RzRz1*)^{21} *bor*::Cam^r	this study
E. coli strains		
MG1655	F$^-$ *ilvG rfb50 rph1*	(Guyer *et al.*, 1981)
MG1655*lacI^{q1}tonA*::Tn*10*		(Park *et al.*, 2006)
MDS12	MG1655 with 12 deletions, totalling 376,180 nt, including cryptic prophages	(Kolisnychenko *et al.*, 2002)
MDS12*ΔtonA*		(Pang *et al.*, 2009)
MDS12*tonA::Tn10*		(Tran *et al.*, 2005)
MDS12*tonA::Tn10*[λ*Cam* Δ(*SR*)]	Lysogen carrying prophage λ*Cam*Δ(*SR*)	this study
MDS12*ΔtonA*[λ*Cam*(*S68^{GFP}R$_{am}$RzRz1*)^{21}]	Lysogen carrying prophage λ*Cam*(*S68^{GFP}R$_{am}$RzRz1*)^{21}	this study
MDS12*ΔtonA*(λ*S^{21}68*)	Lysogen carrying prophage λ*S^{21}68*	this study
LE392 *tonA*::Tn*10*	K-12 *hsdR574*(rK$^-$mK$^+$) *supE44 supF58* Δ(*lacIZY*)*6 galK2 galT22 metB1 trpR55 tonA*::Tn*10*	(Tran *et al.*, 2007)
plasmids		
pTP2	pBR322 origin, pR′ promoter, *(S68/R/Rz/Rz1)^{21}*	(Park *et al.*, 2006)
pR'S^{21}68	pTP2 (*R$_{am}$/Rz$_{am}$/Rz1$_{am}$)^{21}*	
pS^{21}68$_{\Delta TMD1}$	pTP2 with the codons encoding TMD1 of *S^{21}68* deleted, (*R$_{am}$/Rz$_{am}$/Rz1$_{am}$)^{21}*	(Pang *et al.*, 2009)
pirsS^{21}68	pR'S^{21}68 with the *irs* tag encoding RYIRS fused to N terminus of S^{21}68	(Pang *et al.*, 2009)
pQ	pSC101 origin with modification, P$_{lac/ara-1}$ promoter, *Q* from λ	(Gründling *et al.*, 2001)
pRE	pJF118EH with *lacI^Q* and P$_{tac}$ replaced by pR' promoter	(Park *et al.*, 2006)
pGFP	pRE with *gfp* gene inserted downstream of the *pR'* promoter	lab stock
pS^{21}68^{GFP}	pR'S^{21}68 with codons encoding linker sequence Pro and Gly (CCCGGG) and the *gfp* gene without Met1 (AUG) inserted between the last codon (GAA) of *S^{21}68* and the stop codon (UAA)	this study
pS^{21}68$_{\Delta TMD1}$^{GFP}	pS^{21}68$_{\Delta TMD1}$ with the linker and *gfp* same as in pS^{21}68^{GFP}	this study
pirsS^{21}68^{GFP}	pirsS^{21}68 with the linker and *gfp* same as in pS^{21}68^{GFP}	this study
p(S68^{GFP}R$_{am}$RzRz1)^{21}	pS^{21}68^{GFP} with wild-type *Rz^{21}* and *Rz1^{21}*	this study

$pS^{21}68_{\Delta TMD1}{}^{GFP}$, or $pirsS^{21}68^{GFP}$ were used for expression of proteins GFP, $S^{21}68\Phi GFP$, $S^{21}68_{\Delta TMD1}\Phi GFP$, or $irsS^{21}68\Phi GFP$, respectively. pGFP contains the *gfp* gene inserted downstream of the *pR'* promoter and replacing the $(SRRzRz1)^{21}$ lysis cassette of the plasmid pTP2 (Park *et al.*, 2006). The other three plasmids were mutated from plasmids $pR'S^{21}68$, $pS^{21}68_{\Delta TMD1}$, and $pirsS^{21}68$, respectively, with codons encoding residues Pro and Gly (CCCGGG) followed by the *gfp* gene without Met1 codon (AUG) inserted right after the last codon (GAA) of $S^{21}68$ and its variants and before the stop codon (UAA).

For comparison of the localization of $S^{21}68\Phi GFP$ in the absence or presence of $irsS^{21}68$, the plasmid pRE (Park *et al.*, 2006) or $pirsS^{21}68$ was transformed into, and transactivated by the lysogen MDS12*ΔtonA*[$\lambda Cam(S68^{GFP}R_{am}RzRz1)^{21}$] individually. This lysogen was obtained by lysogenizing the phage $\lambda Cam(S68^{GFP}R_{am}RzRz1)^{21}$ with *E. coli* MDS12*ΔtonA* (Pang *et al.*, 2009). The phage $\lambda Cam(S68^{GFP}R_{am}RzRz1)^{21}$ was isolated from clear plaques formed by a french pressate of *E. coli* MDS12*tonA::Tn10*[$\lambda Cam\Delta(SR)$] carrying plasmid $p(S68^{GFP}R_{am}RzRz1)^{21}$ on the amber suppressor *E. coli* strain LE392 *tonA*::Tn*10* (Tran *et al.*, 2007). Plasmid $p(S68^{GFP}R_{am}RzRz1)^{21}$ is identical to $pS^{21}68^{GFP}$, except that the Rz^{21} and $Rz1^{21}$ genes are wild-type. The french pressate was obtained by passing the induced culture through a French pressure cell (Spectronic Instruments; Rochester, MY) at 16,000 psi. 1% chloroform was added to the french pressate. Whole cells and cell debris were removed by centrifugation in a clinical centrifuge for 15 minutes at 4°C.

Media, culture growth, and general DNA manipulation

Cultures were grown in standard Luria- Bertani (LB) media supplemented with antibiotics where needed: kanamycin (40 μg/ml), ampicillin (100 μg/ml), and chloramphenicol (10 μg/ml). Plasmid pQ was induced by 1 mM isopropyl-β-D-thiogalactopyranoside (IPTG) and 0.2% arabinose. Plasmids carried by lysogens were induced by shifting the culture into 42°C for 15 m. Lysis profiles were obtained by monitoring A_{550} after thermal or IPTG/ arabinose inductions, as described previously (Smith & Young, 1998, Tran *et al.*, 2005). 2mM dinitrophenol (DNP) was added into each culture whenever indicated. Site-directed mutagenesis, cloning steps and DNA sequencing have been described elsewhere (Smith & Young, 1998).

TCA precipitation, SDS-PAGE and Western blotting

Ten percent TCA was used to immediately stop cell growth and precipitate protein as previously described (Park *et al.*, 2006). Precipitates were resuspended in sample loading buffer with the addition of 5% β-mercaptoethanol. SDS-PAGE and Western blotting were performed as described (Pang *et al.*, 2009). Proteins were separated on 10% Tris-Tricine gels and transferred to 0.1 μm nitrocellulose membrane (Whatman, NJ). GFP fusion protein was detected by Mouse monoclonal α-GFP antibodies (Stressgen, Ann Arbor, MI). Blots were developed by using the chromogenic substrate 4-chloro-1-naphthol (Sigma). Band intensity was determined by software ImageJ (http://rsbweb.nih.gov/ij/) (Abramoff *et al.*, 2004). The amount of S^{21}68ΦGFP

present in the induced cultures was calculated using the standard curve generated from samples containing the purified GFP protein.

Fluorescent microscopy

One ml of the induced culture was harvested at the time of triggering, or 60 m after induction for irsS^{21}68, or for the non-lethal S^{21}68 mutants, at the time the wild-type S^{21}68 triggers. Cell pellets were washed twice with phosphate buffered saline (PBS) pH7.2, and resuspended in 500 µl PBS. Five µl of the cell suspension was taken for analysis on the Zeiss Axio Observer microscope equipped with 100 × oil immersion objective (NA 1.4) and a Zeiss AxioCam HSm CCD camera. Fluorescence filter FITC was used for detecting GFP fused proteins (excitation: blue 490/20 nm; emission: green 528/38 nm). Data were collected and analyzed by the software AxioVision. Images were saved as TIFF files.

CHAPTER VI

CONCLUSIONS AND FUTURE DIRECTIONS

Like all dsDNA phages of Gram-negative hosts, bacteriophage 21 lyses the host using a three-step mechanism. In this case, the holin S^{21} forms pinholes in the membrane, which collapses the pmf and triggers the immediate release and activation of the SAR-endolysin R^{21} in the periplasm. The peptidoglycan is then degraded by R^{21}, which in turn allows the disruption of the outer membrane by the spanin proteins Rz^{21} and $Rz1^{21}$. As in the *S* gene of phage λ, S^{21} has a dual-start motif, encoding both a short polypeptide, $S^{21}68$, which is the real holin, and the longer polypeptide, $S^{21}71$, which is an antiholin. However, S^{21} has a profoundly different hole formation pathway, as published in the work of Park *et al.* (2006). The TMD2 of $S^{21}68$ alone is able to conduct the holin function, while the TMD1 has unprecedented dynamic topology. It is a SAR domain, which inserts in the membrane initially, and then releases from it spontaneously. Moreover, its removal from the membrane is required for the holin function, and correlates with the lysis timing. The positive charge(s) added to the N-terminus of TMD1, as in the case of $S^{21}71$ and the strong antiholin $irsS^{21}68$, significantly delay or block its release, and therefore delay or completely abolish the triggering of lysis. Recently, detailed study of S^{21} became more attractive with the finding that it forms small holes, or so called pinholes in the membrane, much smaller than those formed by the canonical holins like λ S and T4 T (Park *et al.*, 2007). The work in this dissertation is thus designed to explore the details of the pinhole formation mechanism of S^{21}, which

may be regarded as the prototype pinholin. The results of this study are summarized as follows:

1. We investigated the structure of the final pinhole by using gel-filtration chromatography, negative-stain transmission electron microscopy, chemical cross-linking, cysteine-accessibility, and computational approaches. The results suggest a structural model of the pinhole, in which pinholins form a symmetric heptamer, with the hydrophilic side of TMD2 lining the central channel of ~ 15 Å in diameter. The structural model also identified two helical-helical interaction surfaces for each TMD2 helix: surface A, comprising residues $W_{36}A_{37}xxG_{40}V_{41}xG_{43}S_{44}xxL_{47}G_{48}xL_{50}T_{51}xxT_{54}$; and surface B, comprising residues $A_{38}xxV_{41}L_{42}xxL_{45}xxxF_{49}xxY_{52}L_{53}xN_{55}L_{56}xF_{58}$. The core of surface A is formed by the glycine zipper motif $G_{40}xxxS_{44}xxxG_{48}$, which makes a sterically unhindered pocket accommodating the side chains of the bulky residues L45, F49 and Y52.

2. We analyzed an extensive collection of S^{21} mutants to identify residues and domains critical to the function and regulation of the pinholin. A wide range of phenotypes, from absolute lysis-defectives to accelerated lysis triggering were observed for mutations mapping to each topological domain. We provided evidence indicating that the membrane-inserted TMD1 acts in trans as an inhibitor of the lethal function of TMD2 within the inactive dimer, the first kinetically important stage towards pinhole formation. In addition, the analysis of the phenotypes of S^{21} mutants provides a model for the structure of the inactive dimer. The model identifies the faces of the two

transmembrane domains involved in intramolecular and intermolecular interactions, as well as interaction with the lipid.

3. We further analyzed the early-lysis mutants and the non-lethal mutants of $S^{21}68$. As a conclusion, a refined model for the S^{21} pinhole formation pathway is proposed. In this model, the individually folded and inserted S^{21} molecules first form an inactive dimer form (ID1), with both TMDs inserted in the membrane. For the inactive dimer formed between $S^{21}68$ and $S^{21}71$, a second inactive dimer (ID2) might form, with only one TMD1 externalized in the periplasm. Then, when both TMD1s are released from the membrane, the activated dimer is formed, with the homotypic interaction between the two A surfaces. The A:A interaction is presumed to be unstable, shifting to A:B interaction and thus allowing S^{21} to oligomerize. Finally, the heptameric pinhole forms, possibly driven by the hydration of the lumenal hydrophilic residues. This study also points out the significance of the glycine zipper motif ($G_{40}xxxS_{44}xxxG_{48}$) in TMD2. This motif is likely involved in three interactions: an intramolecular, heterotypic interaction with TMD1 in the inactive dimer stage; an intermolecular homotypic interaction with itself in the activated dimer stage; and a heterotypic, intermolecular interaction with interface B in the oligomer stage and the pinhole.

4. We observed the localization of GFP fusion constructs of $S^{21}68$ and its variants using fluorescence microscopy. Functional pinholins such as $S^{21}68$, $S^{21}68_{\Delta TMD1}$, and $S^{21}68_{V46C}$ all formed numerous small aggregates, designated as 'rafts'. In contrast, the non-lethal $S^{21}68$ and $S^{21}68_{\Delta TMD1}$ mutants were distributed evenly in the membrane. In addition, the GFP fusion of the antiholin irs$S^{21}68$ was uniformly dispersed as well.

Finally, irsS^{21}68 was able to prevent S^{21}68ΦGFP from triggering to a punctate distribution. These results demonstrate conclusively that formation of the rafts is correlated with pinhole formation.

These results point the way to future work. In particular, several projects should have high priority:

1. Determination of the final structure of the pinhole. Although the heptameric structure model has been suggested by the biochemical and computational analysis presented in Chapter II, the structure still needs to be determined. So far, the antiholin irsS^{21}68 can be successfully purified in 0.1% (w/v) DDM (n-dodecyl-β-D-Maltopyranoside) with a relatively higher yield (0.8 mg protein /L culture) than S^{21}68 (0.1 mg protein /L culture). In detergent, irsS^{21}68 forms a ring-like structure undistinguishable from S^{21}68 (Pang *et al.*, 2009). Thus it is possible to crystallize irsS^{21}68 and solve the structure of the final pinhole.

2. Determination of the structure of the inactive dimer. So far, a low resolution structure is suggested by the genetic analysis of the *S^{21}* mutants. It can be refined through at least three ways. One way is to build a computational model for this structure. As in Chapter II, the software suite CHI can be used to model the interaction between TMD1 and TMD2 in the inactive dimer. Another approach is to adopt the cysteine-scanning method to map the TMD1-TMD2 interaction faces. According to the inactive dimer structure suggested in Chapter III, a pair of cysteines can be engineered in TMD1 and TMD2 respectively with possible TMD1-TMD2 interactions. If these cysteines interact in trans, they will be able to form copper-phenanthroline-mediated disulfide-

bond-linked dimers (Gründling *et al.*, 2000b, Sun & Kaback, 1997). If they interact in cis, the copper-phenanthroline-mediated disulfide-bond formation can be verified by the insensitivity of the solubilized protein to pegylation (Lu & Deutsch, 2001). Obviously, the third way is the structural studies through crystallization, if the inactive dimer structure can be retained with the trans and cis disulfide bonds formed between the engineered cysteines of TMD1 and TMD2.

3. Verification of the intermediate stages in the pinhole formation pathway. Mutational analysis suggested a detailed pinhole formation pathway, based on the rationale that mutants were found blocked in various intermediate stages. These putative intermediate stages need to be verified in a more direct way showing the population of these states occurs in a sequential manner. This can be achieved by incorporating the photo-cross-linking technique as shown in Ieva and Bernstein (2009). This technique uses the co-expression of an amber suppressor tRNA and an aminoacyl-tRNA synthetase to incorporate the photo-cross-linkable amino acid *p*-benzoyl-L-phenylalanine (*p*Bpa) at an amber codon engineered into a protein of interest (Farrell *et al.*, 2005). Upon exposure under UV light, *p*Bpa will cross-link with any protein molecule in its close proximity. Using this technique, *p*Bpa can be introduced into $S^{21}68$ at proposed helical-helical interaction faces. Cells grown in minimal media supplemented with *p*Bpa will be photo-cross-linked by being exposed to UV light at various times after induction of $S^{21}68$. Hypothetically the pinhole formation intermediates will be revealed by SDS-PAGE and immuno-blotting.

4. To evaluate the advantage of lysis with both pinholin and SAR-endolysin versus with SAR-endolysin alone. It has been shown that phages carrying R^{21} along had much slower lysis kinetics, and formed heterogeneous and relatively smaller plaques, compared to the lysis carried by S^{21} and R^{21} together (Park *et al.*, 2007). It suggests that lysis by R^{21} alone is not phenotypically uniform in terms of all cells having the precisely same lysis time. Besides that, it is possible that cells expressing R^{21} alone decrease the pmf more gradually than with pinholins together, since the R^{21} is released spontaneously to degrade the cell wall without pinholins. Both hypotheses can be tested by the 'spinning bug' experiment as performed by Gründling *et al.* (2001). Individual cells expressing both S^{21}68 and R^{21} or R^{21} alone can be tethered to the flow chamber by a single flagellum through the flagellar filament-specific antibody. After induction of synchronized expression of lysis proteins, the membrane integrity can be measured through continuous monitor of the rotational velocity of each cell, which is proportional to the pmf to at least -160 mV (Gründling *et al.*, 2001, Fung & Berg, 1995). In addition, lysis by SAR-endolysins alone may be more difficult to alter lysis timing by incorporating mutants. Because the function of SAR-endolysin is to degrade the cell wall, any mutation that affects the lysis timing may only result from altering its expression, or its enzymatic activity. This can be tested by analysis of the phenotypes of random mutants generated on R^{21}. Recently, Zheng *et al.* (2008) compared the lysis fitness of the holin-endolysin lysis system and the single gene *E*- mediated lysis system. The E protein from phage ϕX174 lyses the host cell by inhibiting the function of MraY, the enzyme involved in cell wall synthesis. Their work has shown that E-mediate lysis

lacks the plasticity of lysis timing, which might be the reason why all the dsDNA phages adopt the holin-endolysin lysis system to better adjust to the environment. Similarly, the incorporation of holins to the SAR-endolysin lysis system may allow lysis timing malleability, which is probably the reason that the holin gene is always found in the phage genome along with the SAR-endolysins (Ry Young, personal communication).

Despite the above questions, other questions will arise as we continue to study the $S^{21}68$ protein. Being a small membrane protein with only 68 amino acids, and two TM helices, $S^{21}68$ is also a good model for study of the membrane protein folding mechanism, and the insertion and release mechanism of SAR domains.

REFERENCES

Abad, C., Martinez-Gil, L., Tamborero, S. & Mingarro, I., (2009) Membrane topology of gp41 and amyloid precursor protein: interfering transmembrane interactions as potential targets for HIV and Alzheimer treatment. *Biochim Biophys Acta* **1788**: 2132-2141.

Abedon, S. T., (2006) Phage ecology. In *The Bacteriophages.* Calendar, R. (ed). Oxford: Oxford University Press, pp. 37-46.

Abramoff, M. D., Magelhaes, P. J. & Ram, S. J., (2004) Image processing with ImageJ. *Biophotonics International* **11**: 36-42.

Ackermann, H.-W., (2001) Frequency of morphological phage descriptions in the year 2000. Brief review. *Arch Virol* **146**: 843-857.

Ackermann, H.-W., (2006) Classification of bacteriophages. In *The Bacteriophages.* Calendar, R. (ed). Oxford: Oxford University Press, pp. 8-16.

Adams, P. D., Arkin, I. T., Engelman, D. M. & Brunger, A. T., (1995) Computational searching and mutagenesis suggest a structure for the pentameric transmembrane domain of phospholamban. *Nature Structure Biology* **2**: 154-162.

Adams, P. D., Engelman, D. M. & Brunger, A. T., (1996) Improved prediction for the structure of the dimeric transmembrane domain of glycophorin A obtained through global searching. *Proteins* **26**: 257-261.

Agu, C. A., Klein, R., Lengler, J., Schilcher, F., Gregor, W., Peterbauer, T., Blasi, U., Salmons, B., Gunzburg, W. H. & Hohenadl, C., (2007) Bacteriophage-encoded toxins: the lambda-holin protein causes caspase-independent non-apoptotic cell death of eukaryotic cells. *Cell Microbiol* **9**: 1753-1765.

Akabas, M. H., Stauffer, D. A., Xu, M. & Karlin, A., (1992) Acetylcholine receptor channel structure probed in cysteine-substitution mutants. *Science* **258**: 307-310.

Aoudia, M. & Zana, R., (1998) Aggregation behavior of sugar surfactants in aqueous solutions: effects of temperature and the addition of nonionic polymers. *J Colloid Interface Sci* **206**: 158-167.

Barenboim, M., Chang, C. Y., dib Hajj, F. & Young, R., (1999) Characterization of the dual start motif of a class II holin gene. *Mol Microbiol* **32**: 715-727.

Bartel, P. L., Roecklein, J. A., SenGupta, D. & Fields, S., (1996) A protein linkage map of *Escherichia coli* bacteriophage T7. *Nat Genet* **12**: 72-77.

Bernhardt, T. G., Roof, W. D. & Young, R., (2000) Genetic evidence that the bacteriophage ϕX174 lysis protein inhibits cell wall synthesis. *Proc Natl Acad Sci USA* **97**: 4297-4302.

Bernhardt, T. G., Struck, D. K. & Young, R., (2001a) The lysis protein E of ϕX174 is a specific inhibitor of the MraY-catalyzed step in peptidoglycan synthesis. *J Biol Chem* **276**: 6093-6097.

Bernhardt, T. G., Wang, I. N., Struck, D. K. & Young, R., (2001b) A protein antibiotic in the phage Qβ virion: diversity in lysis targets. *Science* **292**: 2326-2329.

Berry, J., Summer, E. J., Struck, D. K. & Young, R., (2008) The final step in the phage infection cycle: the Rz and Rz1 lysis proteins link the inner and outer membranes. *Mol Microbiol* **70**: 341-351.

Bigelow, H. R., Petrey, D. S., Liu, J., Przybylski, D. & Rost, B., (2004) Predicting transmembrane beta-barrels in proteomes. *Nucleic Acids Res* **32**: 2566-2577.

Bläsi, U., Chang, C. Y., Zagotta, M. T., Nam, K. & Young, R., (1990) The lethal λ *S* gene encodes its own inhibitor. *EMBO Journal* **9**: 981-989.

Bläsi, U., Fraisl, P., Chang, C. Y., Zhang, N. & Young, R., (1999) The C-terminal sequence of the lambda holin constitutes a cytoplasmic regulatory domain. *J Bacteriol* **181**: 2922-2929.

Bläsi, U., Nam, K., Hartz, D., Gold, L. & Young, R., (1989) Dual translational initiation sites control function of the λ S gene. *EMBO Journal* **8**: 3501-3510.

Bläsi, U. & Young, R., (1996) Two beginnings for a single purpose: the dual-start holins in the regulation of phage lysis. *Mol Microbiol* **21**: 675-682.

Bocharov, E. V., Pustovalova, Y. E., Pavlov, K. V., Volynsky, P. E., Goncharuk, M. V., Ermolyuk, Y. S., Karpunin, D. V., Schulga, A. A., Kirpichnikov, M. P., Efremov, R. G., Maslennikov, I. V. & Arseniev, A. S., (2007) Unique dimeric structure of BNip3 transmembrane domain suggests membrane permeabilization as a cell death trigger. *J Biol Chem* **282**: 16256-16266.

Bonovich, M. T. & Young, R., (1991) Dual start motif in two lambdoid *S* genes unrelated to lambda *S*. *J Bacteriol* **173**: 2897-2905.

Brosig, B. & Langosch, D., (1998) The dimerization motif of the glycophorin A transmembrane segment in membranes: importance of glycine residues. *Protein Sci* **7**: 1052-1056.

Campbell, A. M., (1969) *Episomes*., New York: Harper and Row.

Casjens, S. R., Eppler, K., Parr, R. & Poteete, A. R., (1989) Nucleotide sequence of the bacteriophage P22 gene 19 to 3 region: identification of a new gene required for lysis. *Virology* **171**: 588-598.

Chang, C. Y., Nam, K. & Young, R., (1995) *S* gene expression and the timing of lysis by bacteriophage lambda. *J Bacteriol* **177**: 3283-3294.

Cosson, P. & Bonifacino, J. S., (1992) Role of transmembrane domain interactions in the assembly of class II MHC molecules. *Science* **258**: 659-662.

Curran, A. R. & Engelman, D. M., (2003) Sequence motifs, polar interactions and conformational changes in helical membrane proteins. *Curr Opin Struct Biol* **13**: 412-417.

Davidson, V. L., Brunden, K. R., Cramer, W. A. & Cohen, F. S., (1984) Studies on the mechanism of action of channel-forming colicins using artificial membranes. *J Membrane Biol* **79**: 105-118.

Deaton, J., Savva, C. G., Sun, J., Holzenburg, A., Berry, J. & Young, R., (2004) Solubilization and delivery by GroEL of megadalton complexes of the lambda holin. *Protein Sci* **13**: 1778-1786.

Delbrück, M., (1942) Interference between bacterial viruses: I. Interference between two bacterial viruses acting on the same host, and the mechanism of virus growth. *Archives of Biochemistry and Biophysics*: 1238-1244.

Dewey, J. S., Savva, C. G., White, R. L., Vitha, S., Holzenburg, A. & Young, R., (2010) Micron-scale holes terminate the phage infection cycle. *Proc Natl Acad Sci USA* **107**: 2219-2223.

Eberhardt, A., Wu, L. J., Errington, J., Vollmer, W. & Veening, J. W., (2009) Cellular localization of choline-utilization proteins in *Streptococcus pneumoniae* using novel fluorescent reporter systems. *Mol Microbiol* **74**: 395-408.

Engelman, D. M., Chen, Y., Chin, C. N., Curran, A. R., Dixon, A. M., Dupuy, A. D., Lee, A. S., Lehnert, U., Matthews, E. E., Reshetnyak, Y. K., Senes, A. & Popot, J. L., (2003) Membrane protein folding: beyond the two stage model. *FEBS Lett* **555**: 122-125.

Farrell, I. S., Toroney, R., Hazen, J. L., Mehl, R. A. & Chin, J. W., (2005) Photo-cross-linking interacting proteins with a genetically encoded benzophenone. *Nat Methods* **2**: 377-384.

Fleming, K. G. & Engelman, D. M., (2001) Computation and mutagenesis suggest a structure for the synaptobrevin transmembrane dimer. *Proteins* **45**: 313-317.

Fu, D., Libson, A., Miercke, L. J., Weitzman, C., Nollert, P., Krucinski, J. & Stroud, R. M., (2000) Structure of a glycerol-conducting channel and the basis for its selectivity. *Science* **290**: 481-486.

Fung, D. C. & Berg, H. C., (1995) Powering the flagellar motor of *Escherichia coli* with an external voltage source. *Nature* **375**: 809-812.

Furthmayr, H. & Marchesi, V. T., (1976) Subunit structure of human erythrocyte glycophorin A. *Biochemistry* **15**: 1137-1144.

Garrett, J., Bruno, C. & Young, R., (1990) Lysis protein S of phage lambda functions in *Saccharomyces cerevisiae*. *J Bacteriol* **172**: 7275-7277.

Giorno, R., Mallozzi, M., Bozue, J., Moody, K. S., Slack, A., Qiu, D., Wang, R., Friedlander, A., Welkos, S. & Driks, A., (2009) Localization and assembly of proteins comprising the outer structures of the *Bacillus anthracis* spore. *Microbiology* **155**: 1133-1145.

Graschopf, A. & Bläsi, U., (1999) Molecular function of the dual-start motif in the λ S holin. *Mol Microbiol* **33**: 569-582.

Gratkowski, H., Lear, J. D. & DeGrado, W. F., (2001) Polar side chains drive the association of model transmembrane peptides. *Proc Natl Acad Sci USA* **98**: 880-885.

Gründling, A., Blasi, U. & Young, R., (2000a) Genetic and biochemical analysis of dimer and oligomer interactions of the lambda S holin. *J Bacteriol* **182**: 6082-6090.

Gründling, A., Bläsi, U. & Young, R., (2000b) Genetic and biochemical analysis of dimer and oligomer interactions of the λ *S* holin. *J Bacteriol* **182**: 6082-6090.

Gründling, A., Manson, M. D. & Young, R., (2001) Holins kill without warning. *Proc Natl Acad Sci USA* **98**: 9348-9352.

Gründling, A., Smith, D. L., Bläsi, U. & Young, R., (2000c) Dimerization between the holin and holin inhibitor of phage lambda. *J Bacteriol* **182**: 6075-6081.

Guyer, M. S., Reed, R. R., Steitz, J. A. & Low, K. B., (1981) Identification of a sex-factor-affinity site in *E. coli* as gamma delta. *Cold Spring Harb Symp Quant Biol* **45** (Pt 1): 135-140.

Hankin, M. E., (1896) The bactericidal action of the waters of the Jamuna and Ganga Rivers on Cholera microbes. *Ann De I' Inst Pasteur* **10**: 511-522.

Hanych, B., Kedzierska, S., Walderich, B., Uznanski, B. & Taylor, A., (1993) Expression of the Rz gene and the overlapping Rz1 reading frame present at the right end of the bacteriophage lambda genome. *Gene* **129**: 1-8.

Haupts, U., Tittor, J. & Oesterhelt, D., (1999) Closing in on bacteriorhodopsin: progress in understanding the molecule. *Annu Rev Biophys Biomol Struct* **28**: 367-399.

Hershey, A. D., (1946a) Mutation of bacteriophage with respect to type of plaque. *Genetics* **31**: 620-640.

Hershey, A. D., (1946b) Spontaneous mutations in bacterial viruses. *Cold Spring Harbor Symposium on Quantitative Biology* **11**: 67-77.

Ieva, R. & Bernstein, H. D., (2009) Interaction of an autotransporter passenger domain with BamA during its translocation across the bacterial outer membrane. *Proc Natl Acad Sci USA* **106**: 19120-19125.

Iida, S. & Arber, W., (1977) Plaque forming specialized transducing phage P1: isolation of P1CmSmSu, a precursor of P1Cm. *Molecular and General Genetics* **153**: 259-269.

Johnson-Boaz, R., Chang, C. Y. & Young, R., (1994) A dominant mutation in the bacteriophage lambda S gene causes premature lysis and an absolute defective plating phenotype. *Mol Microbiol* **13**: 495-504.

Jorgensen, W. L. & Tirado-Rives, J., (1988) The OPLS [optimized potentials for liquid simulations] potential functions for proteins, energy minimizations for crystals of cyclic peptides and crambin. *Journal of the American Chemical Society* **110**: 1657-1666.

Kahn, T. W. & Engelman, D. M., (1992) Bacteriorhodopsin can be refolded from two independently stable transmembrane helices and the complementary five-helix fragment. *Biochemistry* **31**: 6144-6151.

Kaplan, R. S., Mayor, J. A., Brauer, D., Kotaria, R., Walters, D. E. & Dean, A. M., (2000) The yeast mitochondrial citrate transport protein. Probing the secondary structure of transmembrane domain iv and identification of residues that likely comprise a portion of the citrate translocation pathway. *J Biol Chem* **275**: 12009-12016.

Kedzierska, S., Wawrzynow, A. & Taylor, A., (1996) The Rz1 gene product of bacteriophage lambda is a lipoprotein localized in the outer membrane of *Escherichia coli. Gene* **168**: 1-8.

Kim, S., Jeon, T. J., Oberai, A., Yang, D., Schmidt, J. J. & Bowie, J. U., (2005) Transmembrane glycine zippers: physiological and pathological roles in membrane proteins. *Proc Natl Acad Sci USA* **102**: 14278-14283.

Kolisnychenko, V., Plunkett, G., III, Herring, C. D., Feher, T., Posfai, J., Blattner, F. R. & Posfai, G., (2002) Engineering a reduced *Escherichia coli* genome. *Genome Res* **12**: 640-647.

Lederberg, E. M. & Lederberg, J., (1953) Genetic studies of lysogenicity in *Escherichia coli*. *Genetics* **38**: 51-64.

Lemmon, M. A., Flanagan, J. M., Hunt, J. F., Adair, B. D., Bormann, B. J., Dempsey, C. E. & Engelman, D. M., (1992a) Glycophorin A dimerization is driven by specific interactions between transmembrane alpha-helices. *J Biol Chem* **267**: 7683-7689.

Lemmon, M. A., Flanagan, J. M., Treutlein, H. R., Zhang, J. & Engelman, D. M., (1992b) Sequence specificity in the dimerization of transmembrane alpha-helices. *Biochemistry* **31**: 12719-12725.

Lenz, O., Dittmar, M. T., Wagner, A., Ferko, B., Vorauer-Uhl, K., Stiegler, G. & Weissenhorn, W., (2005) Trimeric membrane-anchored gp41 inhibits HIV membrane fusion. *J Biol Chem* **280**: 4095-4101.

Lev, N., Fridmann-Sirkis, Y., Blank, L., Bitler, A., Epand, R. F., Epand, R. M. & Shai, Y., (2009) Conformational stability and membrane interaction of the full-length ectodomain of HIV-1 gp41: implication for mode of action. *Biochemistry* **48**: 3166-3175.

Liu, Y., Engelman, D. M. & Gerstein, M., (2002) Genomic analysis of membrane protein families: abundance and conserved motifs. *Genome Biol* **3**: 54.1-54.12.

Lu, J. & Deutsch, C., (2001) Pegylation: a method for assessing topological accessibilities in Kv1.3. *Biochemistry* **40**: 13288-13301.

Ludtke, S. J., Baldwin, P. R. & Chiu, W., (1999) EMAN: semiautomated software for high-resolution single-particle reconstructions. *J Struct Biol* **128**: 82-97.

Luirink, J., von Heijne, G., Houben, E. & de Gier, J. W., (2005) Biogenesis of inner membrane proteins in *Escherichia coli*. *Annu Rev Microbiol* **59**: 329-355.

Lutz, R. & Bujard, H., (1997) Independent and tight regulation of transcriptional units in *Escherichia coli* via the LacR/O, the TetR/O and AraC/I1-I2 regulatory elements. *Nucleic Acids Res* **25**: 1203-1210.

Lwoff, A., (1953) Lysogeny. *Bacteriological Reviews* **17**:269-337.

MacKenzie, K. R., Prestegard, J. H. & Engelman, D. M., (1997) A transmembrane helix dimer: structure and implications. *Science* **276**: 131-133.

Markov, D., Christie, G. E., Sauer, B., Calendar, R., Park, T., Young, R. & Severinov, K., (2004) P2 growth restriction on an rpoC mutant is suppressed by alleles of the Rz1 homolog lysC. *J Bacteriology* **186**: 4628-4637.

Marti, T., (1998) Refolding of bacteriorhodopsin from expressed polypeptide fragments. *J Biol Chem* **273**: 9312-9322.

McDonald, I. K. & Thornton, J. M., (1994) Satisfying hydrogen bonding potential in proteins. *J Mol Biol* **238**: 777-793.

Meng, G., Fronzes, R., Chandran, V., Remaut, H. & Waksman, G., (2009) Protein oligomerization in the bacterial outer membrane (Review). *Mol Membr Biol* **26**: 136-145.

Miller, J. H., (1992) *A Short Course in Bacterial Genetics: A Laboratory Manual and Handbook for Escherichia coli and Related Bacteria*. Cold Spring Harbor, NY: Cold Spring Harbor Laboratory Press.

Miroux, B. & Walker, J. E., (1996) Over-production of proteins in *Escherichia coli*: mutant hosts that allow synthesis of some membrane proteins and globular proteins at high levels. *J Mol Biol* **260**: 289-298.

Miyauchi, K., Curran, R., Matthews, E., Komano, J., Hoshino, T., Engelman, D. M. & Matsuda, Z., (2006) Mutations of conserved glycine residues within the membrane-spanning domain of human immunodeficiency virus type 1 gp41 can inhibit membrane fusion and incorporation of Env onto virions. *Jpn J Infect Dis* **59**: 77-84.

Moore, D. T., Berger, B. W. & DeGrado, W. F., (2008) Protein-protein interactions in the membrane: sequence, structural, and biological motifs. *Structure* **16**: 991-1001.

Nascimento, J. G., Guerreiro-Pereira, M. C., Costa, S. F., Sao-Jose, C. & Santos, M. A., (2008) Nisin-triggered activity of Lys44, the secreted endolysin from *Oenococcus oeni* phage fOg44. *J Bacteriol* **190**: 457-461.

Pang, T., Park, T. & Young, R., (2010) Mutational analysis of the S^{21} pinholin. *Mol Microbiol* **(In press)**.

Pang, T., Savva, C. G., Fleming, K. G., Struck, D. K. & Young, R., (2009) Structure of the lethal phage pinhole. *Proc Natl Acad Sci USA* **106**: 18966-18971.

Park, T., Struck, D. K., Dankenbring, C. A. & Young, R., (2007) The pinholin of lambdoid phage 21: control of lysis by membrane depolarization. *J Bacteriol* **189**: 9135-9139.

Park, T., Struck, D. K., Deaton, J. F. & Young, R., (2006) Topological dynamics of holins in programmed bacterial lysis. *Proc Natl Acad Sci USA* **103**: 19713-19718.

Pattabiraman, N., Ward, K. B. & Fleming, P. J., (1995) Occluded molecular surface: analysis of protein packing. *J Mol Recognit* **8**: 334-344.

Plotkowski, M. L., Kim, S., Phillips, M. L., Partridge, A. W., Deber, C. M. & Bowie, J. U., (2007) Transmembrane domain of myelin protein zero can form dimers: possible implications for myelin construction. *Biochemistry* **46**: 12164-12173.

Popot, J. L. & Engelman, D. M., (1990) Membrane protein folding and oligomerization: the two-stage model. *Biochemistry* **29**: 4031-4037.

Popot, J. L. & Engelman, D. M., (2000) Helical membrane protein folding, stability, and evolution. *Annu Rev Biochem* **69**: 881-922.

Prince, S. M., Papiz, M. Z., Freer, A. A., McDermott, G., Hawthornthwaite-Lawless, A. M., Cogdell, R. J. & Isaacs, N. W., (1997) Apoprotein structure in the LH2 complex from *Rhodopseudomonas acidophila* strain 10050: modular assembly and protein pigment interactions. *J Mol Biol* **268**: 412-423.

Raab, R., Neal, G., Garrett, J., Grimaila, R., Fusselman, R. & Young, R., (1986) Mutational analysis of bacteriophage lambda lysis gene *S*. *J Bacteriology* **167**: 1035-1042.

Raab, R., Neal, G., Sohaskey, C., Smith, J. & Young, R., (1988) Dominance in lambda *S* mutations and evidence for translational control. *J Mol Biol* **199**: 95-105.

Ramanculov, E. & Young, R., (2001a) An ancient player unmasked: T4 *rI* encodes a *t* -specific antiholin. *Mol Microbiol* **41**: 575-583.

Ramanculov, E. & Young, R., (2001b) Functional analysis of the T4 *t* holin in a lambda context. *Mol Genet Genomics* **265**: 345-353.

Ramanculov, E. & Young, R., (2001c) Genetic analysis of the T4 holin: timing and topology. *Gene* **265**: 25-36.

Ramanculov, E. M., (2001) Bacteriophage T4 lysis and lysis inhibition: A molecular perspective. Ph.D. dissertation. College Station: Texas A&M University.

Rosevear, P., VanAken, T., Baxter, J. & Ferguson-Miller, S., (1980) Alkyl glycoside detergents: a simpler synthesis and their effects on kinetic and physical properties of cytochrome c oxidase. *Biochemistry* **19**: 4108-4115.

Russ, W. P. & Engelman, D. M., (2000) The GxxxG motif: a framework for transmembrane helix-helix association. *J Mol Biol* **296**: 911-919.

Sanders, C. R. & Myers, J. K., (2004) Disease-related misassembly of membrane proteins. *Annu Rev Biophys Biomol Struct* **33**: 25-51.

Sao-Jose, C., Parreira, R., Vieira, G. & Santos, M. A., (2000) The N-terminal region of the *Oenococcus oeni* bacteriophage fOg44 lysin behaves as a bona fide signal peptide in *Escherichia coli* and as a *cis*-inhibitory element, preventing lytic activity on oenococcal cells. *J Bacteriol* **182**: 5823-5831.

Savva, C. G., Dewey, J. S., Deaton, J., White, R. L., Struck, D. K., Holzenburg, A. & Young, R., (2008) The holin of bacteriophage lambda forms rings with large diameter. *Mol Microbiol* **69**: 784-793.

Schein, S. J., Kagan, B. L. & Finkelstein, A., (1978) Colicin K acts by forming voltage-dependent channels in phospholipid bilayer membranes. *Nature* **276**: 159-163.

Senes, A., Engel, D. E. & DeGrado, W. F., (2004) Folding of helical membrane proteins: the role of polar, GxxxG-like and proline motifs. *Curr Opin Struct Biol* **14**: 465-479.

Senes, A., Gerstein, M. & Engelman, D. M., (2000) Statistical analysis of amino acid patterns in transmembrane helices: the GxxxG motif occurs frequently and in association with beta-branched residues at neighboring positions. *J Mol Biol* **296**: 921-936.

Senes, A., Ubarretxena-Belandia, I. & Engelman, D. M., (2001) The Calpha ---H...O hydrogen bond: a determinant of stability and specificity in transmembrane helix interactions. *Proc Natl Acad Sci USA* **98**: 9056-9061.

Smith, D. L., Struck, D. K., Scholtz, J. M. & Young, R., (1998) Purification and biochemical characterization of the lambda holin. *J Bacteriol* **180**: 2531-2540.

Smith, D. L. & Young, R., (1998) Oligohistidine tag mutagenesis of the lambda holin gene. *J Bacteriol* **180**: 4199-4211.

Stent, G. S., (1963) The Twort-D'Herelle phenomenon. In: *Molecular Biology of Bacterial Virus.* Stent, G. S. (ed.). San Francisco: W. H. Freeman and Company, pp. 1-21.

Strop, P. & Brunger, A. T., (2005) Refractive index-based determination of detergent concentration and its application to the study of membrane proteins. *Protein Sci* **14**: 2207-2211.

Summer, E. J., Berry, J., Tran, T. A., Niu, L., Struck, D. K. & Young, R., (2007) Rz / Rz1 lysis gene equivalents in phages of Gram-negative hosts. *J Mol Biol* **373**: 1098-1112.

Sun, J. & Kaback, H. R., (1997) Proximity of periplasmic loops in the lactose permease of *Escherichia coli* determined by site-directed cross-linking. *Biochemistry* **36**: 11959-11965.

Sun, Q., Kuty, G. F., Arockiasamy, A., Xu, M., Young, R. & Sacchettini, J. C., (2009) Regulation of a muralytic enzyme by dynamic membrane topology. *Nat Struct Mol Biol* **16**: 1192-1194.

Tamm, L. K., Hong, H. & Liang, B., (2004) Folding and assembly of beta-barrel membrane proteins. *Biochim Biophys Acta* **1666**: 250-263.

Therien, A. G., Grant, F. E. & Deber, C. M., (2001) Interhelical hydrogen bonds in the CFTR membrane domain. *Nat Struct Biol* **8**: 597-601.

Tran, T. A., Struck, D. K. & Young, R., (2005) Periplasmic domains define holin-antiholin interactions in T4 lysis inhibition. *J Bacteriol* **187**: 6631-6640.

Tran, T. A., Struck, D. K. & Young, R., (2007) The T4 RI antiholin has an N-terminal signal anchor release domain that targets it for degradation by DegP. *J Bacteriol* **189**: 7618-7625.

Tsukihara, T., Aoyama, H., Yamashita, E., Tomizaki, T., Yamaguchi, H., Shinzawa-Itoh, K., Nakashima, R., Yaono, R. & Yoshikawa, S., (1996) The whole structure of the 13-subunit oxidized cytochrome c oxidase at 2.8 A. *Science* **272**: 1136-1144.

Valentine, R. C., Shapiro, B. M. & Stadtman, E. R., (1968) Regulation of glutamine synthetase. XII. Electron microscopy of the enzyme from *Escherichia coli*. *Biochemistry* **7**: 2143-2152.

VanAken, T., Foxall-VanAken, S., Castleman, S. & Ferguson-Miller, S., (1986) Alkyl glycoside detergents: synthesis and applications to the study of membrane proteins. *Methods Enzymol* **125**: 27-35.

Wagner, P. L., Livny, J., Neely, M. N., Acheson, D. W., Friedman, D. I. & Waldor, M. K., (2002) Bacteriophage control of Shiga toxin 1 production and release by *Escherichia coli*. *Mol Microbiol* **44**: 957-970.

Wagner, P. L. & Waldor, M. K., (2002) Bacteriophage control of bacterial virulence. *Infect Immun* **70**: 3985-3993.

Wahome, P. G., Cowan, A. E., Setlow, B. & Setlow, P., (2009) Levels and localization of mechanosensitive channel proteins in *Bacillus subtilis*. *Arch Microbiol* **191**: 403-414.

Wallin, E. & von Heijne, G., (1998) Genome-wide analysis of integral membrane proteins from eubacterial, archaean, and eukaryotic organisms. *Protein Sci* **7**: 1029-1038.

Walters, R. F. & DeGrado, W. F., (2006) Helix-packing motifs in membrane proteins. *Proc Natl Acad Sci USA* **103**: 13658-13663.

Wang, I. N., Deaton, J. & Young, R., (2003) Sizing the holin lesion with an endolysin-beta-galactosidase fusion. *J Bacteriol* **185**: 779-787.

Wang, I. N., Smith, D. L. & Young, R., (2000) Holins: the protein clocks of bacteriophage infections. *Annu Rev Microbiol* **54**: 799-825.

White, R., (2008) What makes the lysis clock tick? A study of the bacteriophage lambda holin. Ph.D. dissertation. College Station: Texas A&M University.

White, R., Tran, T. A., Dankenbring, C. A., Deaton, J. & Young, R., (2010) The N-terminal transmembrane domain of λ S is required for holin but not antiholin function. *J Bacteriol* **192**: 725-33.

Xu, M., Arulandu, A., Struck, D. K., Swanson, S., Sacchettini, J. C. & Young, R., (2005) Disulfide isomerization after membrane release of its SAR domain activates P1 lysozyme. *Science* **307**: 113-117.

Xu, M., Struck, D. K., Deaton, J., Wang, I. N. & Young, R., (2004) The signal arrest-release (SAR) sequence mediates export and control of the phage P1 endolysin *Proc Natl Acad Sci USA* **101**: 6415-6420.

Young, R., (1992) Bacteriophage lysis: mechanism and regulation. *Microbiol Rev* **56**: 430-481.

Young, R., (2002) Bacteriophage holins: deadly diversity. *J Mol Microbiol Biotechnol* **4**: 21-36.

Young, R. & Bläsi, U., (1995) Holins: form and function in bacteriophage lysis. *FEMS Microbiology Reviews* **17**: 191-205.

Young, R. & Wang, I. N., (2006) Phage lysis. In *The Bacteriophages.* Calendar, R. (ed). Oxford: Oxford University Press, pp. 104-126.

Young, R., Way, S., Yin, J. & Syvanen, M., (1979) Transposition mutagenesis of bacteriophage lambda: a new gene affecting cell lysis. *J Molelcular Biology* **132**: 307-322.

Young, R. & White, R. L., (2008) Lysis of the host by bacteriophage. In *Encyclopedia of Virology,* Third Edition. Mahy, B. W. J. and van Regenmortel, M. H. V. (eds). Boston: Academic Press, pp. 248-258.

Zhang, N. & Young, R., (1999) Complementation and characterization of the nested Rz and Rz1 reading frames in the genome of bacteriophage lambda. *Molecular and General Genetics* **262**: 659-667.

Zheng, Y., Struck, D. K., Dankenbring, C. A. & Young, R., (2008) Evolutionary dominance of holin lysis systems derives from superior genetic malleability. *Microbiology* **154**: 1710-1718.

Zhou, F. X., Merianos, H. J., Brunger, A. T. & Engelman, D. M., (2001) Polar residues drive association of polyleucine transmembrane helices. *Proc Natl Acad Sci USA* **98**: 2250-2255.

VITA

Ting Pang received her Bachelor of Science degree in Biotechnology from Wuhan University in 2004. She entered the Department of Biochemistry and Biophysics at Texas A&M University in September 2004 and received her Ph.D. degree in May 2010. Her research interests include molecular biology and genetics of viruses, and the biochemical studies of membrane proteins.

Ms. Pang may be reached at Department of Biochemistry and Biophysics, Texas A&M University, TAMU 2128, College Station, TX 77843. Her e-mail address is tingpangbiobio@yahoo.com.